NASA CR-114618

AVAILABLE TO THE PUBLIC

STUDY OF BALLISTIC MODE MERCURY ORBITER MISSIONS

Volume II

TECHNICAL REPORT

July 1973

Prepared Under Contract No. NAS2-7268

by

MARTIN MARIETTA CORPORATION
Denver, Colorado 80201

for

AMES RESEARCH CENTER
NATIONAL AERONAUTICS AND SPACE ADMINISTRATION

STUDY OF BALLISTIC MODE MERCURY ORBITER MISSIONS
Volume II

TECHNICAL REPORT

by

W. S. Cook, G. R. Hollenbeck, P. S. Lewis,
D. G. Roos, & D. E. Wainwright

JULY 1973

Prepared Under Contract No. NAS2-7268

by

MARTIN MARIETTA CORPORATION

Denver, Colorado 80201

for

AMES RESEARCH CENTER

NATIONAL AERONAUTICS AND SPACE ADMINISTRATION

Approved: G. R. Hook

G. R. Hook
Program Manager

FOREWORD

This report was prepared under Contract NAS2-7268, Study of Ballistic Mode Mercury Orbiter Missions, to present data and conclusions drawn from a six-month study by Martin Marietta Corporation's Denver Division. Four specific mission opportunities were studied, corresponding to launches in 1977, 1980, 1985, and 1988. Results of investigations of alternate flight techniques to enhance mission performance of these opportunities, as well as to generate new opportunities, are also reported.

The interplanetary trajectory characteristics which provided the bases for generation of mission and spacecraft design support data, science rationales, and critical technology items contained herein are assembled in a handbook format in a separate report. This is entitled "Ballistic Mode Mercury Orbiter Mission Opportunity Handbook," NASA CR-2298, and was published under the same contract in May 1973.

A condensed Summary Report, NASA CR-114617, encompassing the entire study contract scope has been published concurrently with this technical report.

Credit is due Ms. Jill Strauss whose conscientious preparation of graphic material contributed significantly to the quality of this report.

TABLE OF CONTENTS

LIST OF FIGURES

LIST OF TABLES

I. INTRODUCTION

I. INTRODUCTION

Advanced missions to the planet Mercury have been addressed in terms of ballistic mode flight compatible with programmed launch vehicles and conventional spacecraft technologies. Data are presented to validate performance capabilities, to support parametric analyses of mission design, to assess science return, and to define spacecraft design constraints and requirements.

Previous investigations of the difficult Mercury Orbiter mission have indicated that the ballistic mode would require a Saturn V class launch vehicle for adequate performance to support a useful mission. As a consequence, most recent effort has been oriented to use of solar electric propulsion as a solution for the performance requirements.

More thorough analysis of the ballistic mode utilizing Venus gravity-assist has resulted in identification of timely, high-performance mission opportunities which are not dependent on extensive new developments. Figure I-1 displays the characteristics of four mission opportunities which formed the baseline scope for this study contract. As shown, performance capabilities range from values adequate to support either spin stabilized or 3-axis stabilized spacecraft types with a Titan IIIE/Centaur launch to a marginal case which would require launch with the Shuttle/Centaur or equivalent.

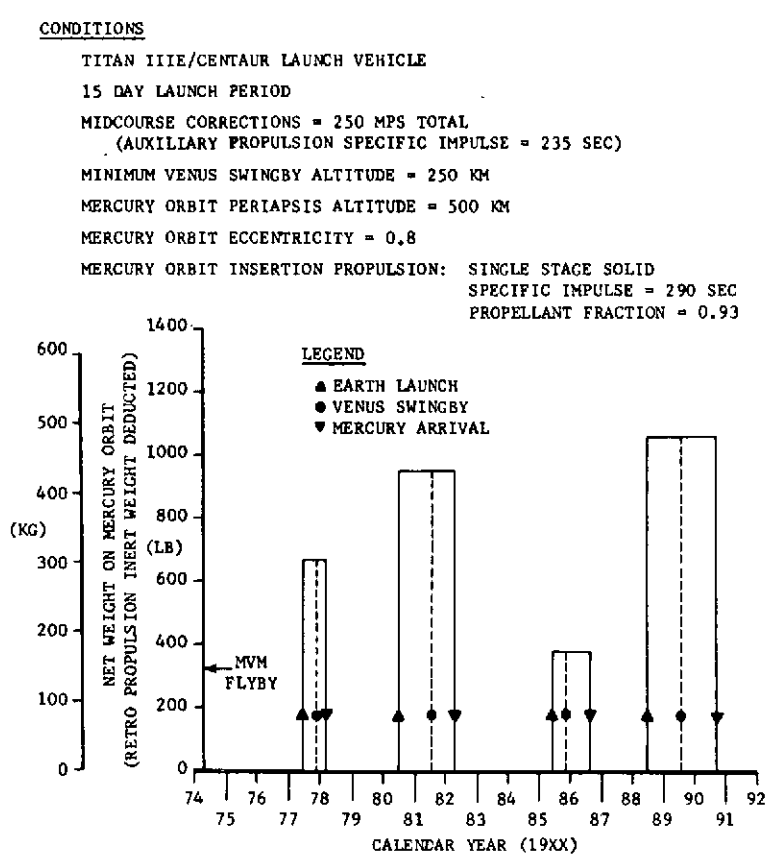

FIGURE I-1 BASELINE MERCURY ORBITER OPPORTUNITIES

The basic planet geometries and event sequences which characterize the baseline missions are typified by the 1980 flight profile presented on Figure I-2. Earth, Venus, and Mercury positions at launch, gravity-assist swingby, and encounter events are near the theoretically ideal alignments for ballistic mode flight. A primary requirement for high performance potential involves achieving Mercury encounter near Mercury perihelion and near the intersection of the Venus and Mercury orbit planes. Secondarily, Venus swingby must also be accomplished near the intersection of the orbit planes. Meeting these conditions will produce a near-tangential encounter with Mercury and minimize the relative approach velocity. The corresponding Earth-to-Venus trajectory must be Type II to achieve the desired Venus encounter geometry.

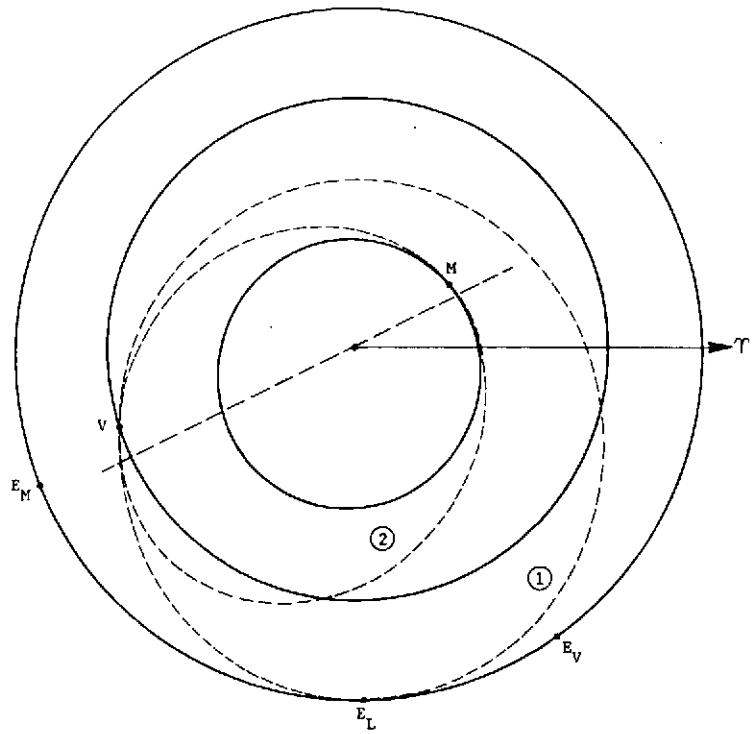

— — — INTERSECTION OF VENUS AND MERCURY ORBIT PLANES
E_L: EARTH AT LAUNCH, 6-24-80
E_V: EARTH AT VENUS SWINGBY, 7-28-81
E_M: EARTH AT MERCURY ENCOUNTER, 4-14-82
V: VENUS AT SWINGBY
M: MERCURY AT ENCOUNTER
① ONE COMPLETE SOLAR REVOLUTION BEFORE VENUS SWINGBY
② ONE COMPLETE SOLAR REVOLUTION BEFORE MERCURY ENCOUNTER

The 1980 mission shown involves two extra solar revolutions of the spacecraft to accommodate planet phasing. Resultant total flight time is about 22 months due to these phasing requirements. Earth positions at the times of the Venus swingby and Mercury encounter events are indicative of the difficult navigation problems typical of ballistic-mode Mercury Orbiter missions.

FIGURE I-2 TYPICAL HELIOCENTRIC FLIGHT PROFILE

As an adjunct to the basic study, exploratory investigations of two alternate flight techniques were conducted. These involved the use of midcourse propulsive maneuvers and multiple Venus swingbys. The impact of these options is illustrated on Figure I-3 in context with the baseline mission opportunities. As shown, performance of the 1985 opportunity can be substantially improved by use of modest midcourse velocity maneuvers. Also, two new high-performance mission opportunities predicated on multiple Venus swingby have been identified for 1983 and 1988 launch. The capabilities depicted for the alternate flight techniques represent verified minimum potential without benefit of complete optimization. The significance of the alternate flight techniques to mission planning options is apparent; however, since detailed analyses have not yet been completed, this report is primarily oriented to the original four baseline mission opportunities with occasional mention of the alternate missions where appropriate.

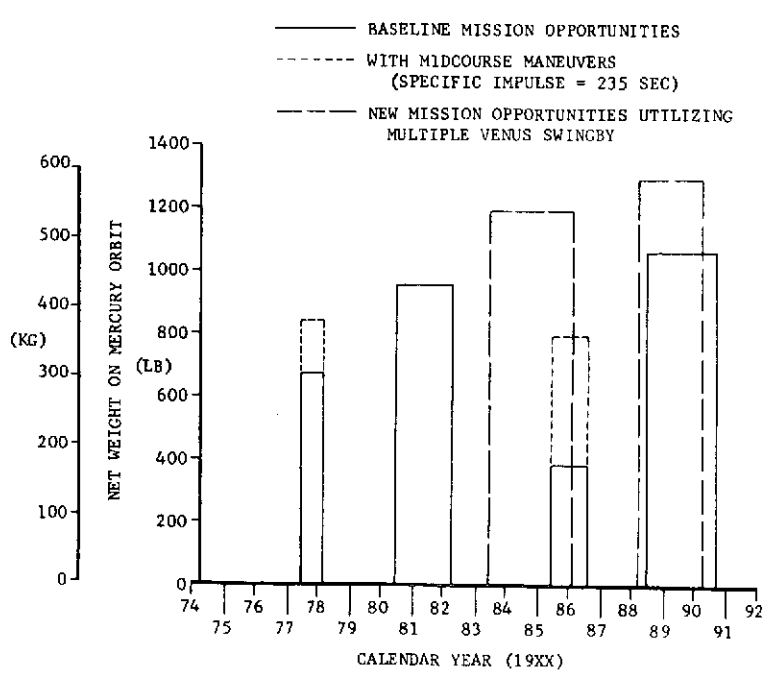

FIGURE I-3 POTENTIAL OF ALTERNATE FLIGHT TECHNIQUES

Detailed documentation of trajectory characteristics data for the aforementioned mission opportunities is contained in a comparison report "Ballistic Mode Mercury Orbiter Mission Opportunity Handbook," NASA CR-2298. Also included are results of navigation analyses for the four baseline cases. For the purpose of continuity, a summary of the handbook data is provided as Section II of this technical report.

Performance capabilities for the baseline mission opportunities have been calculated for two launch vehicles (Titan IIIE/Centaur and Shuttle/Centaur), representative spacecraft propulsion systems and the spectrum of accessible Mercury orbits. Additional requirements associated with low inclination orbits and post-insertion modifications of orbit geometry are treated parametrically. Orbit dispersions resulting from Mercury approach uncertainties and orbit insertion errors have been analyzed and orbit trim maneuvers computed. The foregoing subjects are addressed in Section III and provide the foundation for subsequent discussions of the orbit analysis and spacecraft design factors.

The spectrum of accessible orbit geometries has been analyzed in terms of stability, exposure to the thermal environment, Earth and solar occultations, etc. to characterize requirements and constraints imposed on spacecraft design and operation. Corresponding implications to science return have been related to science objectives and orbit geometry options. Both of these subjects represent orbit selection considerations which are discussed and correlated in Section IV. Section V further extends the science analysis for a representative orbit selected to illustrate some matters in a degree of detail incompatible with parametric treatment.

While design effort was not included in the study scope, technology assessments were conducted for major subsystems appropriate to spin-stabilized and 3-axis stabilized spacecraft configurations. These investigations are related to the current and projected state-of-the-art in Section VI.

A summary of primary conclusions derived from the six-month study effort is presented in Section VII. Items of potential significance to advanced Mercury mission planning which were not resolved in the course of this study are recommended for future investigation.

The appendix to this report contains an assembly of environmental data relevant to spacecraft design. Also included are summaries of side investigations relating to operational options and advanced mission modes. Specifically, opportunities to utilize Arecibo capabilities and to enhance cruise phase science with such activities as comet viewing are identified. Sizing and operational considerations for orbiter-dependent subsatellites and lander vehicles are presented at the conceptual level.

II. MISSION OPPORTUNITY DATA

II. MISSION OPPORTUNITY DATA

The analyses and discussions in this report are, to a large extent, predicated on interplanetary trajectory characteristics data documented in detail in a companion volume entitled "Ballistic Mode Mercury Orbiter Mission Opportunity Handbook," NASA CR-2298. For the convenience of the reader, summary results from the Handbook are presented in this section.

A. PERFORMANCE PARAMETERS

The 1977 mission opportunity has been analyzed for a broad spectrum of Earth launch dates and Mercury arrival dates. Figure II-1 presents the primary performance parameter for Mercury orbiter missions, i.e., relative approach velocity at Mercury. To facilitate use of the data, the envelope of minimum achievable velocity values is shown.

The parametric variations of launch energy requirements for the 1977 opportunity are displayed in Figure II-2. No attempt was made to minimize this parameter due to the overriding significance of Mercury approach velocity. Determination of best performance for a particular launch vehicle and orbit insertion propulsion type does involve some second order tradeoffs between launch requirements and Mercury arrival conditions. Sufficient data are provided to accommodate such optimizations. For convenience, launch energy corresponding to minimum Mercury approach velocity for each Earth launch date is indicated.

Preliminary investigations of the 1980 mission opportunity revealed severe constraints on Mercury arrival date. The entire region of best performance corresponds to a variation of about 1.3 days in Mercury arrival (4-13.7-82 to 4-15-82). Accordingly, it was necessary to optimize Mercury arrival date and present data for this special condition.

Figure II-3 shows the minimized Mercury approach velocities as a function of Earth launch date and the corresponding launch energy requirements. Also shown are the effects of constraining the Venus swingby altitude to a set of values encompassing the expected range of navigation capabilities. Whereas 1977 missions did not require an extremely close swingby of Venus, the 1980 opportunity is characterized by performance incentives to minimize swingby altitude. However, as shown by Figure II-3, higher minimum altitudes which

increase achievable relative velocity at Mercury are partially compensated by a corresponding reduction of launch energy for typical Earth launch periods.

A performance improvement option applicable to the 1980 missions involves use of modest velocity maneuvers in the vicinity of Venus. Figure II-3 presents the direct effect of such maneuvers showing an advantage factor in reducing Mercury approach velocity of about 2 (i.e., a 100 mps maneuver at Venus reduces Mercury arrival speed by about 200 mps). If these maneuvers are applied at Venus departure in conjunction with the post-Venus navigation midcourse correction, the net cost of the maneuver is considerably less than the nominal magnitude. For example, a Venus velocity maneuver of 100 mps statistically combined with the post-Venus midcourse correction involves a net increase of only 26 mps. For this penalty on auxiliary propulsion requirements, the benefits of a 100 mps Venus maneuver as shown on Figure II-3 can be realized.

Planetary geometries for the 1985 mission opportunity depart significantly from idealized alignments. As a consequence, performance potential is relatively poor. The Mission Opportunity Handbook presents the effectiveness of an alternate flight technique for this opportunity involving application of midcourse velocity maneuvers near perihelion of the Earth-Venus transfer trajectory. The net improvment potential of this technique is depicted on Figure I-3.

Even though larger launch vehicles such as Shuttle/Centaur may be operational by the mid 1980's, the improved capabilities of the midcourse maneuver technique may be basic to a useful 1985 Mercury Orbiter mission. However, complete optimizations of the technique have not been accomplished and parametric data are not yet available. Accordingly, the pure ballistic flight mode is presented in this report as representative of the basic characteristics of the 1985 mission opportunity.

Figures II-4 and II-5 show the primary performance parameters for 1985 missions. The relative velocities at Mercury, in excess of 8 km/sec, are responsible for the low performance. It is this parameter which can be significantly improved with midcourse maneuvers. Launch energy requirements as shown are representative of both techniques. General similarities with the 1977 missions are apparent and include insensitivity to Venus altitude constraints.

The high-performance 1988 mission opportunity is similar to the 1980 case.

Mercury arrival dates for best performance span a period of about 2 days (9-17-90 to 9-18-90) and Venus swingby altitude constraints are again a consideration.

A peculiarity in the 1988 planetary alignments produced an interruption in the Earth launch period for the pure ballistic flight mode. It was determined that a velocity maneuver of 75 mps in the vicinity of Venus was effective in bridging the launch period gap. Accordingly, the data presented in Figure II-6 for the 1988 mission opportunity are contingent on provision for the velocity maneuver.

Statistical combination of the 75 mps Venus maneuver with the post-Venus navigation midcourse correction indicates a net equivalent cost of 17 mps. These requirements are summarized in Subsection II-B and must be considered together with the parametric data presented in this subsection for calculation of total performance capabilities.

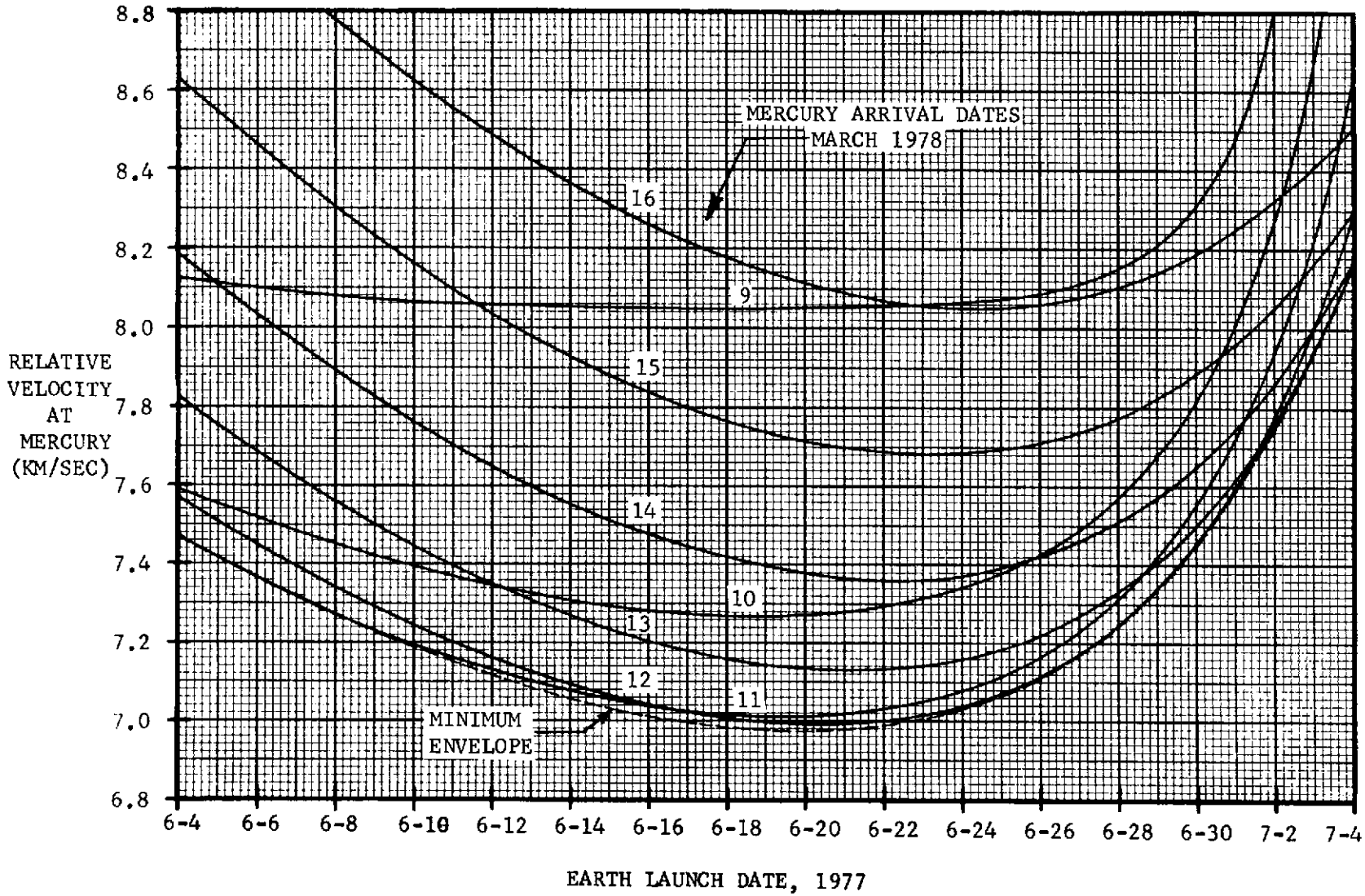

FIGURE II-1 RELATIVE VELOCITY AT MERCURY VS. LAUNCH/ARRIVAL DATE, 1977 OPPORTUNITY

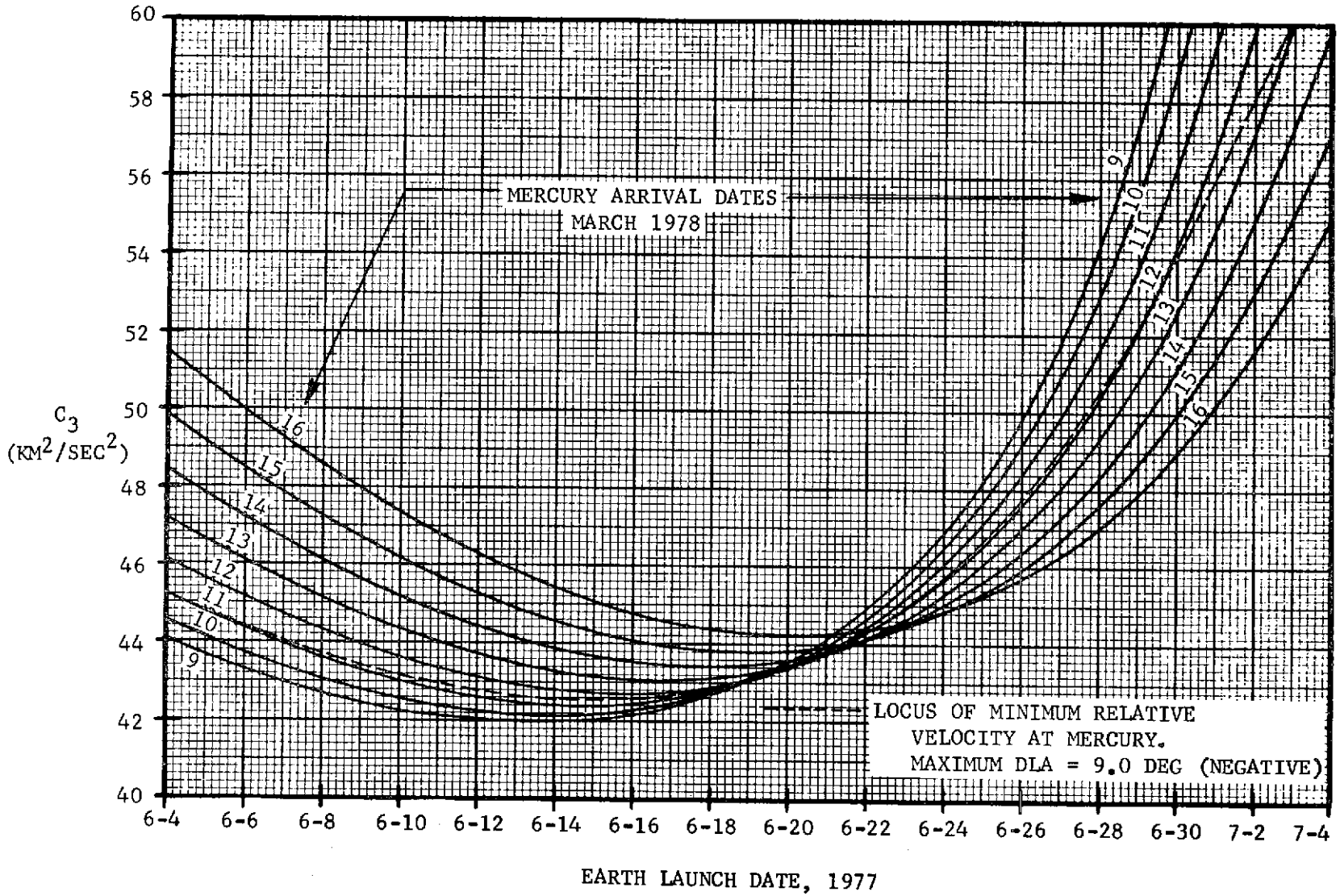

FIGURE II-2 C_3 VS. LAUNCH/ARRIVAL DATE, 1977 OPPORTUNITY

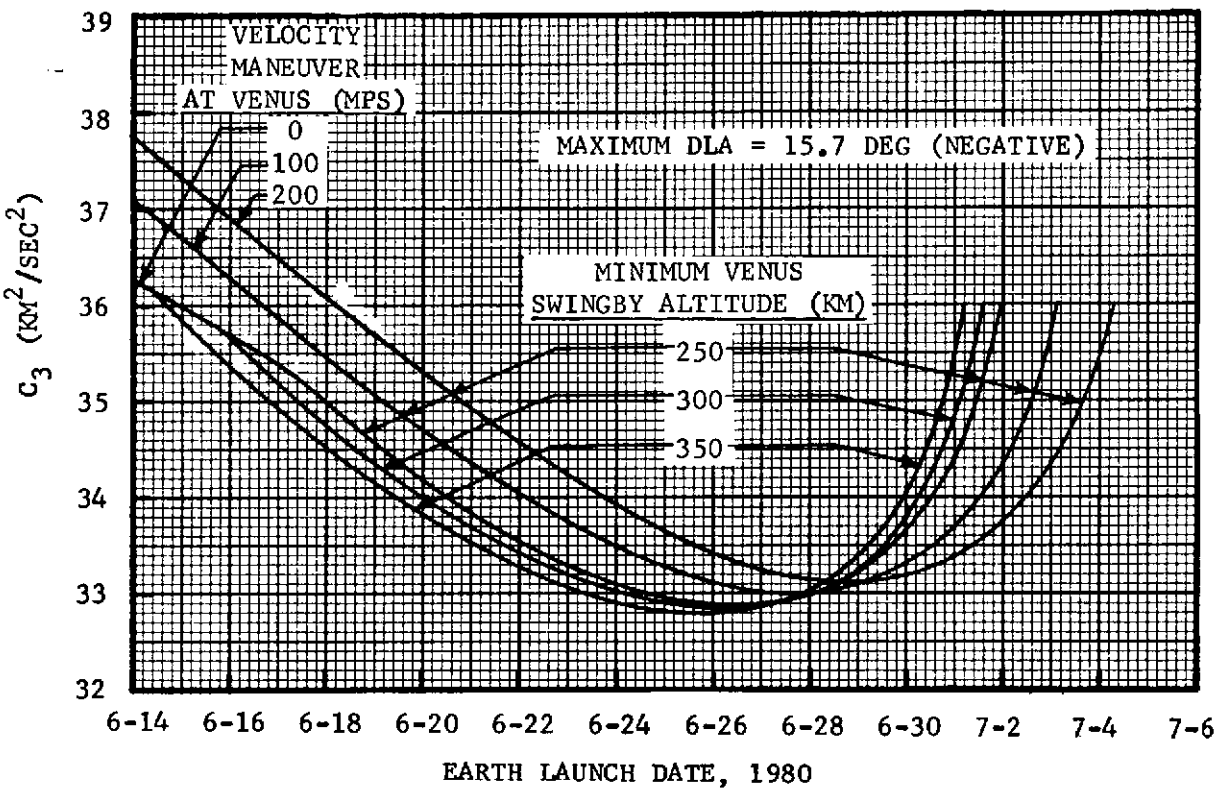

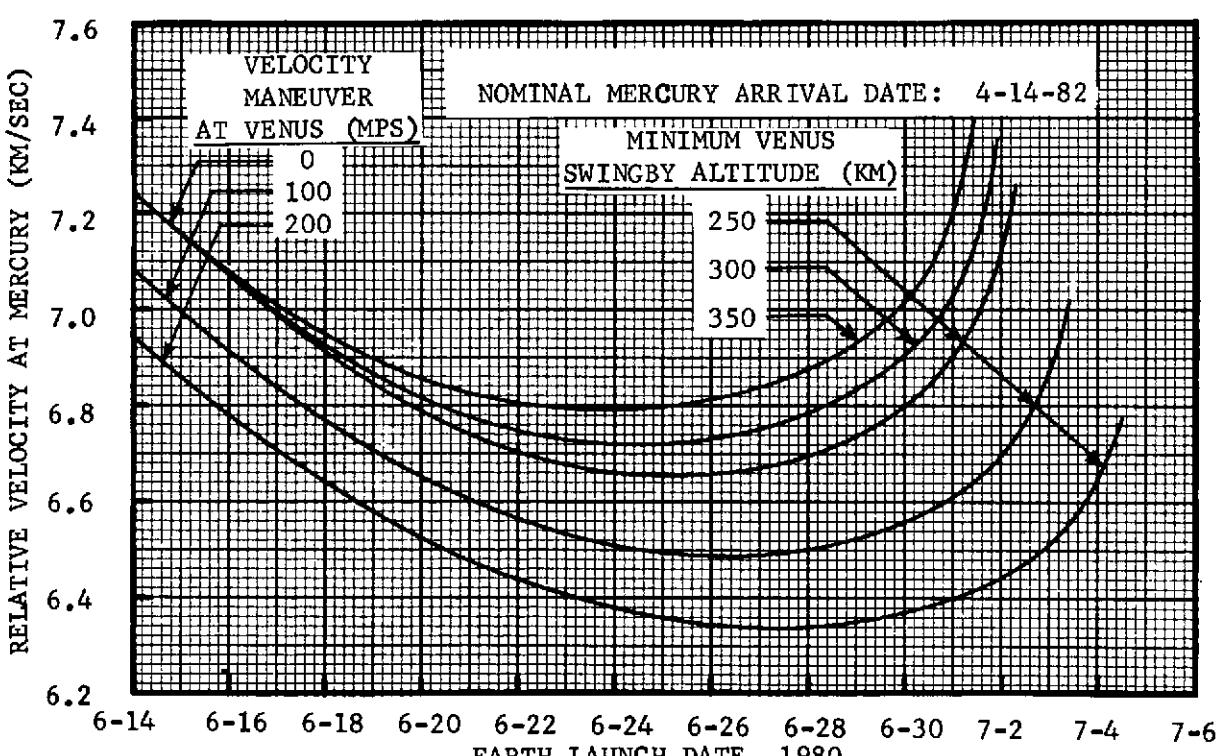

FIGURE II-3 MINIMUM RELATIVE VELOCITY AT MERCURY AND CORRESPONDING C_3 VS. LAUNCH DATE, 1980 OPPORTUNITY

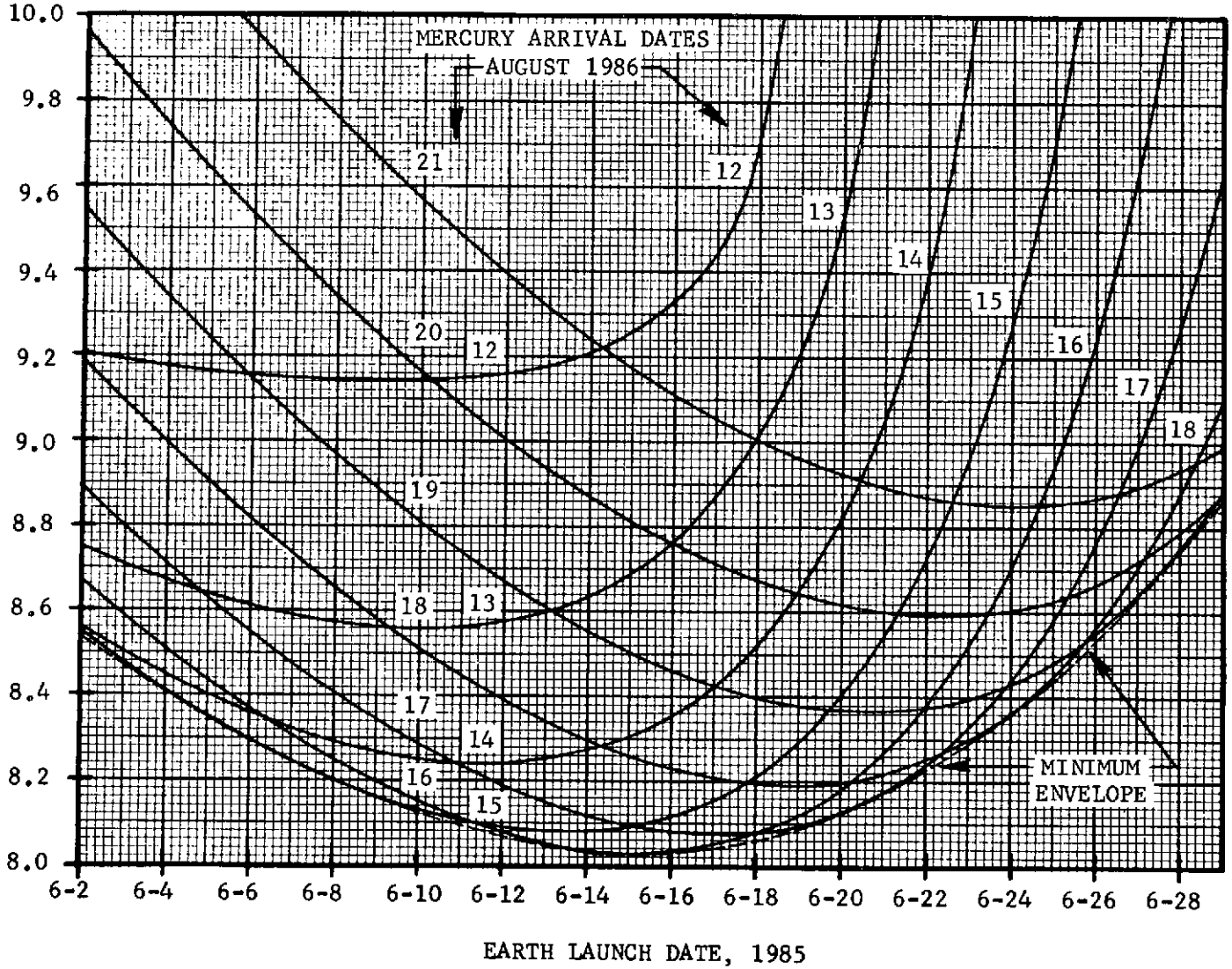

FIGURE II-4 RELATIVE VELOCITY AT MERCURY VS. LAUNCH/ARRIVAL DATE, 1985 OPPORTUNITY

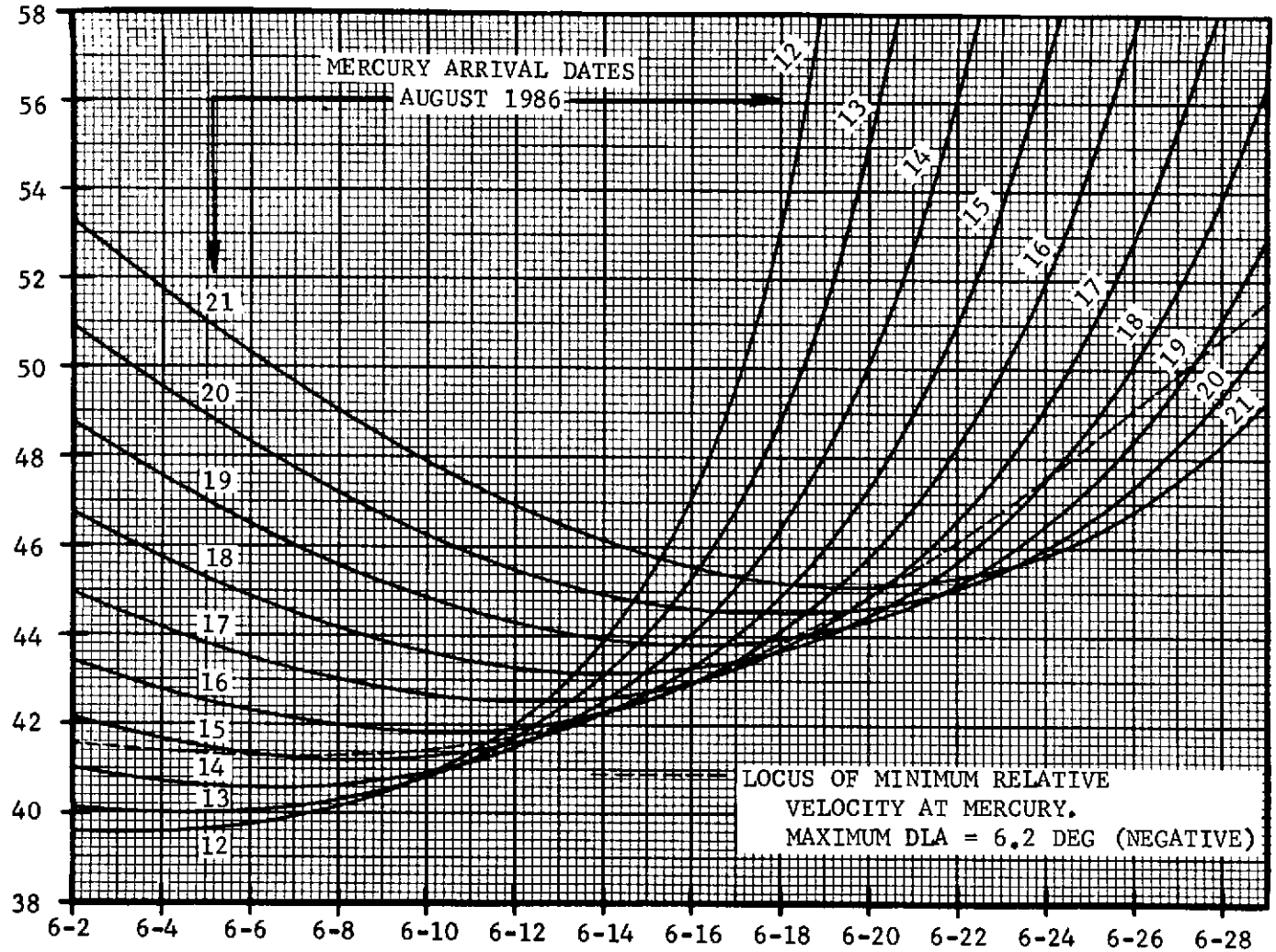

FIGURE II-5 C_3 VS. LAUNCH/ARRIVAL DATE, 1985 OPPORTUNITY

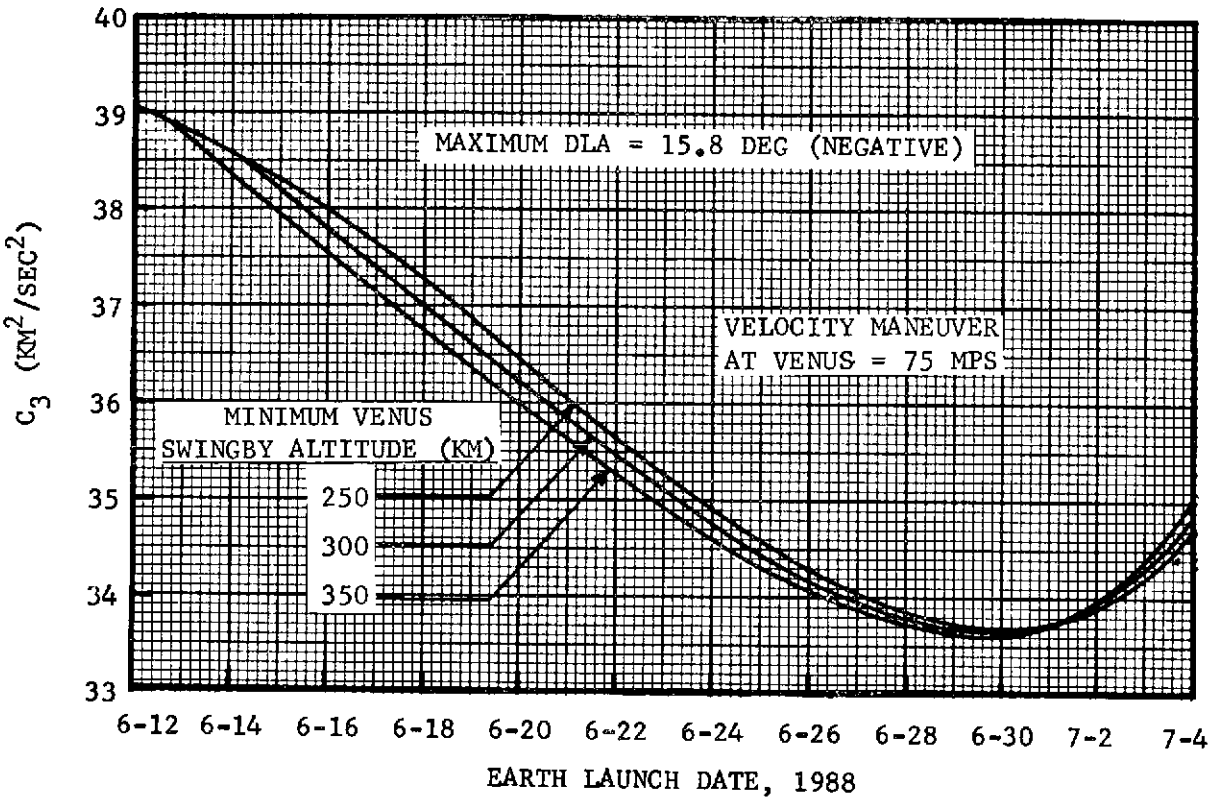

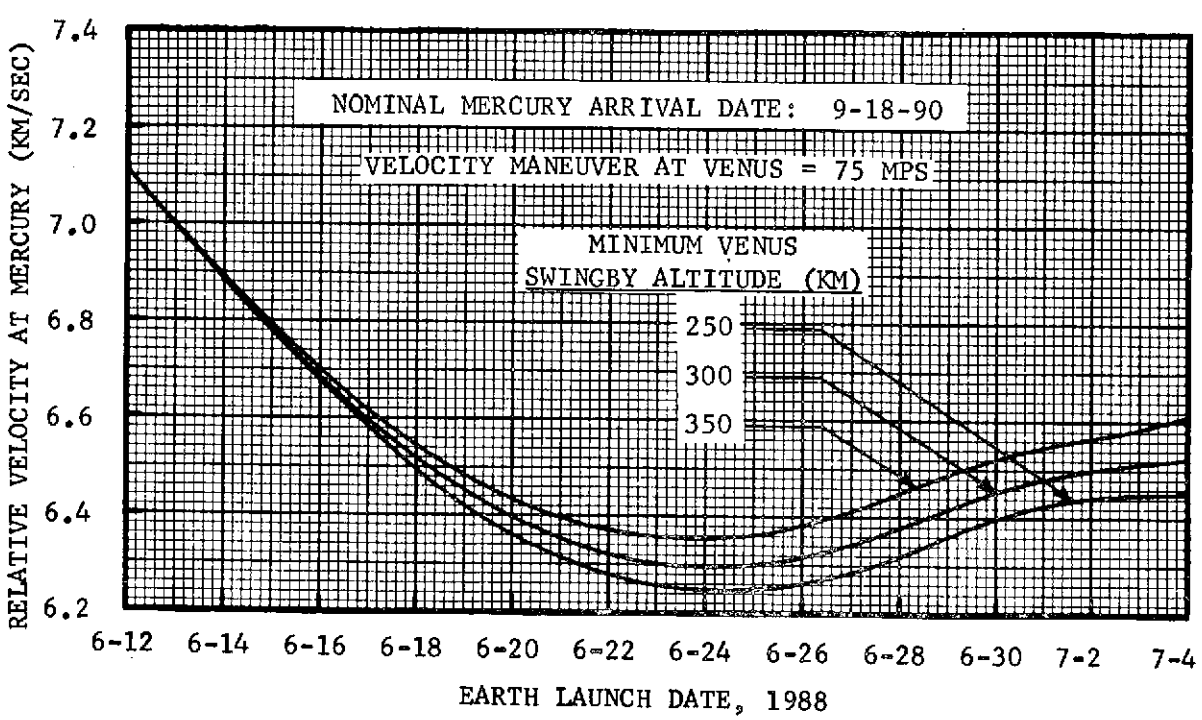

FIGURE II-6 MINIMUM RELATIVE VELOCITY AT MERCURY AND CORRESPONDING C_3 VS. LAUNCH DATE, 1988 OPPORTUNITY

THIS

PAGE

BLANK

B. NAVIGATION REQUIREMENTS

Complete navigation analyses have been conducted for each of the baseline mission opportunities and documented in detail in the Mission Opportunity Handbook. Table II-1 summarizes the primary results of these analyses. The major assumptions qualifying these data are:

1) Conservative estimates of DSN station location errors for the 1980 time period (with charged particle calibration).

Sigma R_S	.73 m
Sigma λ	2.04 m
Sigma Z_h	10 m
Correlation λ_i λ_j	.9

2) Dual frequency doppler (S and X band)

The potential improvements offered by QVLBI, optical navigation, and/or a ranging transponder are <u>not</u> reflected in the Table II-1 data.

TABLE II-1 STATISTICAL DESCRIPTION OF MANEUVERS

MISSION YEAR	MANEUVER TIME (DAYS)	MEAN ΔV (MPS)	SIGMA ΔV (MPS)		MEAN PLUS THREE SIGMA (MPS)
1977	Earth Launch +10	6.90	4.57		20.6
	Venus Encounter -3	3.94	2.76		12.2
	Venus Encounter +2	62.15	41.40		186.4
	Mercury Encounter -30	2.26	1.68		7.3
				TOTAL	226.5
1980	E+10	7.53	5.12		22.9
	E+260	.06	.04		.2
	V-3	1.08	.72		3.2
	V+2	66.04	41.84		206.6*
	M-100	.98	.58		2.7
	M-3	1.32	.99		4.3
				TOTAL	239.9
1985	E+10	6.95	4.61		20.8
	V-3	1.23	.71		3.4
	V+2	69.04	47.34		211.1
	M-100	1.20	.78		3.8
	M-3	1.00	.75		3.2
				TOTAL	242.3
1988	E+10	7.45	5.05		22.6
	E+260	.06	.04		.2
	V-3	1.23	.84		3.8
	V+2	71.70	51.43		226.0**
	M-290	1.16	.67		3.2
	M-100	.43	.28		1.3
	M-8	2.40	1.82		7.8
				TOTAL	264.9

*233 mps when combined with 100 mps planned velocity maneuver at Venus.

** Statistical combination of 226 mps midcourse correction and 75 mps required velocity maneuver at Venus results in 243 mps at V+2 and 281.9 mps equivalent total.

Trajectory dispersions were propagated through encounter with the Mercury sphere of influence. One sigma dispersion levels are presented in Figure II-7 for each of the four baseline mission opportunities.

A major contributor to the encounter dispersions is the assumed value of Mercury ephemeris errors. Current predictions for the 1980 time period range as high as 90 km for one sigma confidence depending on the planetary geometries existing at the time knowledge update is attempted. For this study, a judgement value of 60 km spherical, one sigma, was employed and represents a primary qualification on dependent analyses. This ephemeris uncertainty value is about double that to which the MVM'73 mission has been designed.

As shown by Figure II-7, improvements in Mercury ephemeris knowledge could greatly decrease dispersions for most of the mission cases. The large R-axis uncertainty for 1980 is due to zero-declination conditions prior to encounter and would not be substantially affected by ephemeris error reduction. A similar condition applies to T-axis dispersions for the 1977 mission which are due to assumed early execution of the final midcourse maneuver dictated by solar interference with doppler tracking during the month prior to Mercury encounter. The effects of the assumed ephemeris error on resultant Mercury orbit dispersions (further discussed in Subsection III-C) do not preclude successful orbit insertion and can be subsequently trimmed with modest maneuvers.

The component of Mercury encounter dispersions affecting periapsis radius uncertainties is determined by B-plane targeting. The example shown on Figure II-7 for the B-vector (along the planet radius) illustrates the dependence on θ_{AIM} and permits interpretation of Subsection III-C data for other targeting assumptions. Figure IV-1 presents a definition of B-plane targeting and shows the spectrum of orbit geometry options.

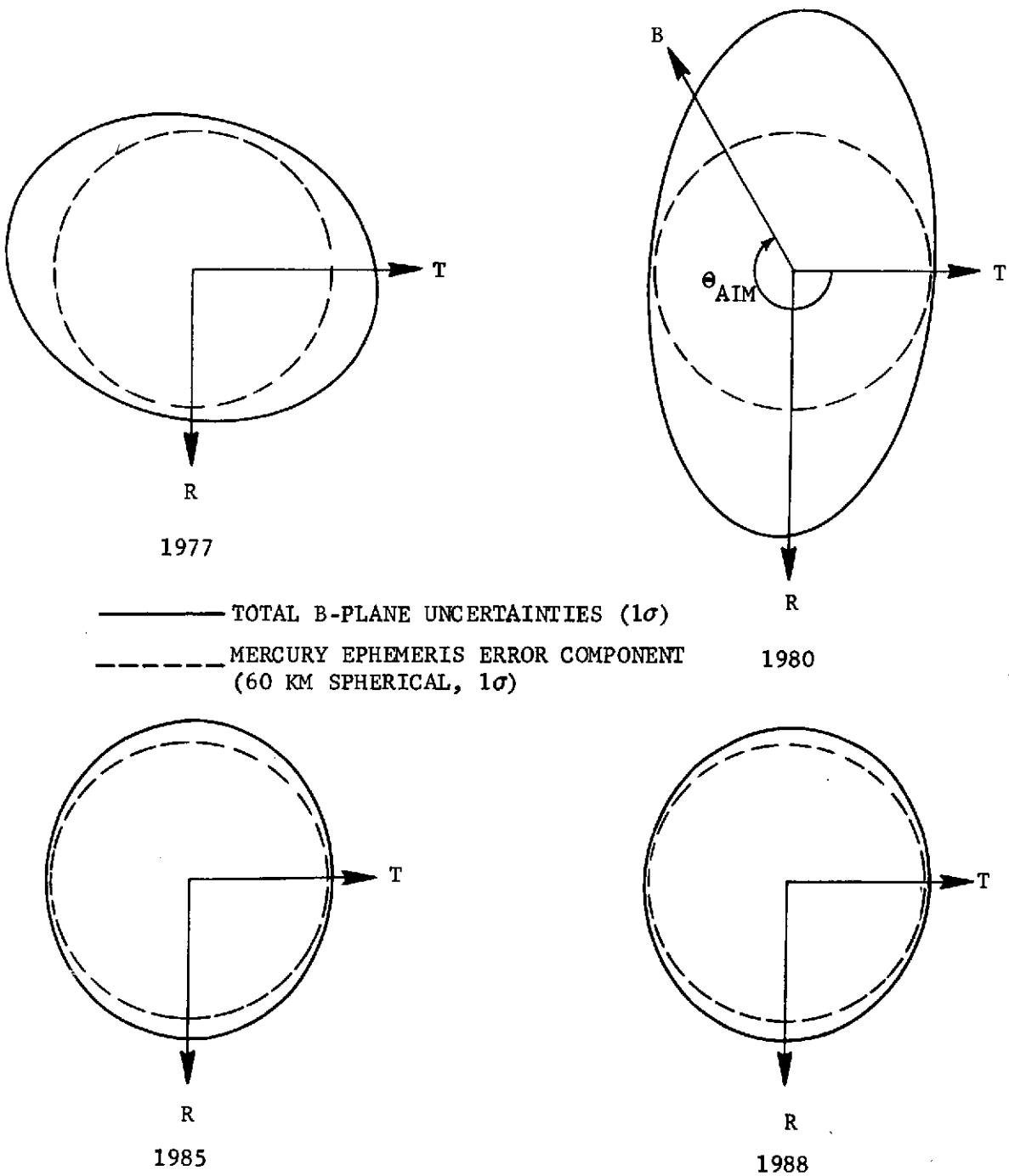

FIGURE II-7 MERCURY ENCOUNTER DISPERSIONS

THIS
PAGE
BLANK

III. PERFORMANCE ANALYSIS

III. PERFORMANCE ANALYSIS

The Handbook data summarized in the preceding section have been utilized to generate estimates of net orbited weight which establish total capabilities available for basic spacecraft systems, science instruments, and on-orbit consumables. Calculations have been performed for the four baseline opportunities and two launch vehicles: Titan IIIE/Centaur and Shuttle/Centaur. Availability of the latter launch system is uncertain but is not expected to apply to ballistic Mercury orbiter missions earlier than the 1985 opportunity.

Analyses of orbit dispersions resulting from Mercury approach uncertainties, retro execution errors, etc. are included in this section. The performance requirements for post-insertion trim of these dispersions are presented.

A. SPACECRAFT SIZING

Launch vehicle capabilities were derived from the current edition of the NASA document "Launch Vehicle Estimating Factors for Advance Mission Planning." Figure III-1 presents extracted data for the range of launch energies applicable to ballistic mode Mercury orbiter missions.

Overall performance is highly dependent on the type of spacecraft propulsion system employed for the large orbit insertion retro maneuver. While detailed design studies and tradeoffs have not been conducted, a conventional solid rocket motor seems appropriate to the cruise phase thermal environment and the high thrust requirements for prompt retro. Accordingly, performance capabilities presented in this report are predicated on the propulsion characteristics listed in Table III-1. Also shown is the specific impulse assumed for an auxiliary propulsion system appropriate to execution of navigation midcourse corrections and other maneuvers of a comparable magnitude. Hardware weights for the latter are included in the calculated values of net spacecraft weight.

Selection of an Earth launch interval is necessary for interpretation of the mission opportunity performance parameters. Due to the short periods of best performance characteristic of Venus-assist Mercury missions, a practical upper limit of about 15 days is indicated. This criterion is consistent with the planned MVM '73 mission.

Figure III-2 illustrates the extreme condition of one day launch periods and corresponding Earth launch date optimization for each opportunity. These

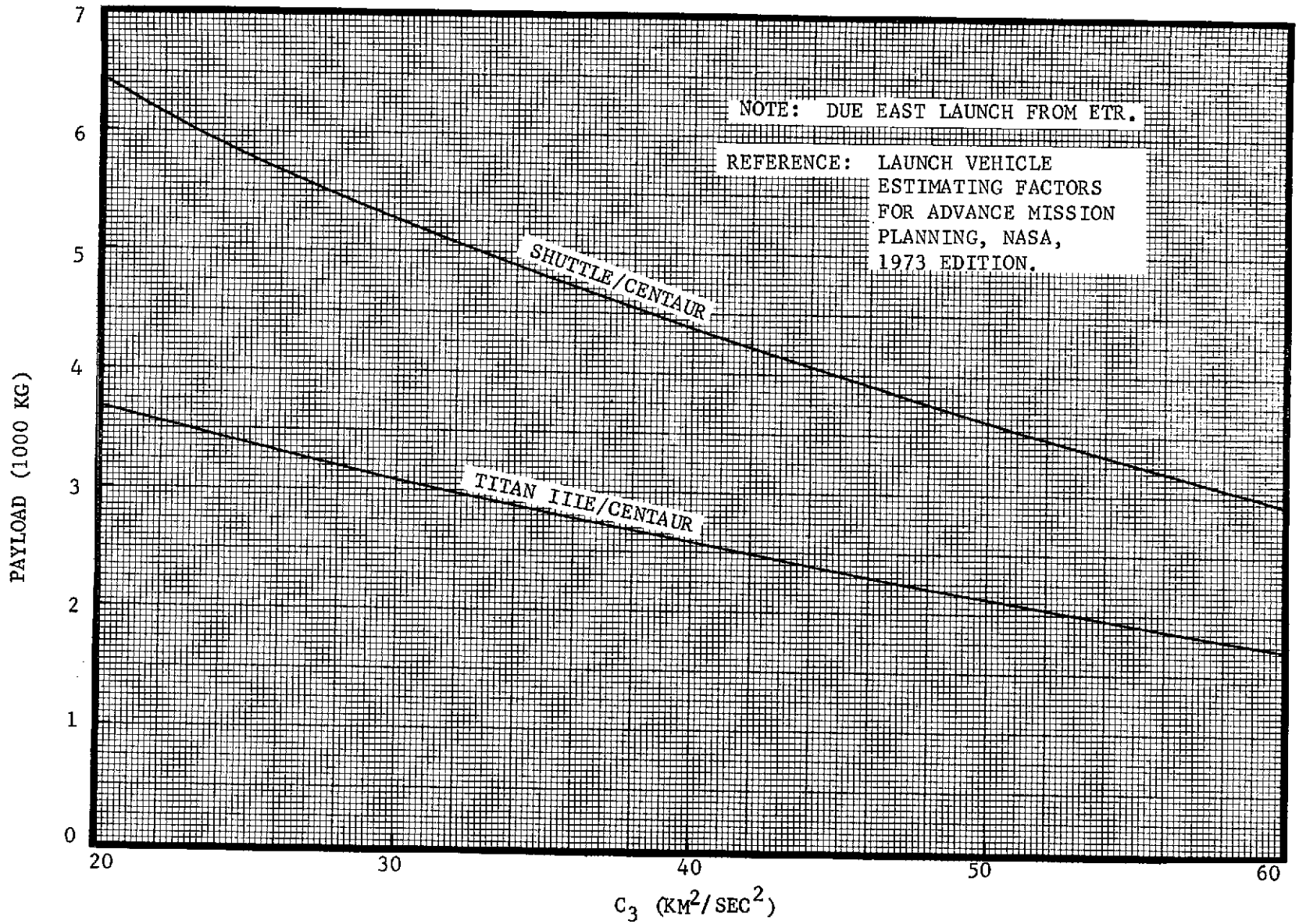

FIGURE III-1 LAUNCH VEHICLE PERFORMANCE CAPABILITIES

TABLE III-1

REPRESENTATIVE SPACECRAFT PROPULSION SYSTEM CHARACTERISTICS

	MINIMUM SPECIFIC IMPULSE (SEC)	PROPELLANT MASS FRACTION
Primary Retro Propulsion (Solid Rocket Motor, TE-364-4 Technology)	290	.93
Auxiliary Propulsion (Hydrazine Mono-propellant)	235	Not Specified

data are based on the Titan IIIE/Centaur launch vehicle but are amenable to general interpretation.

As shown by the figure, performance is not seriously degraded by consideration of a 15-day launch span. A minor exception is the 1980 opportunity which, due to pronounced asymmetry, displays about 15% improvement for reduction to a 7-day launch period.

Corresponding retro propulsion sizing is also shown on the figure for single day tailored optimization. The prospects of performance degradation associated with a fixed weight solid motor for operation over a span of earth launch dates is indicated by variation trends. In this regard, the 1980 mission displays remarkable consistency.

Determination of a best performance Earth launch period involves secondary tradeoffs between launch energy and Mercury arrival conditions. This effect is illustrated on Figure III-3 for 15-day launch periods and the 1977 mission (for which a total spectrum of Mercury arrival date data is available). As shown, neither the condition for minimum relative velocity at Mercury (worst values for 15-day span) nor the condition for minimum launch energy (worst

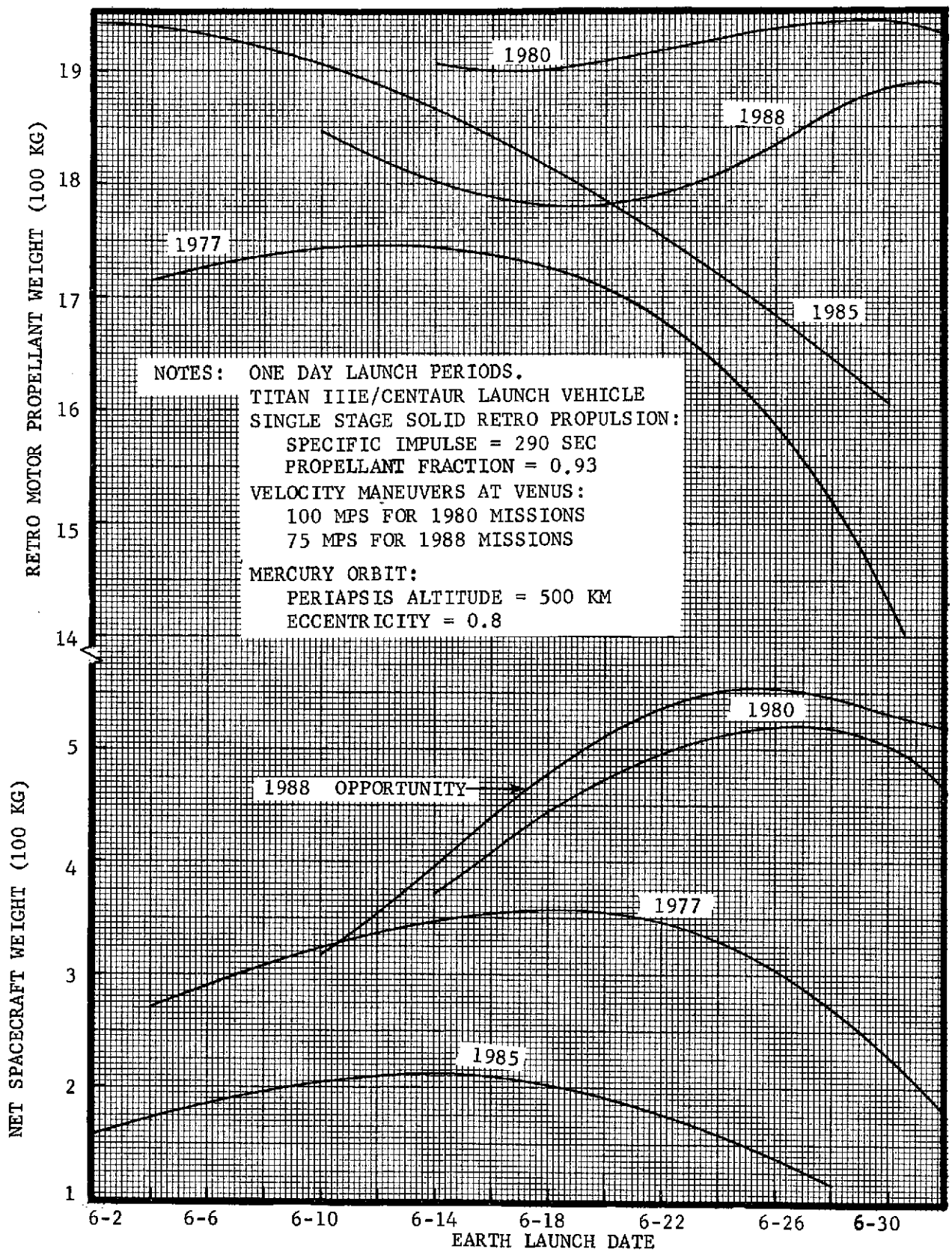

FIGURE III-2 NET SPACECRAFT WEIGHT AND RETRO PROPULSION SIZING FOR MAXIMUM PERFORMANCE

values for 15-day span) represent the true optimum. However, the psuedo-optimum case of best relative velocity at Mercury is within about 2% of optimum (considered typical) and represents the only data type available for the 1980 and 1988 opportunities. Accordingly, performance values in subsequent report sections are consistently quoted for the case of 15-day launch periods based on best relative velocity at Mercury.

Table III-2 summarizes performance parameters for each of the mission opportunities and shows histories of spacecraft weight through the major propulsion phases. The Titan IIIE/Centaur launch vehicle was employed for these examples.

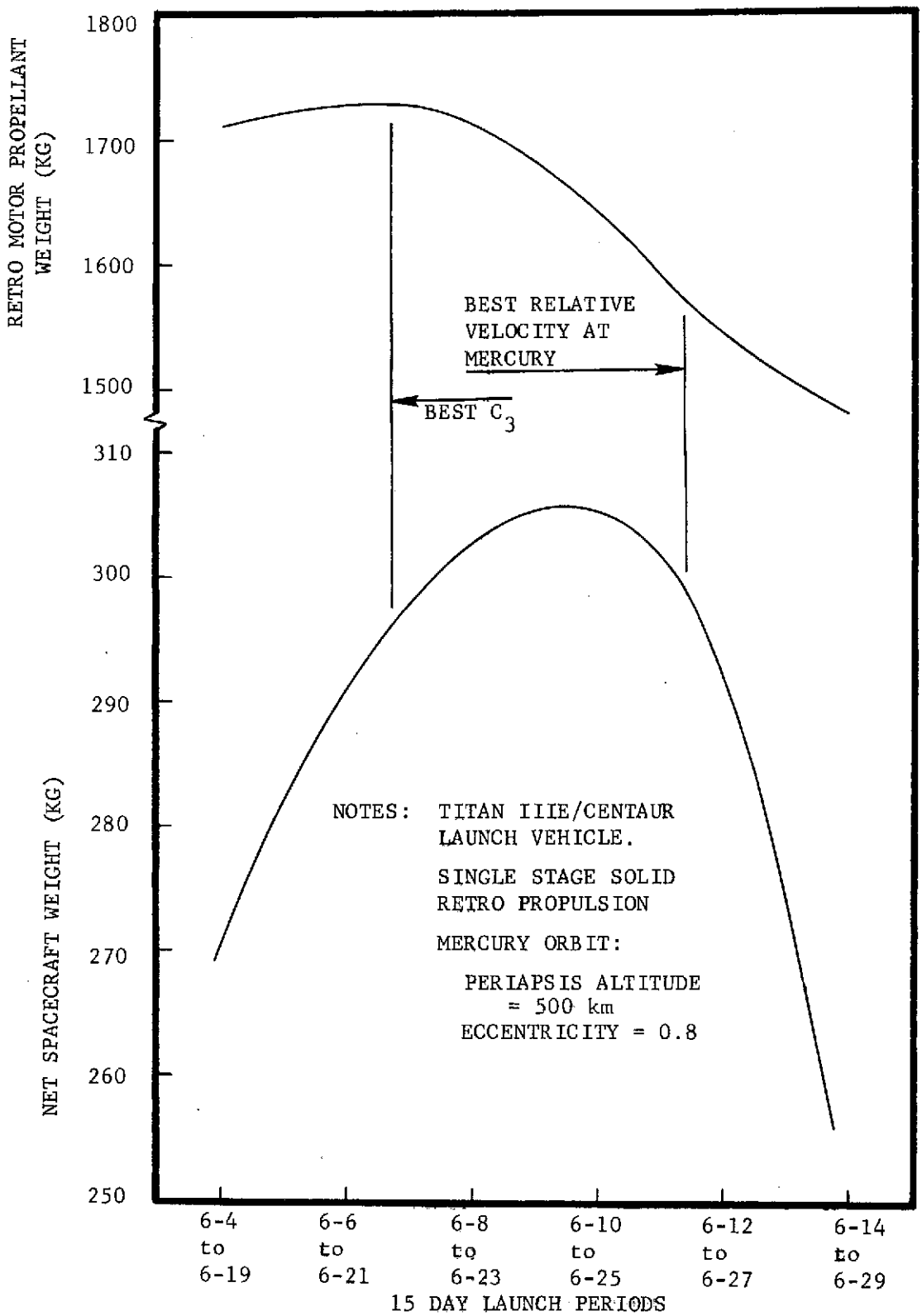

FIGURE III-3 FIFTEEN DAY LAUNCH PERIOD OPTIMIZATION, 1977 OPPORTUNITY

TABLE III-2 BASELINE PERFORMANCE CAPABILITIES

	LAUNCH YEAR			
	1977	1980[1]	1985	1988[2]
15 DAY LAUNCH PERIOD (Based on Minimum Relative velocity at Mercury	6-11.4 to 6-26.4	6-17.6 to 7-2.6	6-7.2 to 6-22.2	6-18.6 to 7-3.6
C_3 (KM^2/SEC^2) (maximum for launch period)	48.26	35.62	46.28	37.03
SPACECRAFT INITIAL WEIGHT (KG) (Titan IIIE/Centaur Minimum Performance, due east launch from ETR).	2195	2785	2285	2715
MIDCOURSE CORRECTION MANEUVERS (MPS)	226.5	265.9	242.3	281.9
MIDCOURSE CORRECTION PROPELLANT (KG) (Specific impulse - 235 sec)	206	304	228	313
SPACECRAFT WEIGHT AT MERCURY ENCOUNTER (KG) (no inert weight jettisoned)	1989	2481	2057	2402
RELATIVE VELOCITY AT MERCURY ENCOUNTER * (KM/SEC) (maximum for launch period)	7.137	6.795	8.240	6.450
ORBIT INSERTION VELOCITY INCREMENT (KM/SEC)(Mercury Orbit periapsis = 500 km, eccentricity = .8)	4.439	4.140	5.423	3.843
ORBIT INSERTION PROPELLANT (KG) (Specific Impulse = 290 sec)	1572	1903	1751	1780
SPACECRAFT WEIGHT ON MERCURY ORBIT (KG)	417	578	306	622
EXPENDED SOLID ROCKET MOTOR (KG) (Propellant Fraction = .93)	118	143	132	134
NET WEIGHT ON MERCURY ORBIT (KG) (including auxiliary propulsion residuals, spacecraft systems, science instruments, etc.	299	435	174	488

NOTES: (1) Minimum Venus Swingby Altitude = 250 km, velocity maneuver at Venus = 100 MPS (Combined with Post-Venus Midcourse Correction)

(2) Minimum Venus Swingby Altitude = 250 km, velocity maneuver at Venus = 75 MPS (Combined with Post-Venus Midcourse Correction)

* Use of non-optimum Mercury arrival dates permit maintaining approach Velocity constant throughout launch period.

B. PERFORMANCE SENSITIVITIES

In this subsection, penalties paid in terms of spacecraft weight in orbit for differences in orbit size, shape, and orientation will be presented. Orbit parameters which will be considered by variation from the reference orbit (500 km periapsis altitude, 0.8 eccentricity) are: periapsis altitude, eccentricity and period variations, apsidal rotations, inclination changes, and in-orbit trims. Reference orbit insertion maneuver requirements for different shaped orbits for each mission year will be given along with velocity increments needed to change the size and orientation of these orbits. For orbit alterations which are not performed at the time of insertion, auxiliary propulsion requirements are also considered.

In analyzing these performance sensitive orbit parameters, a relationship between the retro velocity requirements for different orbits and the resultant net weight in Mercury orbit is required. A graphical presentation of this relationship can be useful for comparing the performance effect of a given orbit insertion velocity increment upon the net spacecraft weight for a particular mission year opportunity. Two launch vehicles, Titan IIIE/Centaur and Shuttle/Centaur, are considered for this comparison in Figure III-4. The variation of net spacecraft weight with retro velocity increment is dependent upon the mission year opportunity. The placement of the four different missions on this plot shows the relative performance of these missions. In this figure, performance requirements are presented for 500 km periapsis altitude orbits extended from circular orbits out to parabolic conditions. This figure is useful for considering maneuver requirements for orbit options other than eccentricity variations. Using any of the other orbit parameter differences to follow, the penalty paid in net spacecraft weight can be calculated by following the particular mission line down the amount indicated by the velocity increment scale. For example, consider the 1980 mission with a deviation from the reference orbit to a 1500 km periapsis altitude which costs ~ 260 mps in orbit insertion velocity increment. Starting at the dot representing .8 orbit eccentricity on the 1980 Titan IIIE/Centaur line and moving 260 mps on the abscissa gives a penalty of 60 kg in net spacecraft weight. Therefore, Figure III-4 will permit evaluation of other differences from the reference orbit which can be included

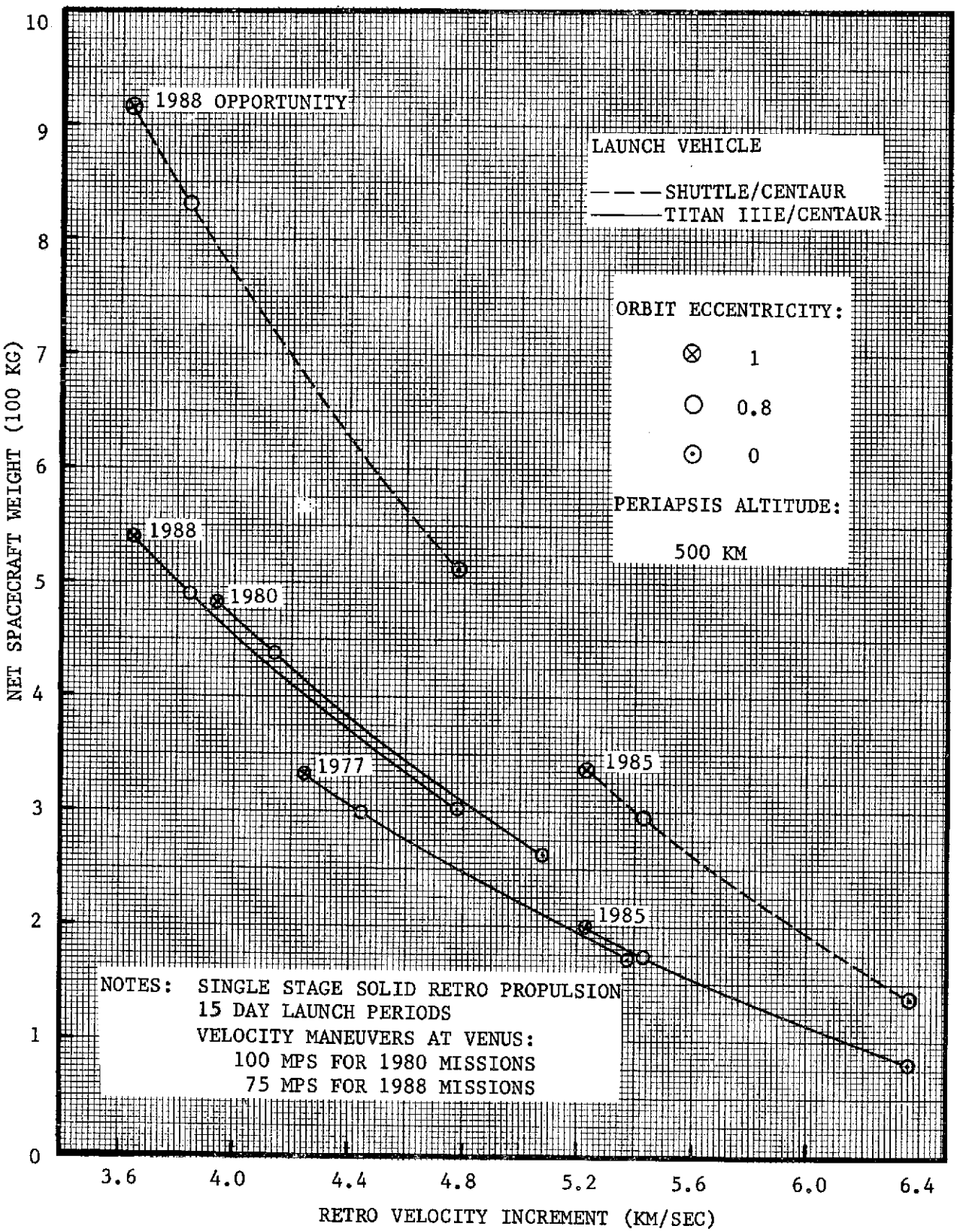

FIGURE III-4 NET SPACECRAFT WEIGHT VS. RETRO VELOCITY INCREMENT

in the retro-propulsion system. Although orbit eccentricities are shown here through 1., it will be shown in the orbit dispersion section that eccentricities larger than .8 are probably not desirable.

The next figure (III-5) considers periapsis altitude variations for any orbit eccentricity. Orbit insertion requirements are shown for altitudes ranging from 0 to 2500 km. Periapsis altitudes higher than 500 km may become especially important once a complete thermal study is accomplished. The cost paid for going from a 500 km h_p to 1000 km is less than 200 mps for all missions and decreases with successive h_p increases. Constant period lines are shown in the event that orbit period is an important consideration. While the standard .8 eccentricity, 500 km h_p orbit has a period just under 21 hours, a 24-hour period might be considered from a mission operations viewpoint. Consistent data transmission to Earth might make this a desirable orbit.

In addition to orbit size and shape variations, orientation changes considered include apsidal rotations and inclination changes. Heretofore, the insertion strategy has been a minimum ΔV strategy with impulsive insertion at periapsis. The line of apsides can be rotated for a small ΔV penalty for small rotations, if this is done at the time of insertion. Such rotations might be desired for a more equatorial periapsis latitude. Figure III-6 shows orbit insertion velocity requirements for the 1980 mission using two orbit eccentricities (.6 and .8). Although these data are for a 500-km h_p, they are representative of a considerable range of periapsis altitude as well as for the other three mission opportunities.

Inclination changes are presented for the possibility of an equatorial orbit. The minimum inclination achievable without any additional ΔV requirement is equal to the declination of the VH_M vector. For this inclination change, the worst declination cases for all four missions are shown (all of which are around -20^o). The results from two methods of achieving lower inclination orbits are shown in Figure III-7. Only one of these ΔV requirements would come out of the retro propulsion system. Another method of achieving the inclination change is to implement the maneuver near apoapsis (at the node of the equator and the spacecraft orbit). To evaluate these maneuver requirements near apoapsis requires the information relating space-

craft net weight to auxiliary propulsion requirements presented in Figure III-8. This exchange ratio is 4.2% per 100 mps for small maneuvers. Another use for the auxiliary propulsion system is in-orbit trims. Due to orbit insertion dispersions, two maneuvers may be required to trim the dispersed orbit back to the preplanned orbit; one at apoapsis to adjust h_p and another at periapsis to adjust orbit period. ΔV requirements for these maneuvers will be presented in the following subsection.

Although basic performance figures have been given for a Mercury orbit of .8 eccentricity with a 500 km periapsis altitude, penalties for other orbits have been considered in Figures III-4 through 8. These figures allow a mission planner to estimate the velocity requirements of any different orbit and determine if it is worth the decrease in spacecraft weight in orbit. The feasibility of these deviations is mission dependent; a 1980 or 1988 Mercury Orbiter mission could afford to invest more for orbit options than can the other two missions.

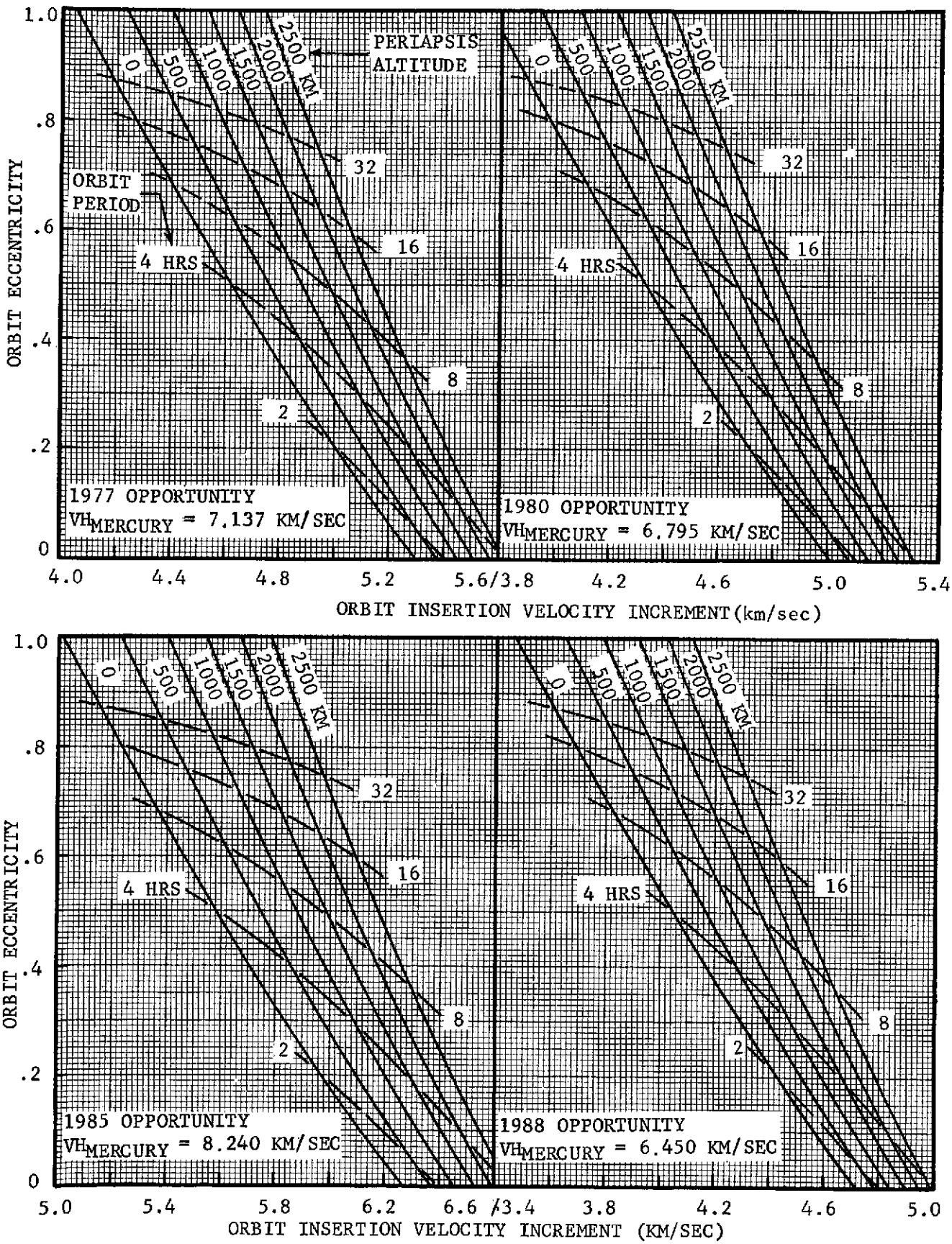

FIGURE III-5 ORBIT INSERTION VELOCITY INCREMENT VS. ORBIT ECCENTRICITY AND PERIAPSIS ALTITUDE

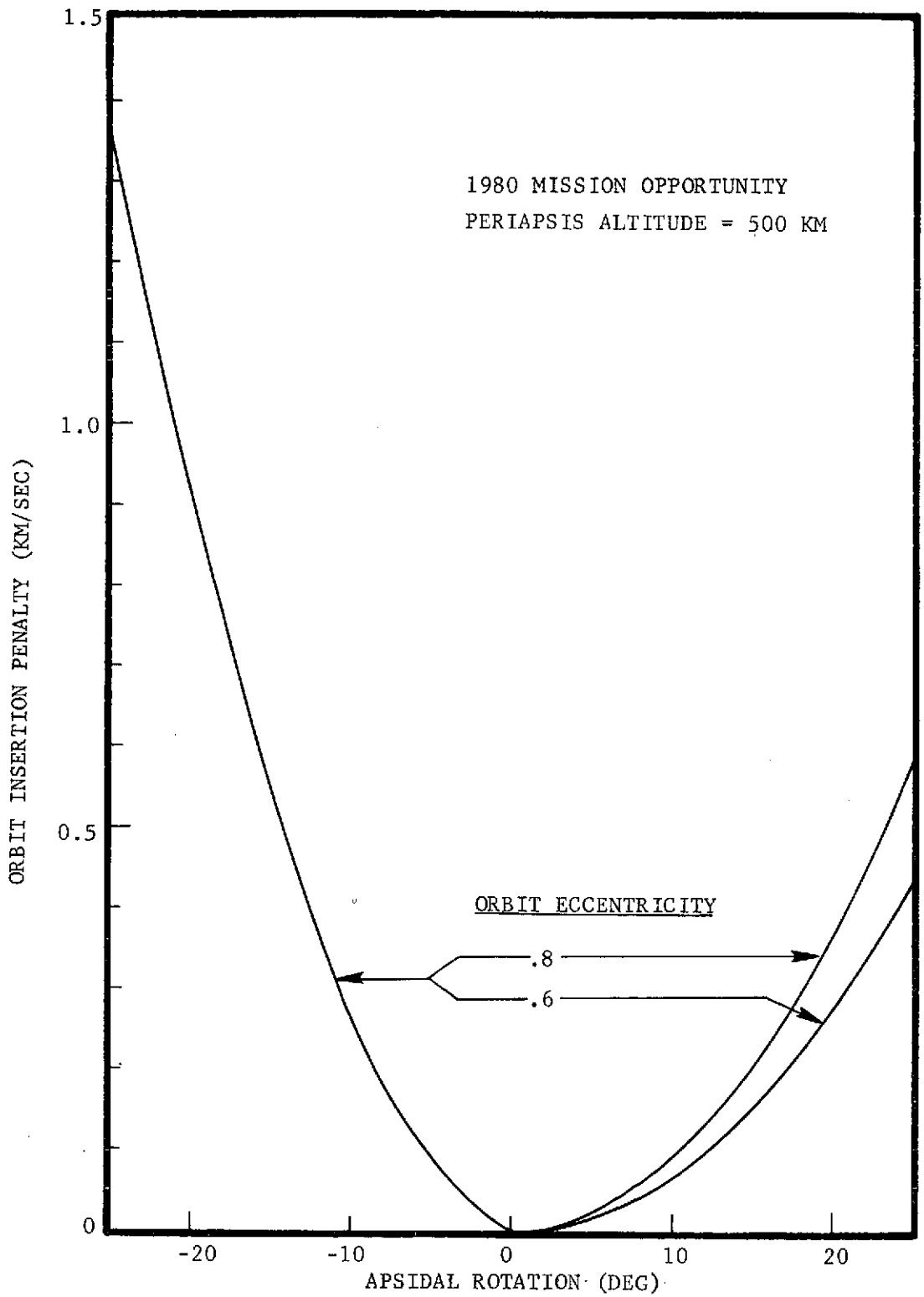

FIGURE III-6 ORBIT INSERTION VELOCITY PENALTY FOR APSIDAL ROTATION

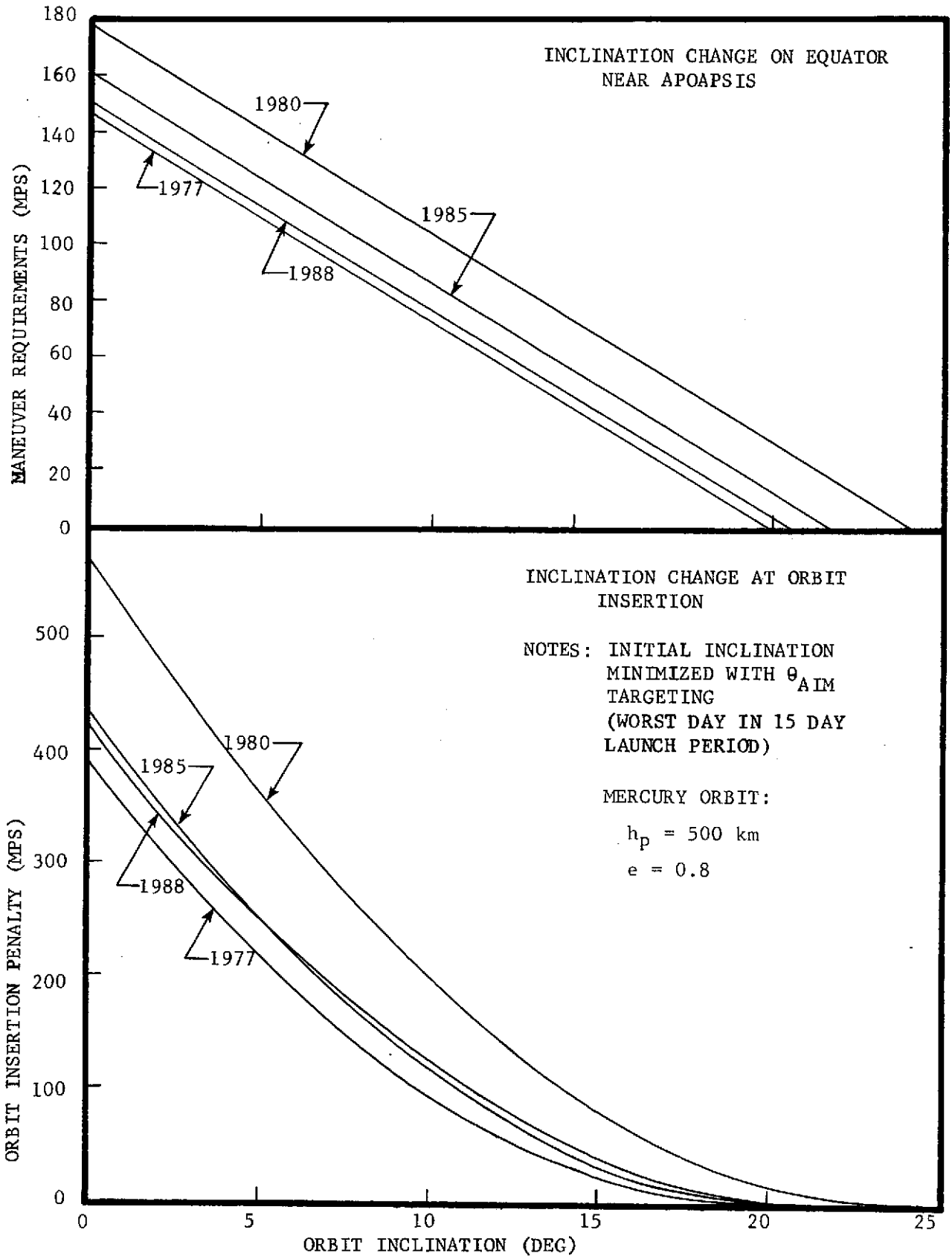

FIGURE III-7 VELOCITY REQUIREMENTS FOR LOW INCLINATION ORBITS

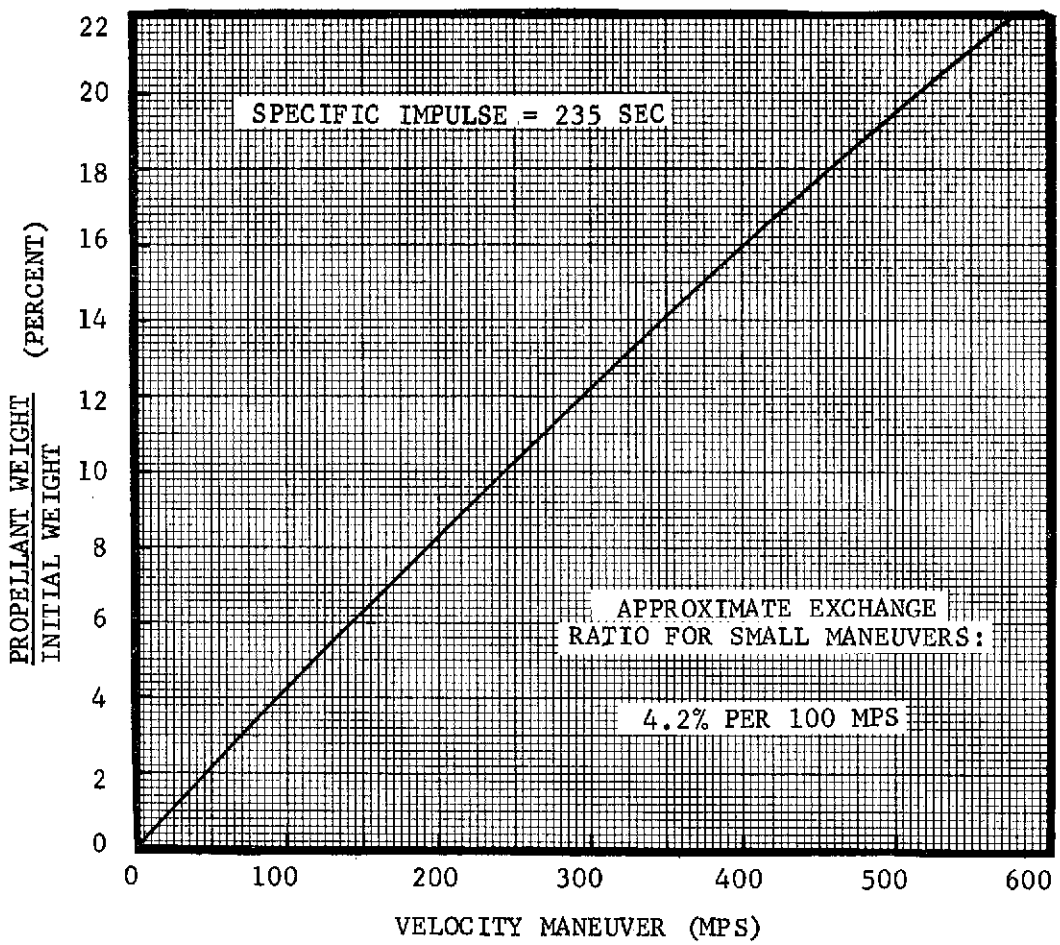

FIGURE III-8 AUXILIARY PROPULSION SYSTEM PERFORMANCE

C. ORBIT DISPERSIONS

Orbit insertion was analyzed for each of the four mission opportunities using Monte Carlo techniques. Navigation cases from the Handbook are used to represent these missions. All results presented in this section will be based on 1000 Monte Carlo samples; dispersions will be shown for key orbit parameters and initial orbit trim maneuvers. For this analysis, the standard error sources include execution errors (3σ) of 1% proportionality (an error in the magnitude of the delivered ΔV) and 1^{o} pointing (an error in the direction of the net delivered ΔV from the commanded direction). Approach uncertainties are based on a 60 km spherical ephemeris error for Mercury and certain orbit determination results which are discussed in detail in the Handbook. The orbit selected to present this data is characterized by a θ_{AIM} of 240^{o} and a periapsis altitude of 500 km. While these values are not intended to be construed as nominal values, they are reasonable from a science standpoint and desirable from a performance standpoint.

For all four opportunities, the orbit dispersions are large. These are caused primarily by large planet relative orbit determination (OD) errors due, in all except the 1980 case, to a 60 km Mercury ephemeris error. For 1980, the large navigation uncertainties are due primarily to a zero-declination geometry problem during the Mercury approach phase. (This means that the 1980 dispersions could be improved with the use of QVLBI). Although these dispersions degrade the mission, the initial orbit can be corrected for a reasonable trim allowance. Results will be explained in detail after a description of the insertion strategy and the Monte Carlo method is presented. Orbit dispersion sensitivities to eccentricity will be shown for the 1980 trajectory followed by a comparison of the four opportunities with .8 eccentricity. Finally, the sensitivities of the dispersions to nominal periapsis altitude, approach uncertainties, and execution errors will be discussed.

A minimum ΔV strategy is assumed for the orbit insertion maneuver which involves a purely retrograde maneuver executed at estimated periapsis of the approach hyperbola. The Monte Carlo technique for sampling this maneuver begins with the planet relative control and knowledge errors which are dominated by the assumed 60 km ephemeris error in all but the 1980 case. Control errors are shown as B-plane uncertainties at Mercury in Figure II-7.

For most missions, the knowledge errors are smaller than the control due to information gained from tracking the S/C after the last midcourse guidance correction. However, since Mercury is such a small planet, and since the V_H is ~7 km/sec, the S/C does not encounter the planet's sphere-of-influence until a half-day before orbit insertion. Not much additional information is gained from tracking past the last midcourse so the knowledge covariance is almost as large as the control covariance. The sequence for considering these errors follows. The control covariance is sampled and the control errors are added to the nominal approach hyperbola state at periapsis. This gives the actual state. Knowledge errors, which come from sampling the knowledge covariances, are added to this to obtain an estimated state. Maneuver direction and timing are dictated by the estimated hyperbola while the size of the ΔV is determined by the nominal hyperbola. With execution errors added to the estimated ΔV, it becomes the actual ΔV. Then finally, the actual ΔV is added to the actual hyperbolic state to obtain the actual elliptical orbit. Statistics are collected for the sample orbits and key orbit parameters: radius of periapsis, velocity at periapsis, eccentricity, and period, along with two maneuvers for initial orbit trim. These will be shown for cumulative probability levels of .997 and .003 since these parameters have non-gaussian distributions.

The Monte Carlo technique is used to obtain initial sample orbits about the design orbit. An orbit lifetime analysis can then be used to investigate the stability of these highly elliptical Mercury orbits under the influence of solar perturbations. These results were subsequently verified with integrated trajectory methods. Using the 1980 mission, any initial orbit with an eccentricity less than or equal to .925 will be captured into orbit about Mercury.

A parametric approach to orbit eccentricity selection based on orbit dispersions will be presented using the 1980 mission opportunity. Referring again to Figure II-7 reveals that the 1980 mission has the worst approach uncertainties and that a θ_{AIM} of 240° results in nearly the worst possible errors for that year. Periapsis velocity dispersions for nominal orbit eccentricies of .6, .7, .8, and .9 are shown in the lower portion of Figure III-9. These results show that periapsis velocity has approximately the same uncertainty for any eccentricity chosen ($\pm$ 100 m/s for .997 probability). However, out of the 1000 samples, about a nominal eccentricity of .8, the worst sample has e=.906.

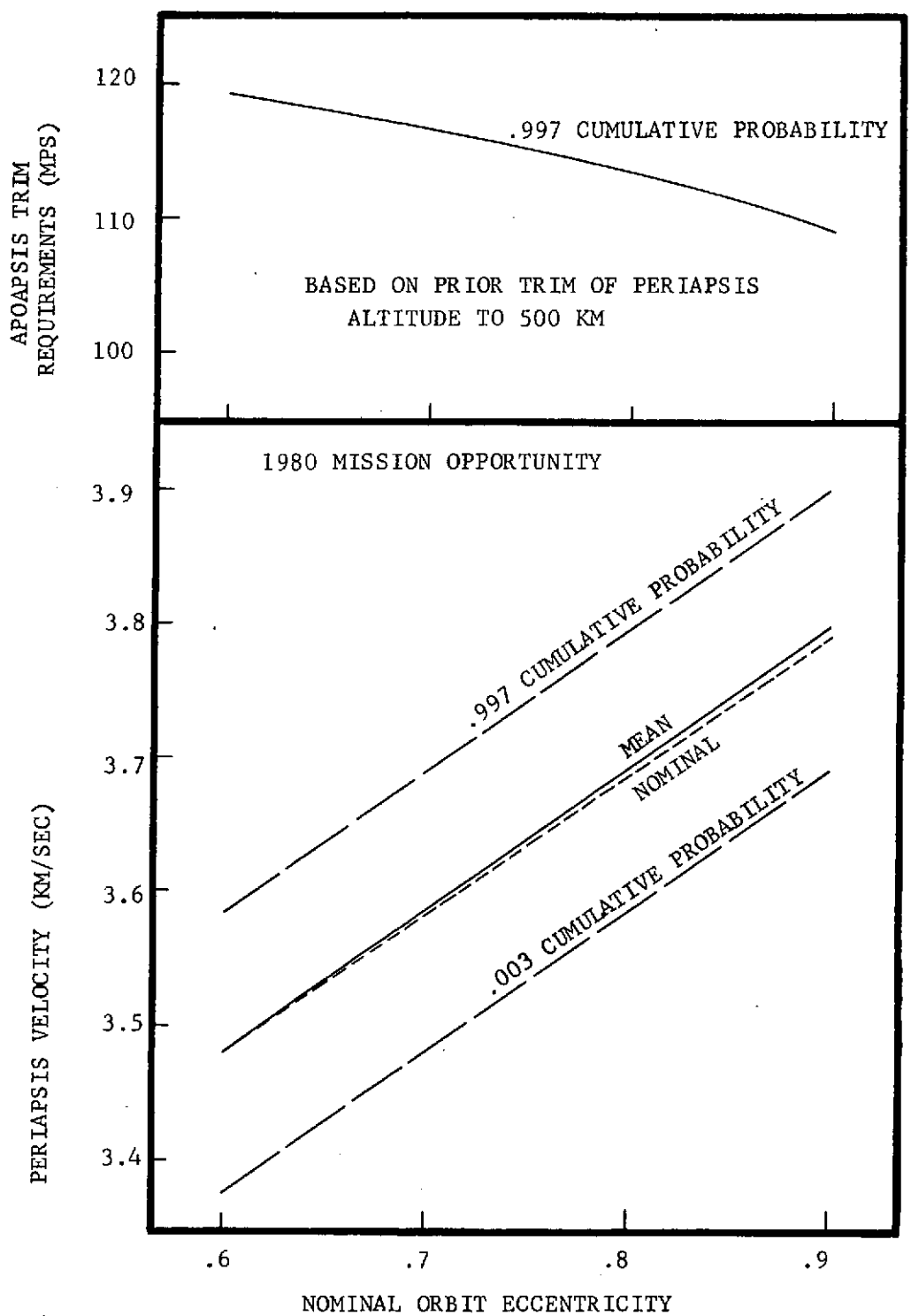

FIGURE III-9 PERIAPSIS VELOCITY DISPERSIONS VS. NOMINAL ORBIT ECCENTRICITY

In view of this, a design value of .8 is a reasonable upper limit. However, any value up through .8 could be selected with assurance that a mission were possible. In Figure III-10, the effect of the orbit insertion dispersions are shown upon the size of the orbit. Period dispersions shown as a function of nominal eccentricity emphasize the large dispersions.

Although these dispersed orbits do not escape for $e \leq .925$, it is assumed that the mission planner would like to trim back to the preplanned orbit. Still, a mission could exist without trimming in the event of failure of the trim propulsion system, which may not be guaranteed in the Mercury environment, and significant data would be returned. However, the large dispersions are trimmable for a reasonable budget of about 5% of the useful weight in orbit. (See Figure III-8). The trim strategy used involves trimming periapsis first, because a low periapsis altitude may have bad thermal implications. This will be denoted as ΔV_{TRIM_1} in the tabular data to follow. But there may be no incentive to lower the altitude at periapsis since it is not believed scientifically necessary to have a low h_p. After adjusting h_p, if desired, the larger trim maneuver (ΔV_{TRIM_2}) is executed at periapsis to adjust the period back to the preplanned value. The .997 probability for this larger ΔV penalty is shown versus eccentricity in the upper portion of Figure III-9.

Monte Carlo results for all four mission opportunities appear in Table III-3. Since 1980 has the worst approach errors, which is the dominating error source, the eccentricity used for that mission can also be used for the other years. Results from this table verify that 1980 has by far the worst dispersions. The .997 probability for the orbit period varies from 56.4 hours in 1980 to 37.2 hours in 1988; consequently, trim requirements range from 112 m/s down to 70 m/s (.997 probability). Dispersed periapsis radii are as low as 2662 km in 1980, which could have a significant thermal impact upon orbits whose initial periapsis is on the sunlit side of Mercury. Choosing a nominal h_p larger than 500 km might be necessary for those orbits.

Another interesting comparison is the dispersions for different periapsis altitude orbits with fixed period. The reference orbit for the 1980 trajectory with .8 eccentricity and θ_{AIM} of 240^o was analyzed for 500, 1000, and 1500 km periapsis altitudes. Instead of holding this eccentricity fixed and

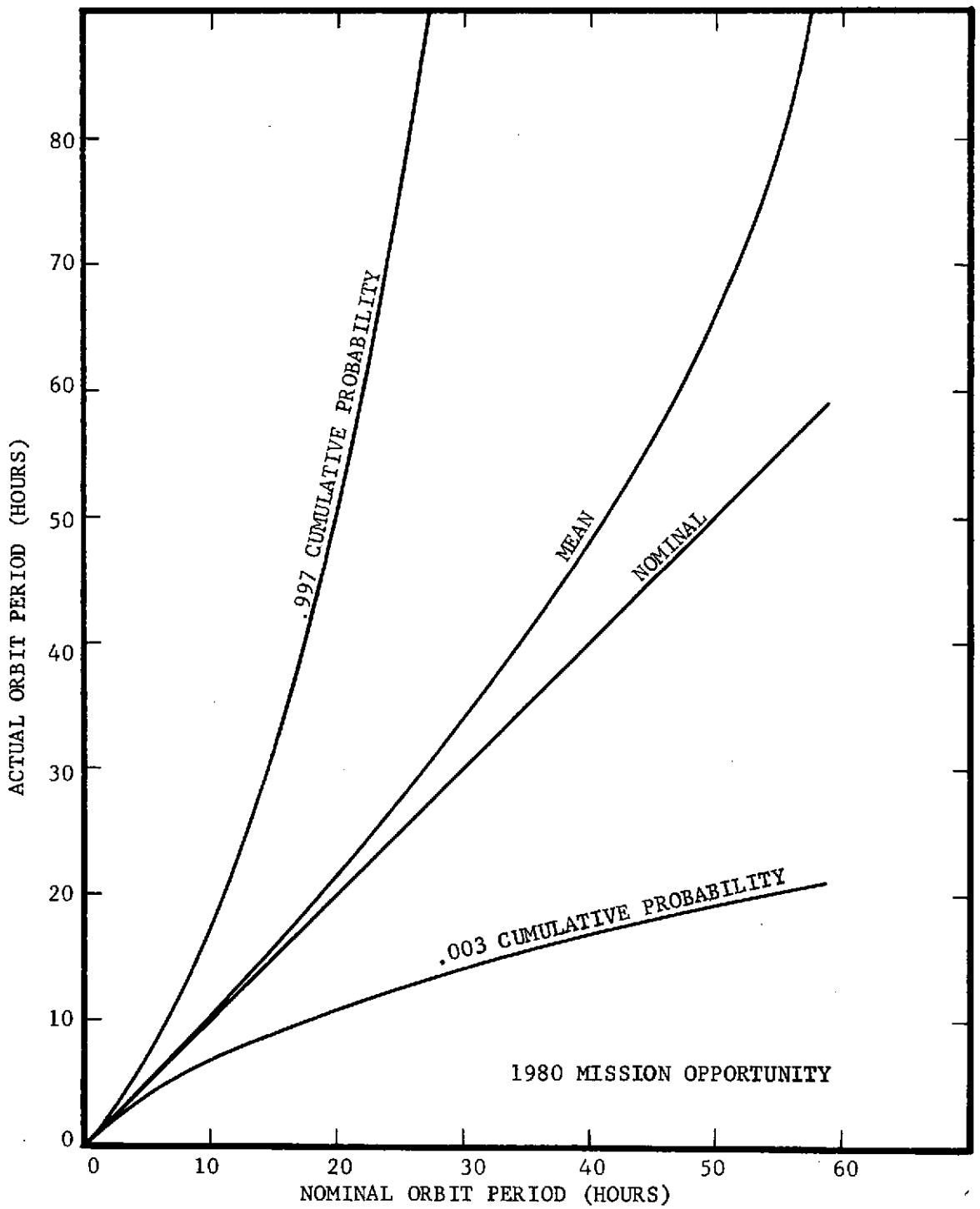

FIGURE III-10 ORBIT PERIOD EFFECTS OF UNTRIMMED INSERTION DISPERSIONS

TABLE III-3 ORBIT DISPERSION RESULTS

	1977				1980			
	Cumulative Probability				Cumulative Probability			
	.003	.997	Mean	Sigma	.003	.997	Mean	Sigma
R_p (km)	2750.	3144.	2935.	71.56	2662.	3220.	2935.	99.15
PERIOD (hrs)	12.63	43.06	21.85	5.32	11.20	56.41	22.33	7.05
V_p (km/sec)	3.613	3.768	3.690	.0274	3.589	3.796	3.691	.0364
ECCENTRICITY	.738	.868	.801	.0254	.725	.888	.801	.0310
ΔV $TRIM_1$ (m/s)	.0460	13.30	3.57	2.73	.0279	18.95	4.95	3.74
ΔV $TRIM_2$ (m/s)	.283	88.90	23.88	17.99	.122	112.9	29.77	22.05
	TOTAL TRIM ΔV 122.2				TOTAL TRIM ΔV 131.9			

	1985				1988			
R_p (km)	2748.	3122.	2935.	66.91	2767.	3103.	2934.	64.07
PERIOD (hrs)	12.05	46.91	22.00	5.85	13.57	37.20	21.48	4.23
V_p (km/sec)	3.616	3.768	3.690	.0263	3.622	3.757	3.690	.0258
ECCENTRICITY	.729	.879	.801	.0279	.749	.858	.801	.0210
ΔV $TRIM_1$ (m/s)	.0216	12.16	3.36	2.53	.0233	11.95	3.22	2.43
ΔV $TRIM_2$ (m/s)	.156	93.87	25.59	19.22	.208	70.57	19.93	14.93
	TOTAL TRIM ΔV 106.0				TOTAL TRIM ΔV 82.5			

enlarging the period, three orbits of the same relative size with a slightly different shape were compared. Although performance and science preferences include the low altitude, results from a complete thermal feasibility study might dictate a higher one. If this were the reason for a higher periapsis, it would be necessary to insert with a higher initial h_p for some θ_{AIMS}. Performance penalties at insertion are addressed in Figure III-5. Although raising periapsis after the S/C is already in orbit is more advantageous for performance (Figure IV-16), this technique would not help an initial thermal problem. Dispersion results are shown for these three orbits in Table III-4. Period uncertainties decrease from 7 hours to 5 to 4 hours for the altitude increases of 500 km steps. Therefore, approximately, one tenth of the increased orbit insertion maneuvers can be saved in the trim maneuvers for the additional altitude of a safer orbit.

The largest contributor to the dispersions is the 60 -100 km uncertainty (all missions) in the height of periapsis resulting from orbit determination errors. Timing uncertainty, also due to these errors, results in executing the right maneuver at the wrong time. Execution errors are the least significant contributors to this problem. Table III-5 shows the sensitivity to execution errors and navigation improvements. Three levels are shown for execution errors, including zero and twice the assumed level used previously. Also, results from 20 km spherical OD uncertainties including ephemeris errors are presented. In order to significantly improve initial orbit dispersions, it is necessary to greatly reduce the planet relative OD errors. Optical navigation which works directly on the S/C error relative to the planet would be a possible answer. This does not necessarily mean that these errors could be reduced to 20 km spherical; but is rather presented as a reasonable lower bound to these errors. The best method of optical navigation, however, requires that the target body have a natural satellite which Mercury does not. If both the S/C error and planet error were reduced independently, they would have to each be decreased below 20 km. This would require both more accurate tracking data types (such as QVLBI) and a significant decrease in Mercury ephemeris errors.

In conclusion, for all four missions, orbit insertion dispersions are large due primarily to planet relative OD errors. This limits the inital orbit to probably no higher than .8 eccentricity. Since a reasonable trim budget

allows the return of the dispersed orbit to the preplanned one, it would probably be desirable to remove any large period dispersions. However, there could be significant data return for the mission if the trim propulsion system failed. Navigational improvements would be needed to decrease these dispersions, but anticipated improvements for the 1980 time frame are not expected to eliminate the need for initial orbit trims.

TABLE III-4 ORBIT DISPERSIONS FOR VARIATIONS IN PERIAPSIS ALTITUDE - 1980 MISSION

	500 km H_p				1000 km H_p			
	Cumulative Probability				Cumulative Probability			
	.003	.997	Mean	Sigma	.003	.997	Mean	Sigma
R_p (km)	2662.	3220.	2935.	99.15	3160.	3720.	3435.	99.41
PERIOD (hrs)	11.20	56.41	22.33	7.05	12.77	43.46	21.76	5.20
V_p (km/sec)	3.589	3.796	3.691	.0364	3.298	3.458	3.379	.0288
ECCENTRICITY	.725	.888	.801	.031	.693	.845	.767	.0284
ΔV $TRIM_1$ (m/s)	.0279	18.95	4.98	3.74	.0177	17.39	4.57	3.44
ΔV $TRIM_2$ (m/s)	.1220	112.9	29.77	22.05	.158	97.46	25.89	19.23
	TOTAL TRIM ΔV	131.9			TOTAL TRIM ΔV	114.9		

	1500 km H_p			
R_p (km)	3658.	4220.	3935.	99.60
PERIOD (hrs)	13.63	37.10	21.47	4.15
V_p (km/sec)	3.057	3.195	3.126	.0242
ECCENTRICITY	.661	.809	.733	.0269
ΔV $TRIM_1$ (m/s)	.0160	16.10	4.24	3.19
ΔV $TRIM_2$ (m/s)	.0988	85.57	23.09	17.22
	TOTAL TRIM ΔV	101.7		

TABLE III-5 ORBIT DISPERSION SENSITIVITIES - 1980 MISSION

	NO EXECUTION ERRORS				1°, 1% EXECUTION ERRORS			
	Cumulative Probability				Cumulative Probability			
	.003	.997	Mean	Sigma	.003	.997	Mean	Sigma
R_p (km)	2663.	3221.	2935.	99.15	2662.	3220.	2935.	99.15
PERIOD (hrs)	11.28	52.52	22.06	6.34	11.20	56.41	22.33	7.05
V_p (km/sec)	3.600	3.793	3.690	.0339	3.589	3.796	3.691	.0364
ECCENTRICITY	.727	.882	.801	.0279	.725	.888	.801	.031
ΔV $TRIM_1$ (m/s)	.0348	19.0	4.98	3.74	.0279	18.95	4.98	3.74
ΔV $TRIM_2$ (m/s)	.0757	104.6	27.94	20.91	.1220	112.9	29.77	22.05
TOTAL TRIM ΔV	123.6				131.9			
	2°, 2% EXECUTION ERRORS				20 km APPROACH UNCERTAINTIES			
R_p (km)	2661.	3219.	29.35	99.15	2879.	2990.	2935.	20.31
PERIOD (hrs)	10.18	75.93	23.17	9.58	16.29	30.08	21.11	2.35
V_p (km/sec)	3.572	3.816	3.691	.0430	3.651	3.737	3.689	.0148
ECCENTRICITY	.707	.910	.802	.0375	.767	.844	.801	.0138
ΔV $TRIM_1$ (m/s)	.0209	18.95	4.98	3.74	.0051	3.735	1.019	.769
ΔV $TRIM_2$ (m/s)	.0169	128.0	34.56	25.86	.1065	44.22	11.79	8.71
TOTAL TRIM ΔV	147.0				48.0			

IV. ORBIT SELECTION CONSIDERATIONS

THIS

PAGE

BLANK

IV. ORBIT SELECTION CONSIDERATIONS

The spectrum of accessible orbits has been analyzed parametrically for determination of basic characteristics relevant to orbit operations and spacecraft design. Specifically, behavior of orbit periapsis altitude under the influence of solar perturbations is presented. Corresponding relationships with the thermal environment and occurrences of Earth and solar occultations are also included. The foregoing considerations are basic to the orbit selection process when correlated with science objectives and spacecraft design factors. The 1980 mission opportunity is employed to illustrate characteristics requiring extensive analysis.

Also presented in this section are postulated science objectives and dependence of science instrument performance on orbit size and orientation parameters. Specific instrument complements and corresponding best orbit geometries cannot be defined in advance of the MVM mission and improved understanding of the priorities appropriate for such matters as atmospheric properties, interactions with the solar wind, etc. Accordingly, science considerations affecting orbit selection are addressed parametrically.

A. ORBIT ORIENTATION

Although it is not the intent of this study to select a best orbit for a Mercury orbiter mission, orbit selection data will be presented and some interpretation of the impact on system design will be included. Polar or near-polar orbits offer advantages of better overall planet coverage for any orbiter mission. Near-polar orbits which approach Mercury over the top (ecliptic north) and result in periapsis locations in Mercury's northern hemisphere offer many advantages for these opportunities. After defining the aiming plane (B-plane) and showing the locations of Mercury approach velocities and related periapses, data which should impact orbit selection will be discussed. Periapsis altitude time histories, worst case IR flux conditions, solar occultation time histories, and Earth occultations time histories will be described as a function of orbit orientation.

A spacecraft approaching Mercury with a given relative velocity (VH) may be aimed to any point on a circular locus with respect to the planet. The standard technique for precise definition of the aiming conditions requires defining the

B-plane and its elements. Figure IV-1 presents a perspective of the B-plane (defined at the sphere of influence) related to the target planet geometry. By definition, the B-plane is normal to the approach relative velocity vector. Rectangular coordinates in this plane consist of the T-axis (parallel to the ecliptic, positive to the right of the VH vector) and the R-axis (normal to the VH and T vectors, positive to celestial south). A consistent set of polar coordinates employs the targeted offset from the planet center and the angular targeting parameter θ_{AIM} to define the B vector illustrated on Figure IV-1. Much of the following parametric data will be presented in terms of the independent variable θ_{AIM}. As shown by Figure IV-1, this parameter represents the primary control for initial orbit orientation with respect to the planet equator, the illuminated surface, the sun and (by implication) the Earth.

Because all of the baseline opportunities reflect the same idealized geometry for the Earth-Venus-Mercury trajectories, the Mercury approach conditions are quite similar. The VH locations throughout 15-day launch periods for all four opportunities are bounded by a 11^{o} by 33^{o} rectangle (Figure IV-2). The S/C-Mercury-Sun geometry at encounter is repetitive to first order, while the position of Earth at encounter changes due to variations in the number of solar revolutions from Earth to Mercury. Major orbit selection parametrics and sensitivities are sufficiently constant to justify a detailed study of the 1980 opportunity orbit selection process and assume that the same results apply to the other opportunities.

All of these approach velocity locations are near the morning terminator with small southern declinations. The locus of periapsis for approach hyperbolas with constant periapsis altitude is a circle parallel to the B-plane. Because the approach velocities are high and Mercury is small, there is less turn in the hyperbolas than for approaches to other planets. The penalties for locating periapsis of the inserted ellipse more than a few degrees from periapsis of the approach hyperbola are quite severe, as discussed in Section III. Hence, the set of orbits available to the mission planner without extra ΔV penalties includes:

1) Near-equatorial orbits with initial periapsis near the antisolar point ($\theta_{AIM} \sim 0^{o}$),

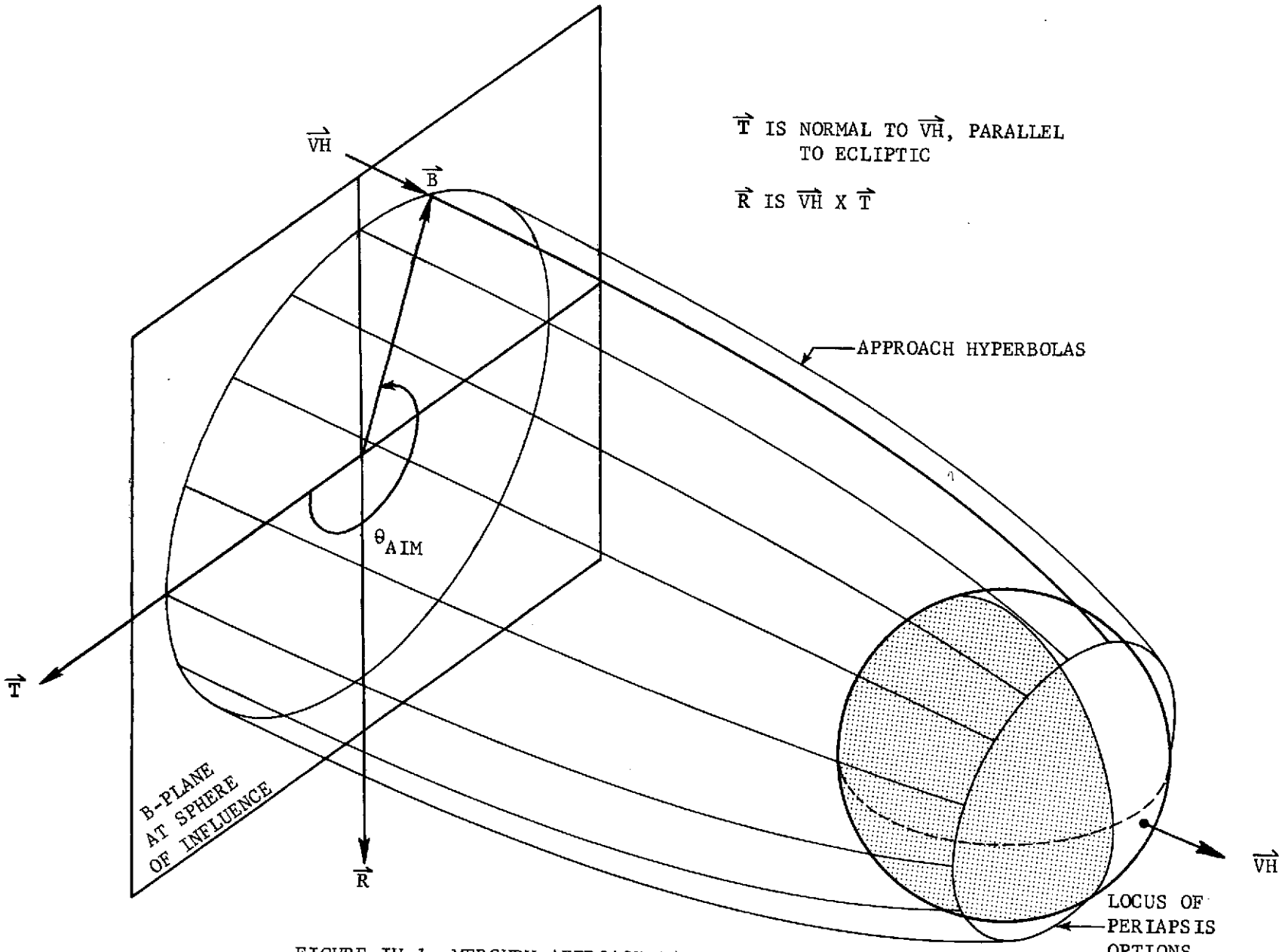

FIGURE IV-1 MERCURY APPROACH TARGETING OPTIONS

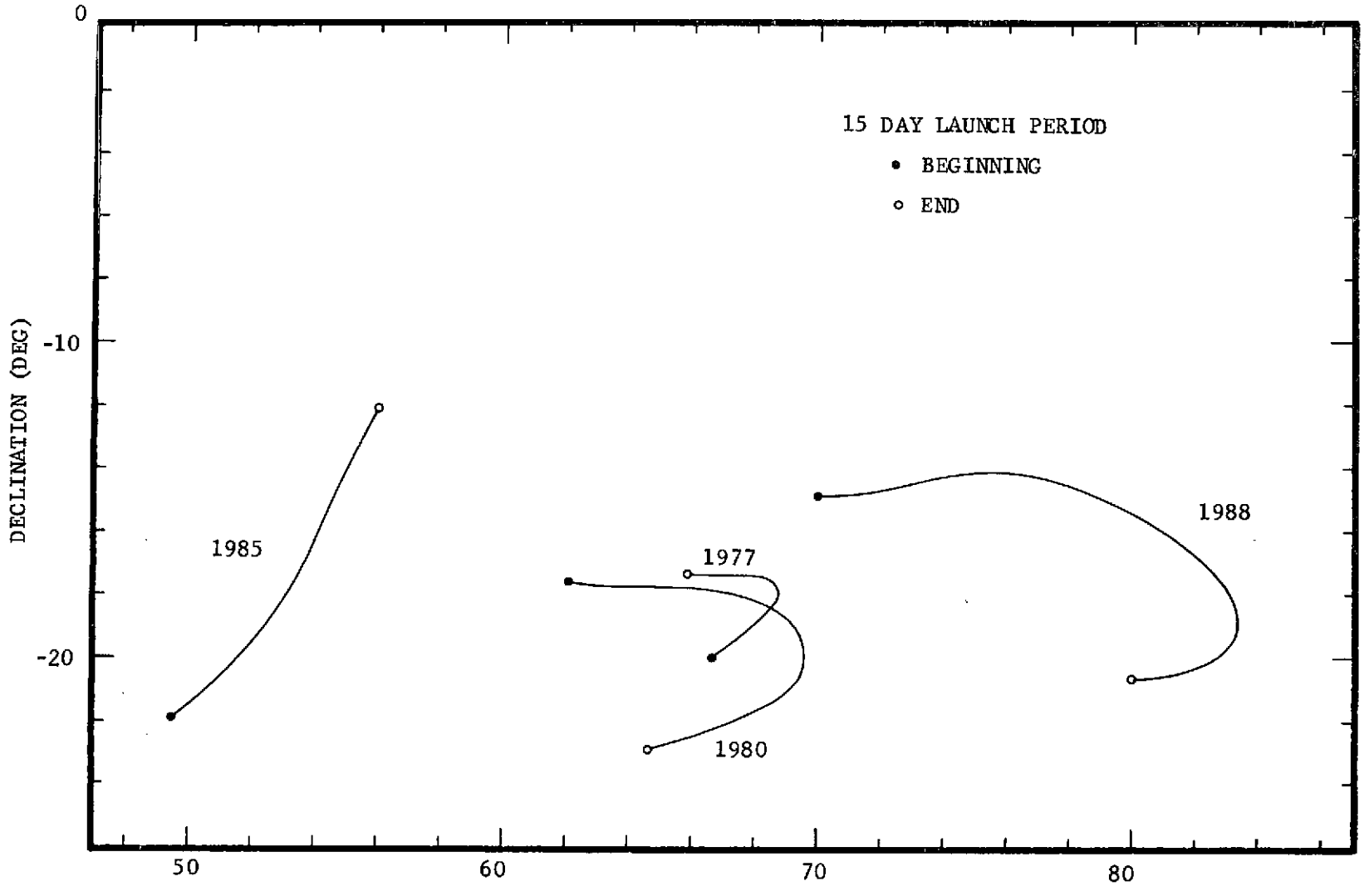

FIGURE IV-2 LOCATIONS OF MERCURY APPROACH RELATIVE VELOCITY VECTORS

2) near-polar orbits with periapsis in the south-pole region ($\theta_{AIM} \sim 90^{o}$),

3) near-equatorial, retrograde orbits with initial periapsis near the subsolar point ($\theta_{AIM} \sim 180^{o}$),

4) near-polar orbits with initial periapsis near the morning terminator and 50^{o} to 70^{o} north ($\theta_{AIM} \sim 270^{o}$).

Obviously, the continuum of aiming conditions contains intermediate inclinations in each quadrant. The variation, as a function of θ_{AIM}, of inclination, latitude of periapsis, longitude of periapsis relative to the prime meridian and relative to the sub-solar point are shown in Figures IV-3 through IV-6 for all four opportunities. These data are based on mid-launch-period Earth launch dates for each opportunity and assume minimum ΔV impulsive insertion strategy.

The remainder of this section will discuss 1980 opportunity orbit selection considerations and the applicability of any conclusions to the other opportunities.

Because Mercury is nearest the Sun and has the smallest mass of any planet, Mercury orbiters experience the largest solar gravitational perturbations of any planetary orbiter. This study has focused on eccentric orbits. Since solar gravitational perturbations are proportional to eccentricity and perturbations caused by anomalies in Mercury's gravitational field are inversely proportional to eccentricity, the highly eccentric orbits are totally dominated by the solar perturbations.

Periapsis altitude variations of as much as 25 km per orbit are possible at Mercury. Figures IV-7 and IV-8 show periapsis altitude time histories as a function of θ_{AIM} from 0^{o} to 330^{o} by 30^{o} steps. (The reader is cautioned to note the inconsistency of ordinate scales on these computer generated plots). Periapsis altitude and latitude at subsolar longitude are critical because a significant thermal environment problem is created by IR radiation from Mercury. It may be seen from the figures that near-equatorial orbits ($\theta_{AIM} = 0^{o}$ and 180^{o}) have large short-term variations but no long-term trends. The time history for θ_{AIM} of 0^{o} has the disadvantage of low altitudes at the subsolar longitude (bad for thermal considerations) and high altitudes at the termi-

nator longitudes (bad for imaging). The opposite situation implies an advantage for θ_{AIM} of 180°. For that initial orbit, periapsis is higher at subsolar longitudes and lower at terminator longitudes. However, the disadvantage for a θ_{AIM} of 180° is that periapsis begins near the subsolar point and orbit insertion dispersions could result in immediate thermal problems.

Approaching Mercury to the south (θ_{AIM} = 60°, 90°, 120°) provides initial orbit conditions that result in decreasing periapsis altitudes. This would mean an early end to the mission unless trim maneuvers were executed to maintain periapsis altitude. Trajectories which approach Mercury to the north (θ_{AIM} = 240°, 270°, 300°) demonstrate the opposite trend of gradually increasing periapsis altitude. A mission planner choosing a θ_{AIM} between 240° and 300° could combine the performance benefits of orbit insertion at 500 km with the thermal conditions corresponsing to 800 km periapsis altitude at the time periapsis crosses the sub-solar meridian. Whatever the initial periapsis altitude, θ_{AIM}s around 270° will provide higher altitudes at a time when higher altitudes are advantageous and lower altitudes at a time when lower altitudes are advantageous.

A Mercury Orbiter S/C will experience IR radiation of an unusual magnitude from both the Sun and Mercury. IR flux from the sun ranges from 2 to 6 million ergs/cm^2-sec depending on Sun-Mercury distance. IR flux from Mercury may reach 10 million ergs/cm^2-sec for short periods of time depending on orbit geometry. For each θ_{AIM} (multiples of 30 deg.), the orbit which experienced maximum IR flux from Mercury during the 176 days after encounter was identified. IR flux as a function of true anomaly is presented in Figures IV-9 and IV-10 for each worst case orbit. Maximum IR flux for any 176-day mission occurs at periapsis of the orbit which has periapsis nearest the subsolar point. Worst case heating would be minimized by using θ_{AIM}s around 90° if trim maneuvers can be guaranteed to maintain periapsis altitude. This occurs because of polar periapsis locations. A safer approach would be to choose a θ_{AIM} around 270° which yields northern periapsis locations and increasing altitude. Any near-equatorial orbit (θ_{AIM} around 0° or 180°) will eventually have periapsis right over the subsolar point thereby amplifying the thermal problems.

Solar occultation time histories for a variety of θ_{AIM}s and the same standard initial orbits (h_p = 500 km, e = .8) are presented in Figures IV-11 and

IV-12. As would be expected, solar occultations are maximized in frequency and duration for near equatorial orbits. Polar orbits experience occultation only when they are edge-on to the sun. Near-equatorial orbits experience short (.4 hrs.) and long (3 hrs.) occultations depending on whether periapsis or apoapsis is occulted. Although many spacecraft subsystems (power, attitude control, etc.) would benefit from no solar occultations, science activities would probably benefit from some solar occultations. The impact of solar occultation on orbit selection cannot be fully understood until MVM results have been analyzed and detailed spacecraft design efforts are undertaken.

Plots of earth occultation time histories for a variety of θ_{AIM}s appear in Figures IV-13 and IV-14. Once again, near-equatorial orbits experience frequent and often lengthy occultations. Near-polar orbits experience occultations only when the orbit is nearly edge-on to Earth. This occurs during the middle of the 176-day time span for the 1980 opportunity. For the other opportunities, the Earth occultations are very similar in magnitude but occur at different times during the 176-day mission because Earth varies in position at Mercury encounter. The data handling problem for a Mercury orbiter is adversely affected by Earth occultations. Potential science value of radio occultation experiments that may influence orbit selection is contingent on MVM findings.

There are several reasons for changing the altitude of periapsis after a successful orbit insertion. For example, an orbit intially established with 500 km periapsis altitude and 0.8 eccentricity may exhibit undesirable behavior of periapsis altitude, excessive thermal flux, etc. Figure IV-15 defines the maneuver requirements for post-insertion modification of periapsis. As shown by the figure, increasing periapsis altitude from 500 km to 1000 km involves a posigrade velocity maneuver at apoapsis of about 30 mps. This technique could be employed to retain some θ_{AIM} targeting options while utilizing the performance benefits of initial orbit insertion at low altitude. Alternatively, some orbit orientations may be benefited by post-insertion lowering of periapsis. Figure IV-15 includes the retrograde maneuver requirements for such orbit modifications.

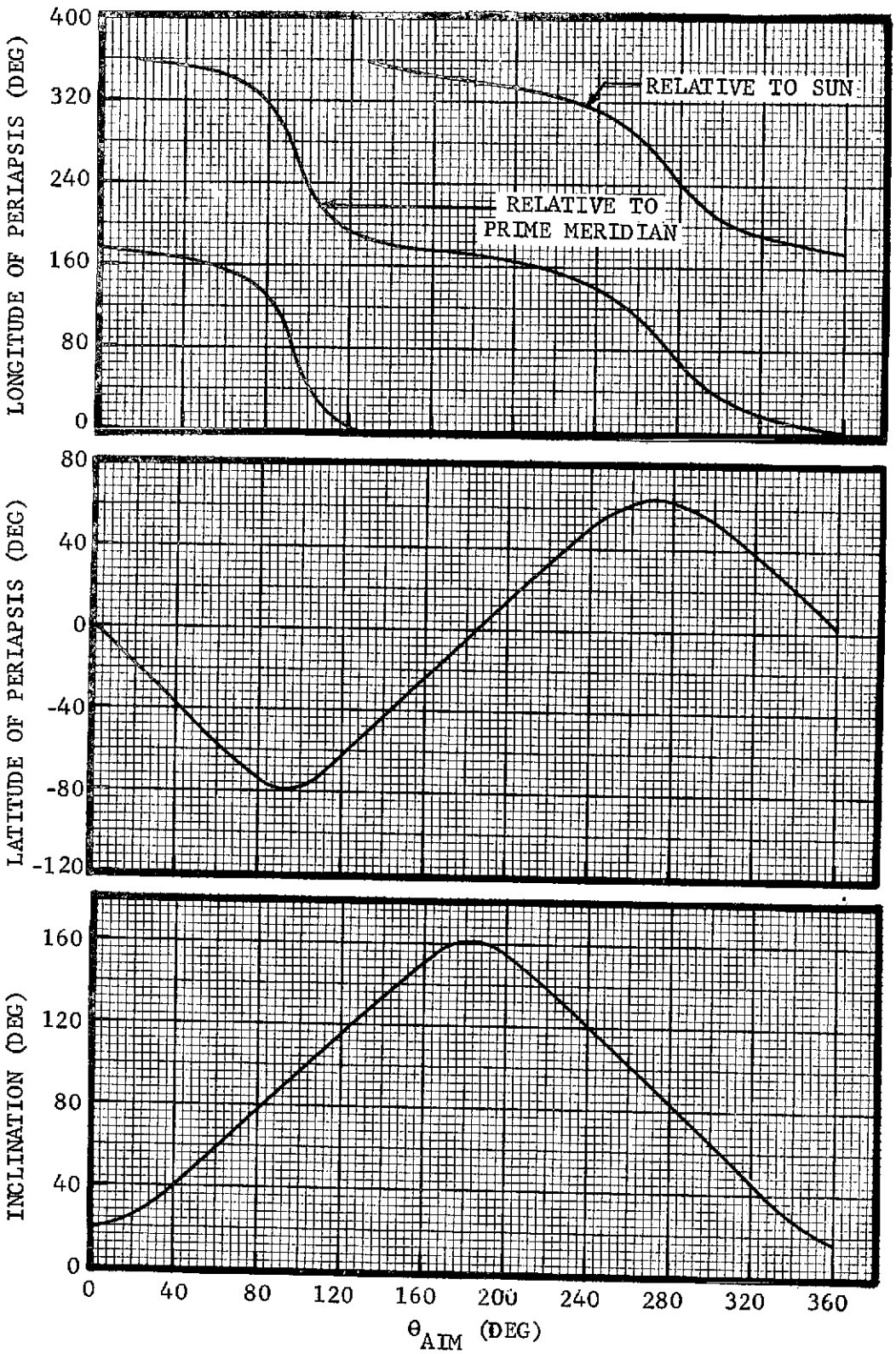

FIGURE IV-3 INITIAL ORBIT ORIENTATION DEPENDENCE ON B-PLANE TARGETING, 1977 MISSION OPPORTUNITY

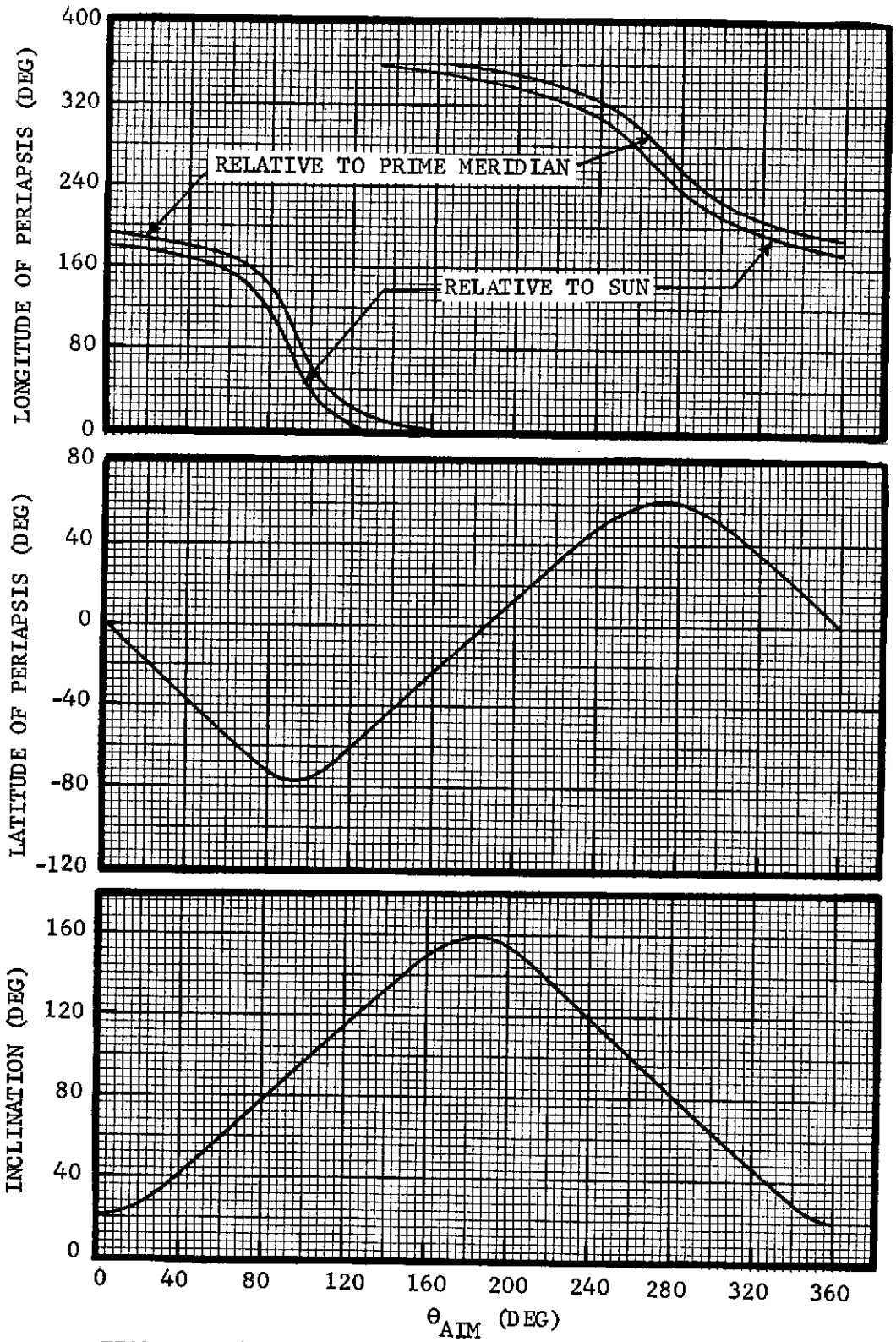

FIGURE IV-4 INITIAL ORBIT ORIENTATION DEPENDENCE ON B-PLANE TARGETING, 1980 MISSION OPPORTUNITY

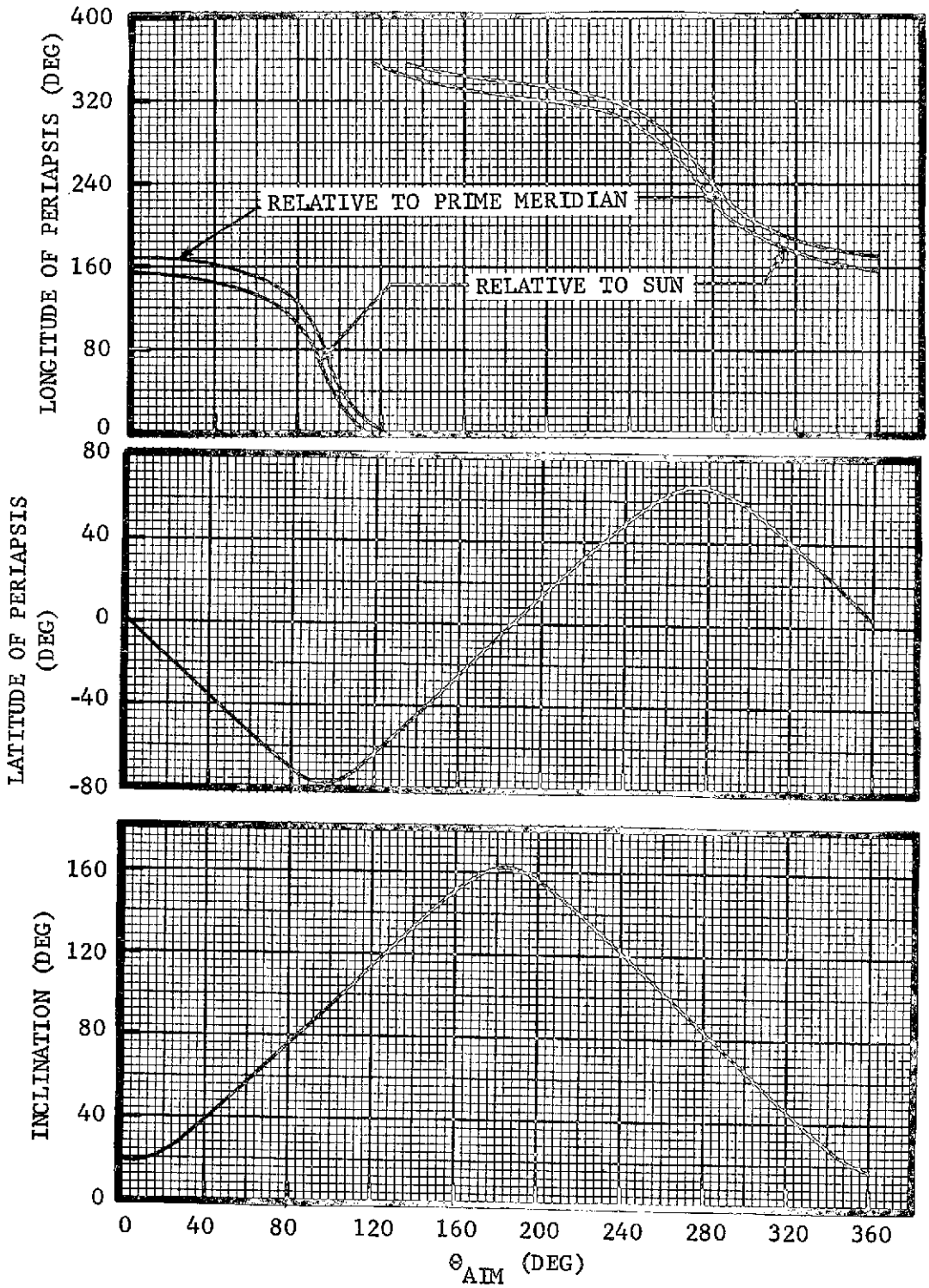

FIGURE IV-5 INITIAL ORBIT ORIENTATION DEPENDENCE ON B-PLANE TARGETING, 1985 MISSION OPPORTUNITY

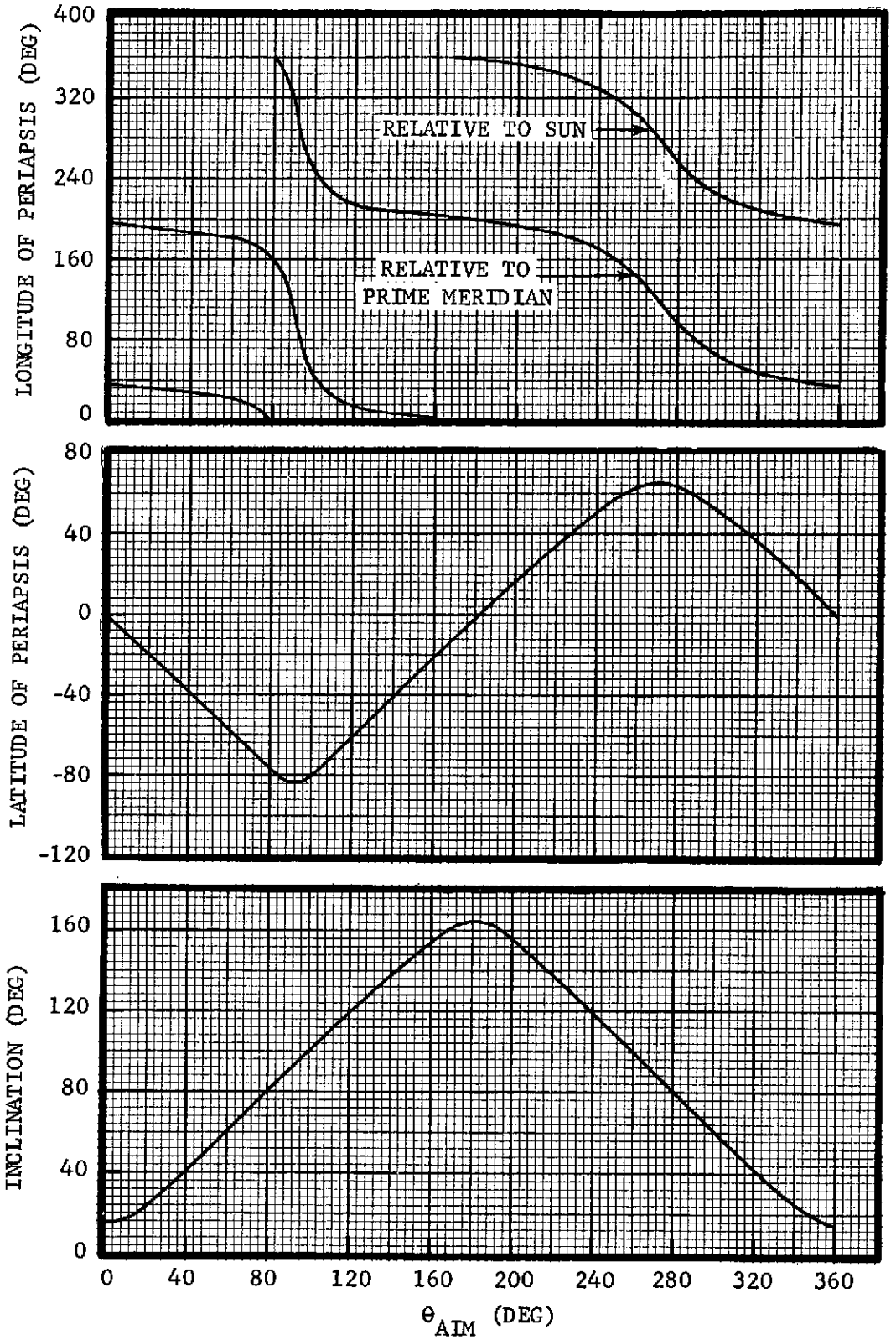

FIGURE IV-6 INITIAL ORBIT ORIENTATION DEPENDENCE ON B-PLANE TARGETING, 1988 MISSION OPPORTUNITY

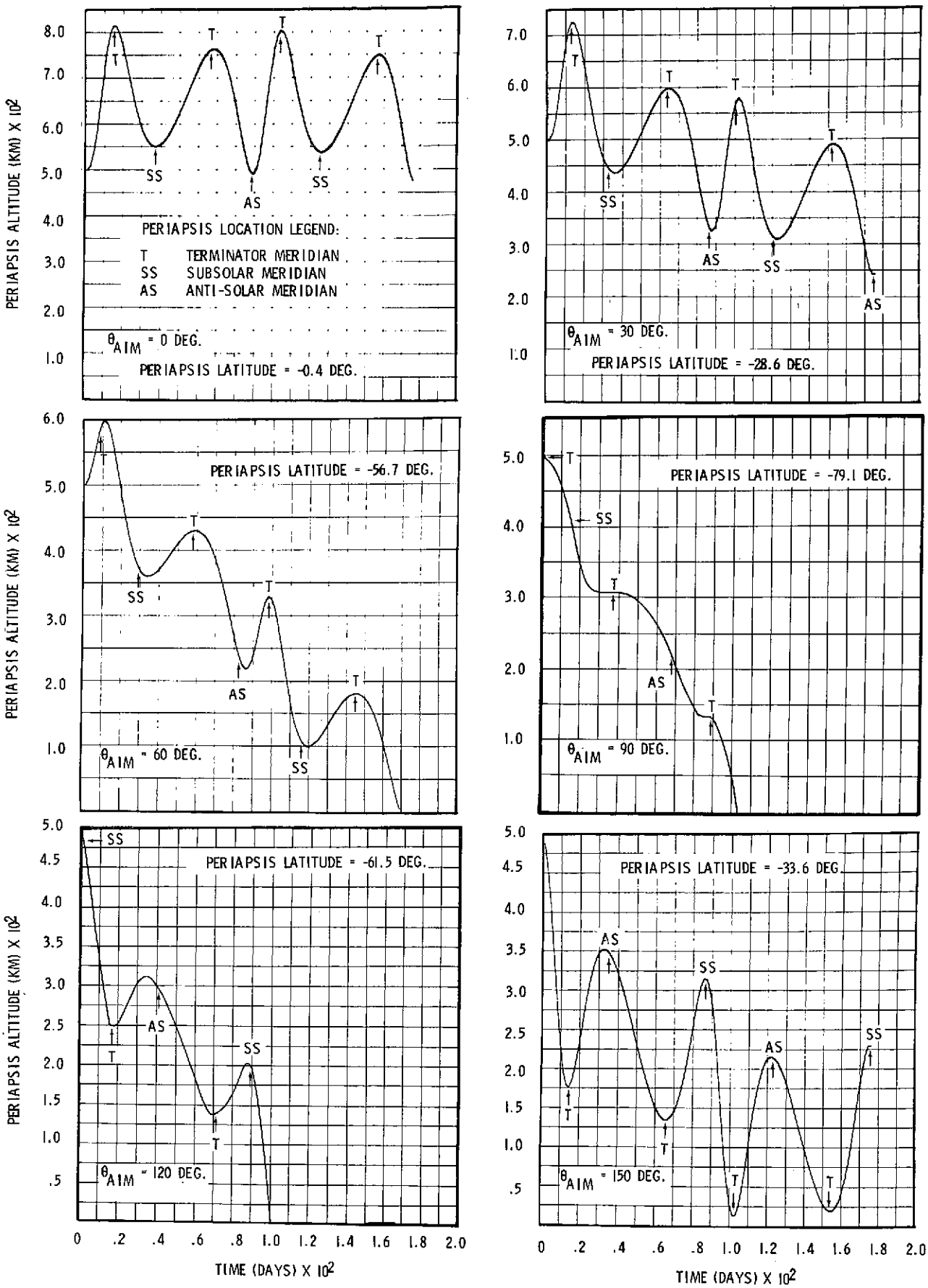

FIGURE IV-7 Periapsis Altitude Time Histories, 1980 Mission Opportunity, θ_{AIM} 0 to 150 Degrees

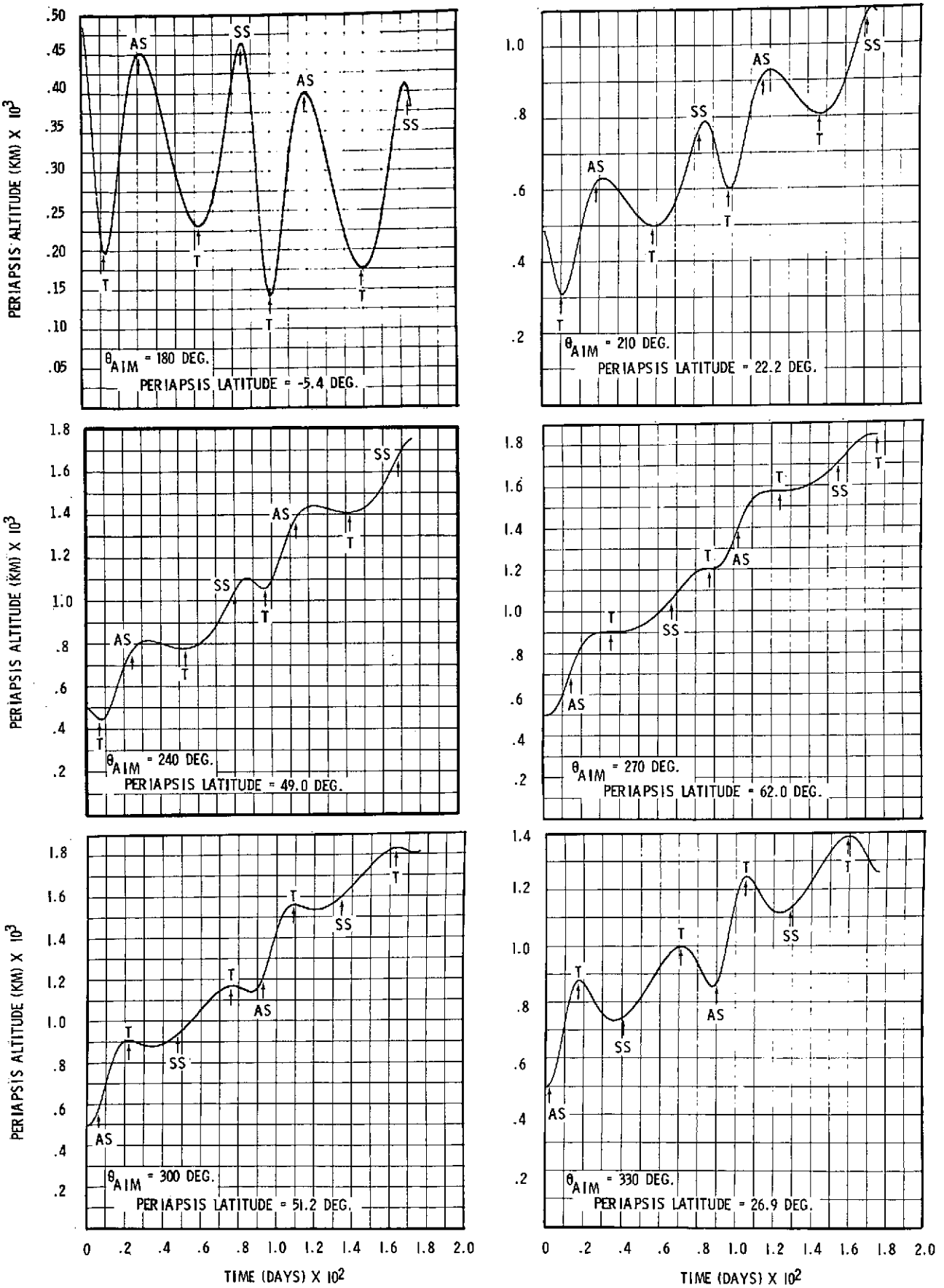

FIGURE IV-8 Periapsis Altitude Time Histories, 1980 Mission Opportunity, θ_{AIM} 180 to 330 Degrees

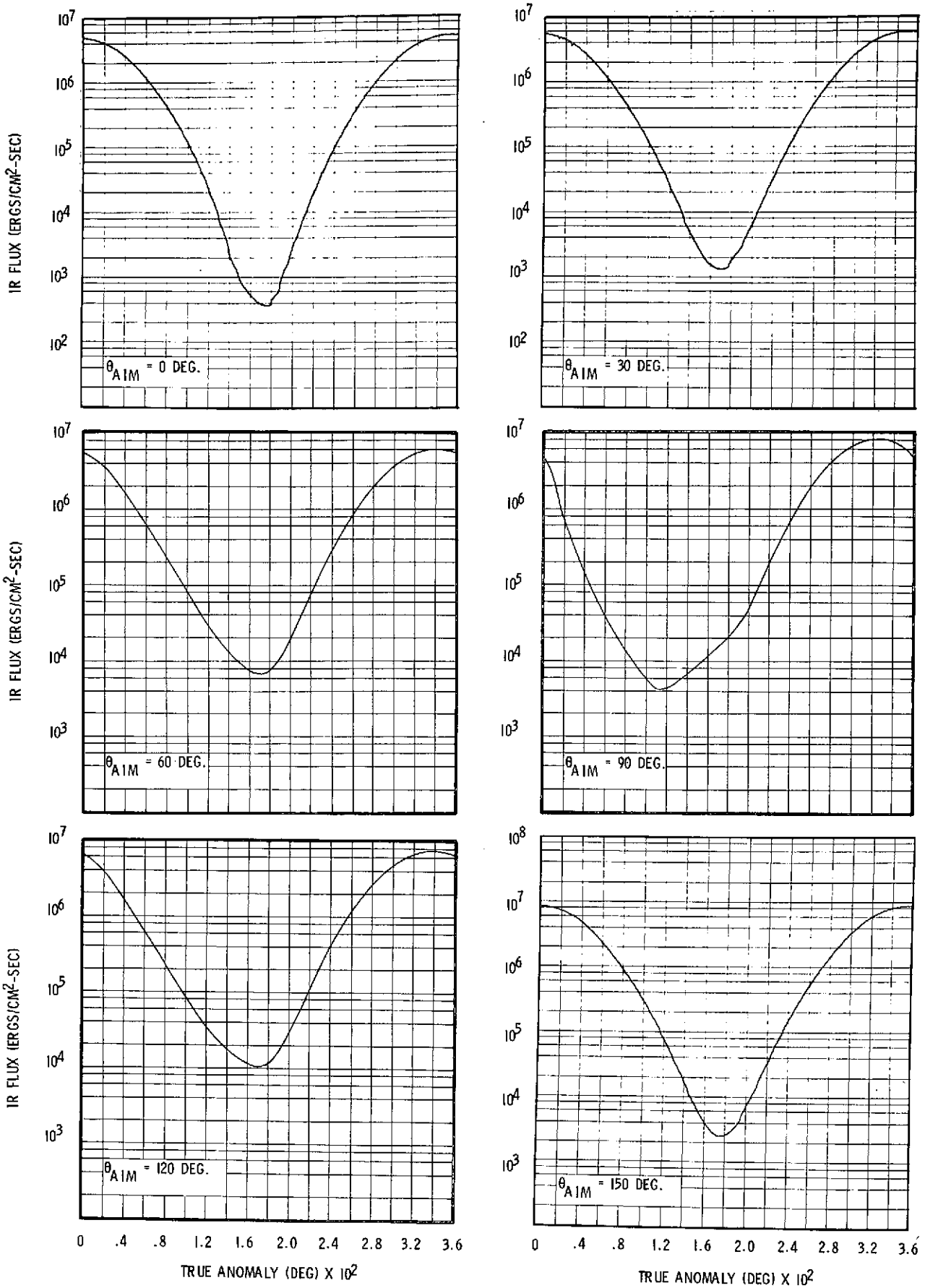

FIGURE IV-9 Worst Orbit IR Flux From Mercury, 1980 Mission Opportunity, θ_{AIM} 0 to 150 Degrees

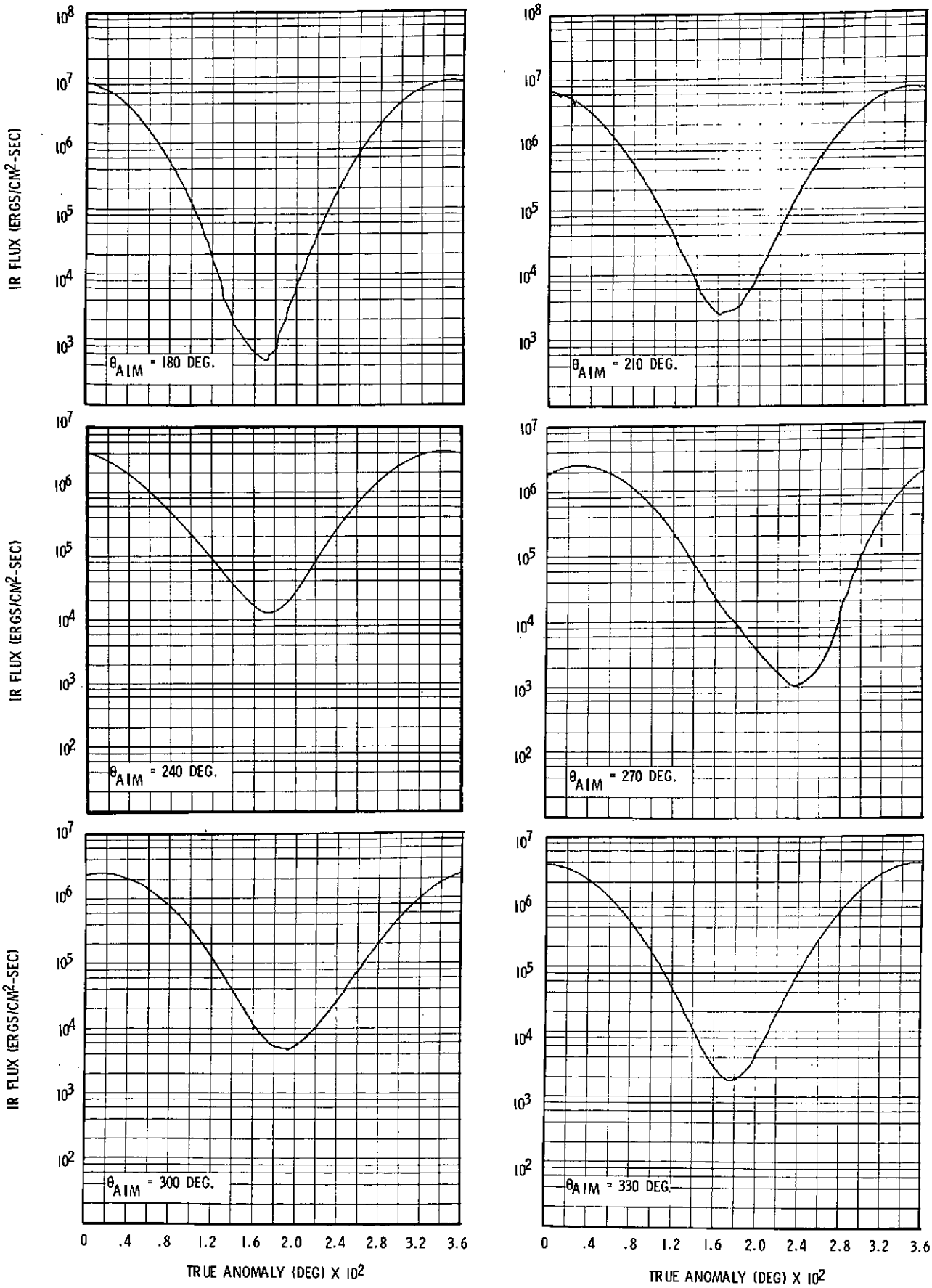

FIGURE IV-10 Worst Orbit IR Flux From Mercury, 1980 Mission Opportunity, θ_{AIM} 180 to 330 Degrees

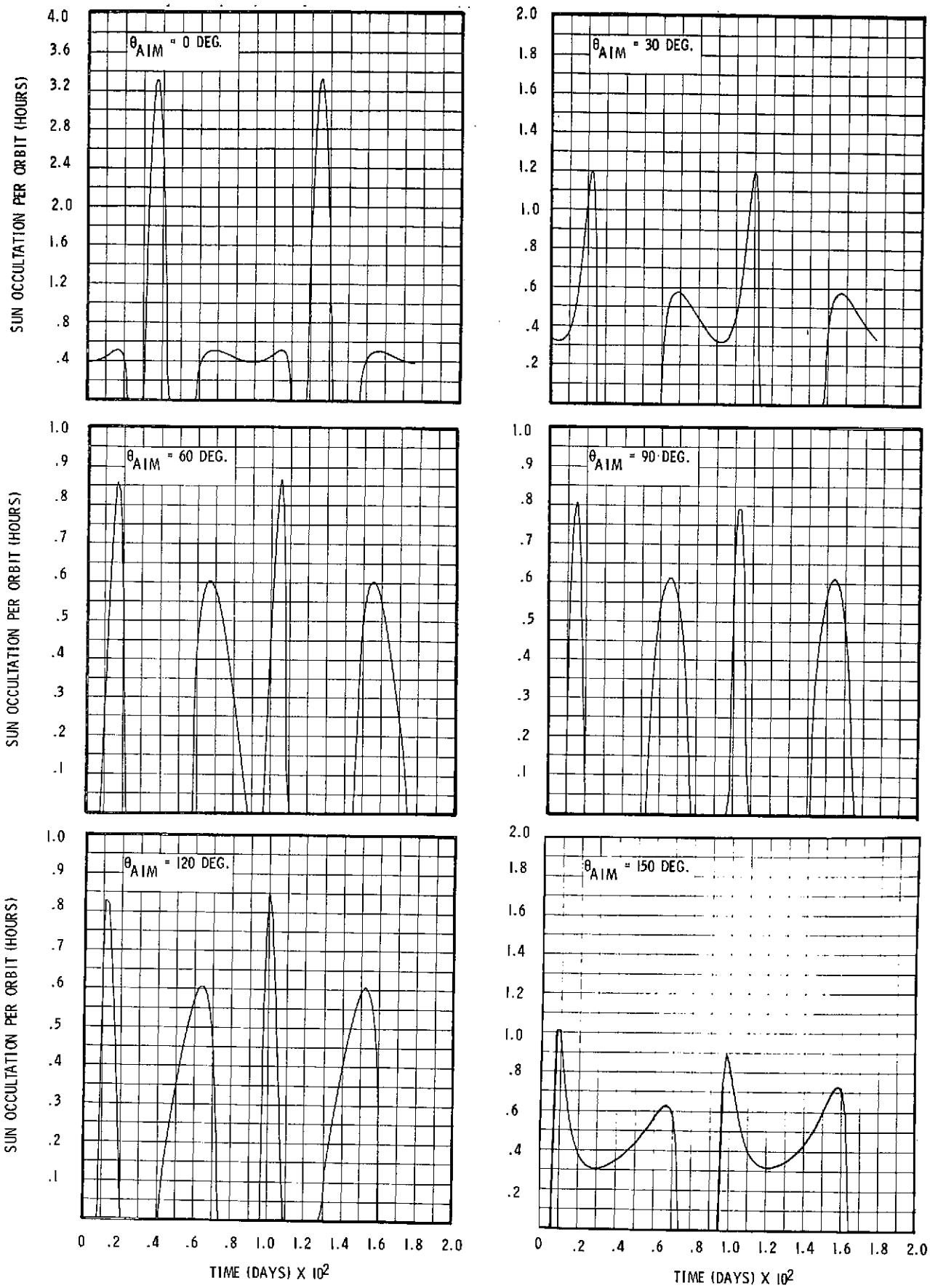

FIGURE IV-11 Solar Occultation Time Histories, 1980 Mission Opportunity, θ_{AIM} 0 to 150 Degrees

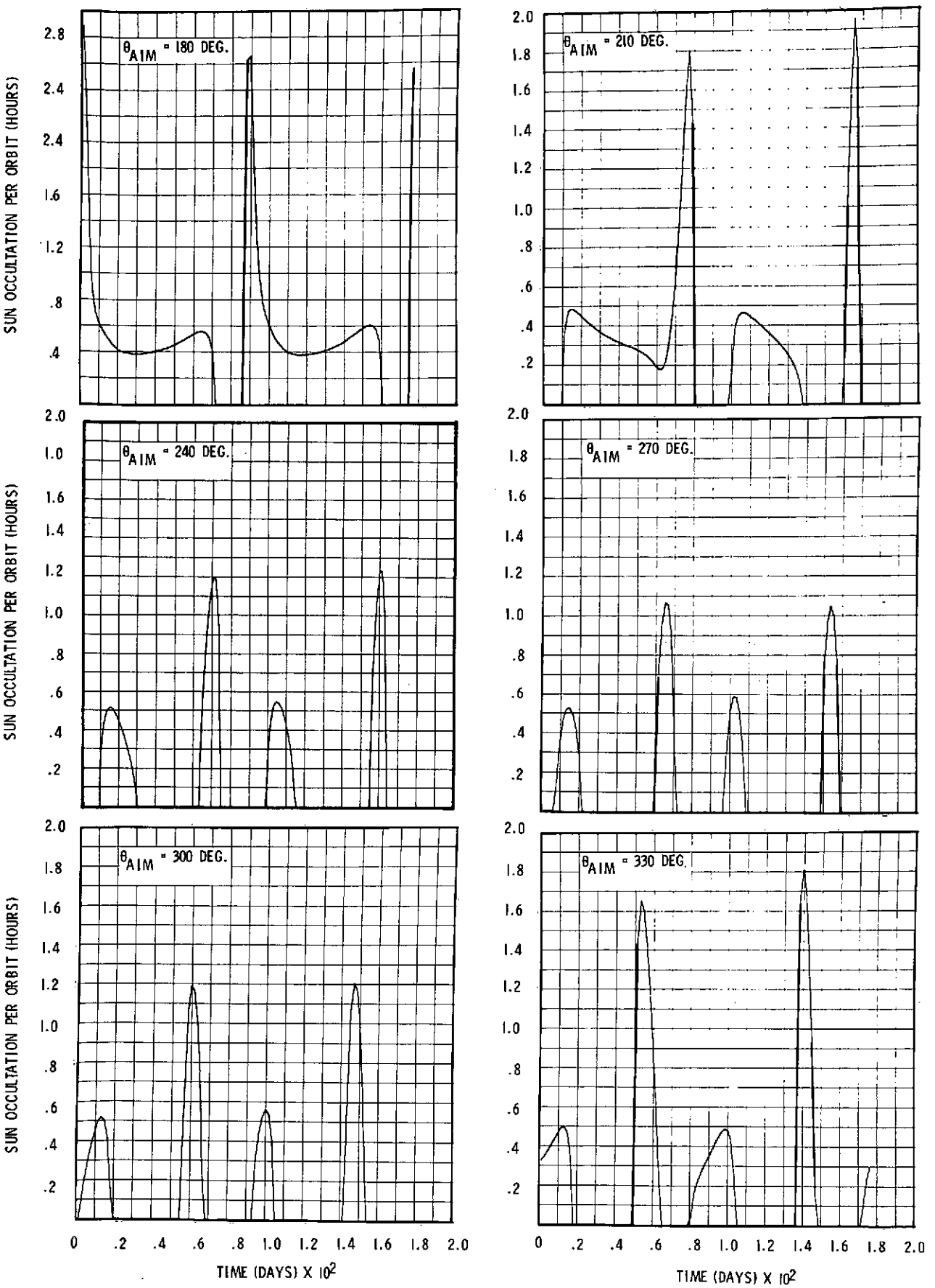

FIGURE IV-12 Solar Occultation Time Histories, 1980 Mission Opportunity, θ_{AIM} 180 to 330 Degrees

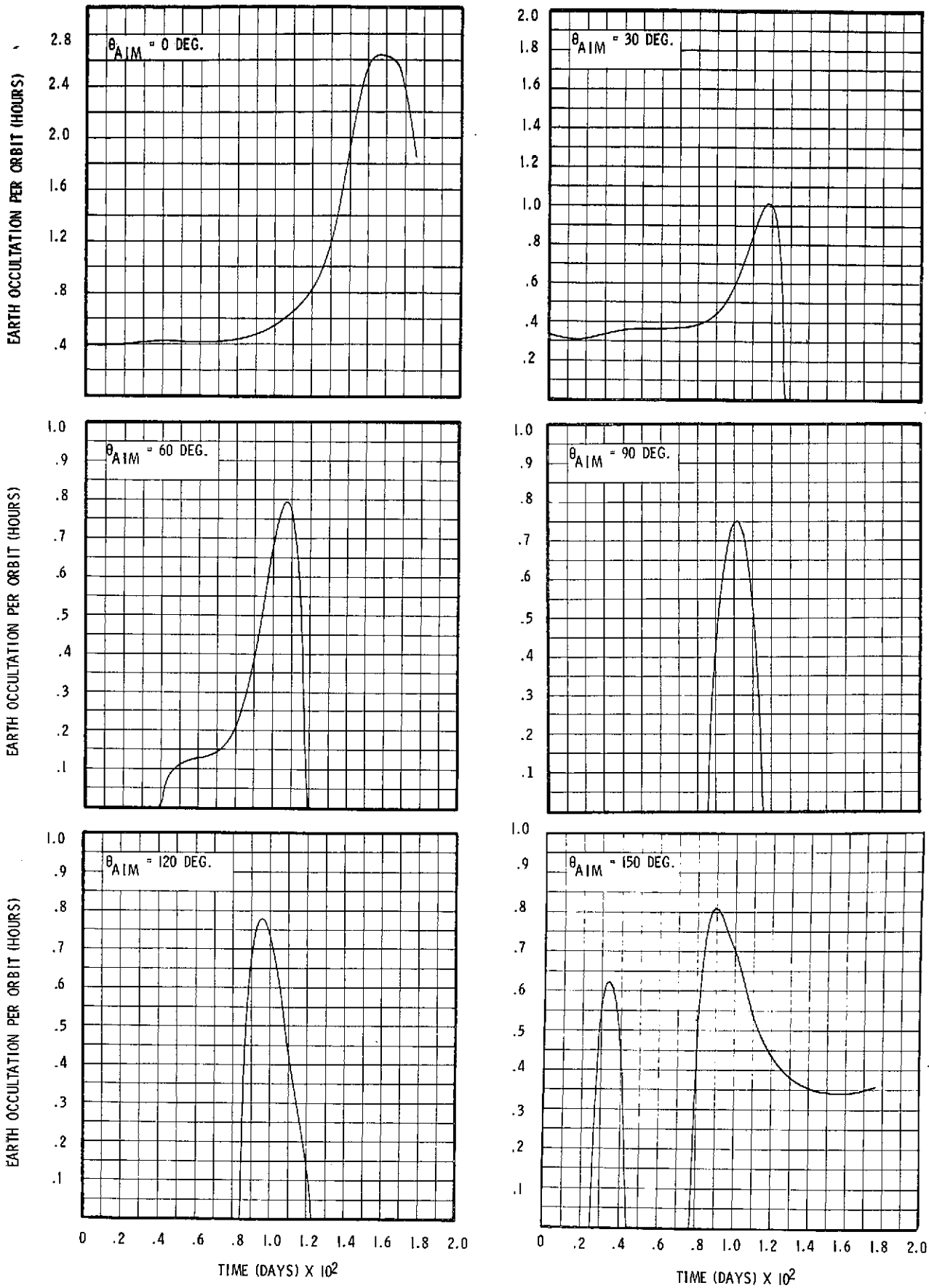

FIGURE IV-13 Earth Occultation Time Histories, 1980 Mission Opportunity, θ_{AIM} 0 to 150 Degrees

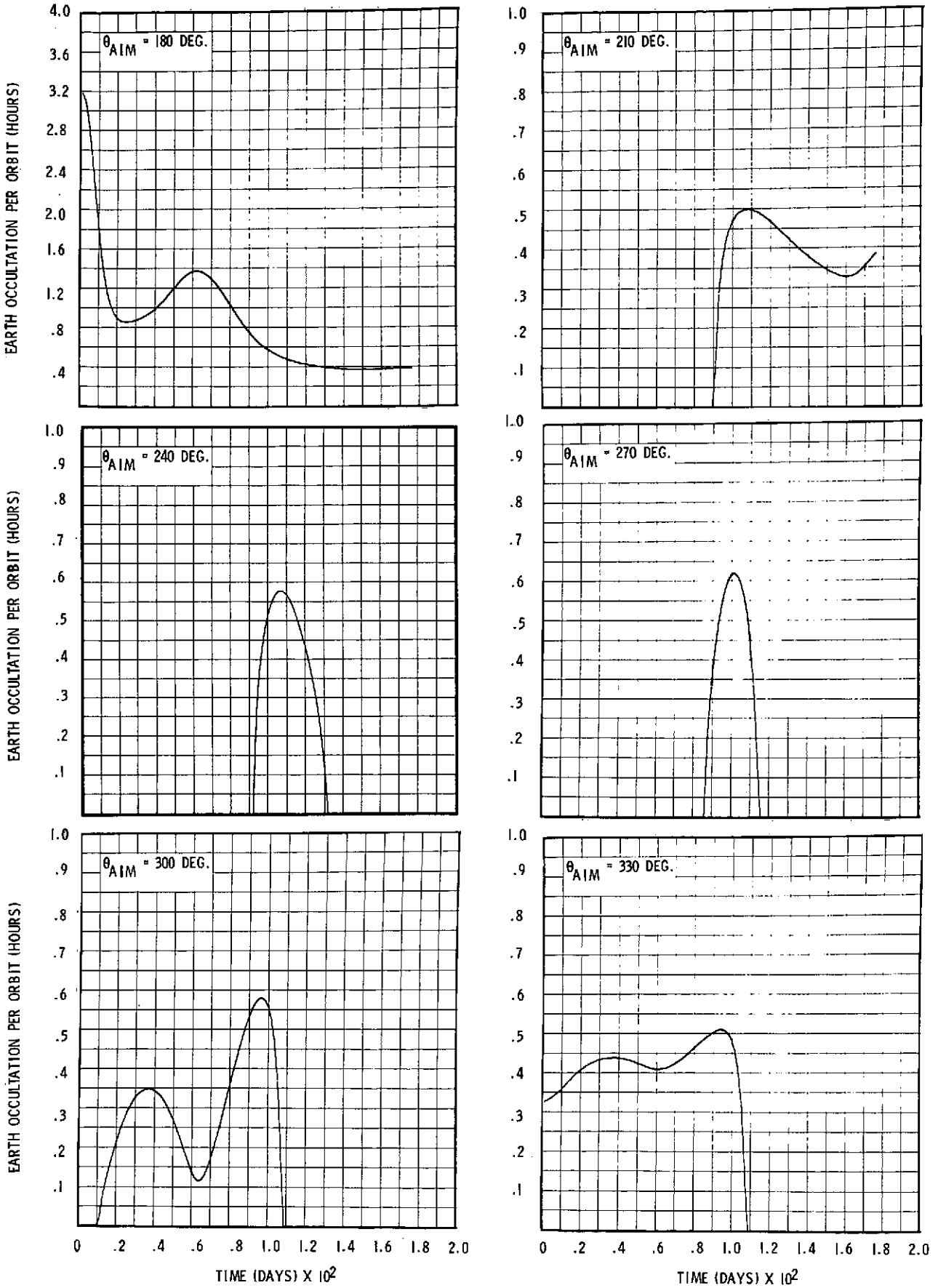

FIGURE IV-14 Earth Occultation Time Histories, 1980 Mission Opportunity, θ_{AIM} 180 to 330 Degrees

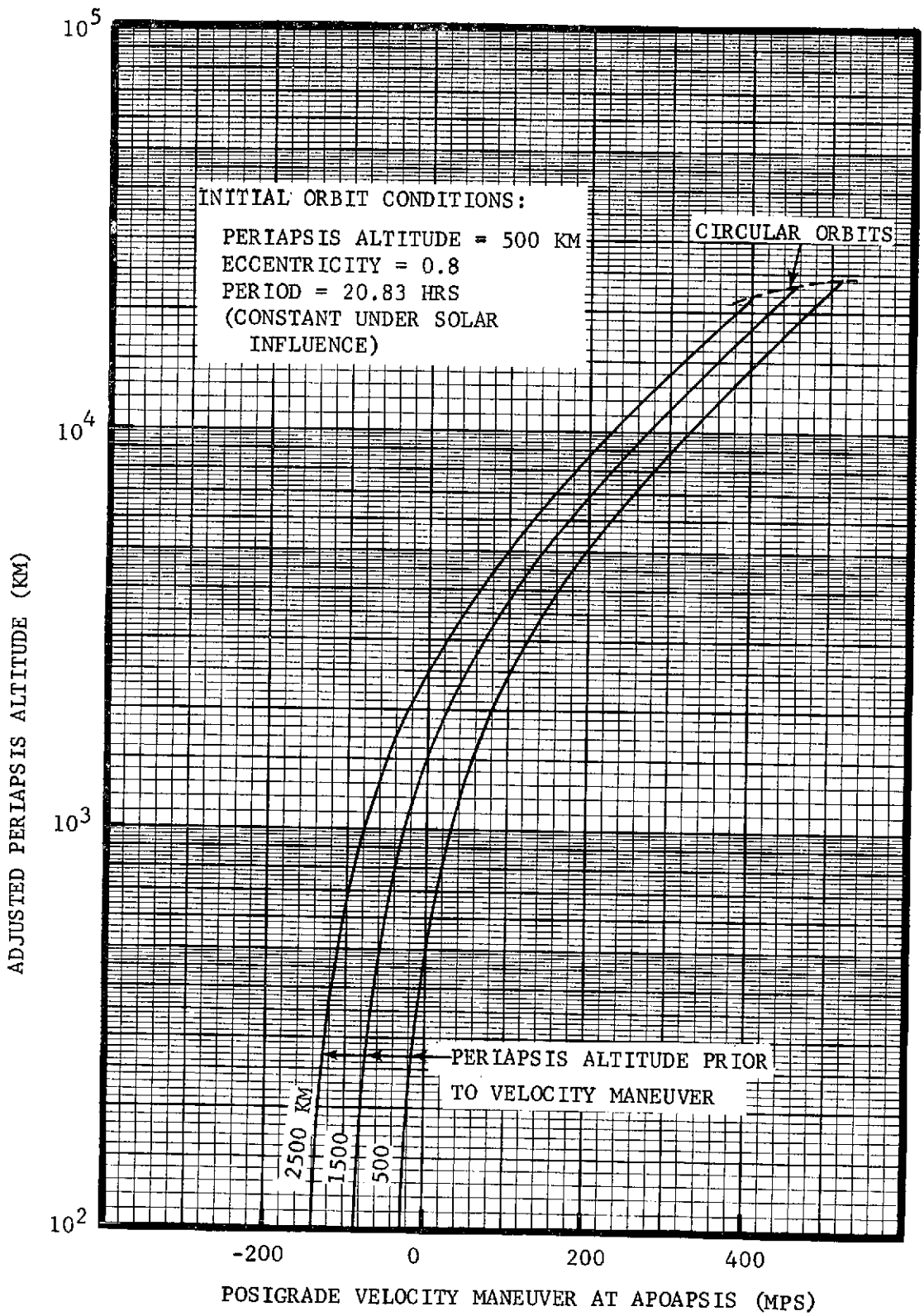

FIGURE IV-15 PERIAPSIS ALTITUDE ADJUSTMENT MANEUVER REQUIREMENTS

B. SCIENCE OBJECTIVES

A primary science objective for any planetary mission is to determine the planet's composition and internal structure. Comparing Mercury's composition and internal structure with that of the other planets is essential to understanding planetary accretion processes. The science objectives and experiments to accomplish these objectives are based on our present knowledge of Mercury which is discussed first in this section. Orbit selection criteria are then presented with the conclusion that a highly inclined eccentric orbit may offer an adequate compromise to the science objectives. The results from MVM'73 are certainly expected to have an impact on experiment and orbit selection; thus, the experiment list and orbit selection criteria presented herein should be considered preliminary. The natural follow-on to a successful orbiter mission is an orbiter/lander mission which is briefly discussed.

1. Present Knowledge of Mercury's Physical Properties

Our present knowledge of Mercury's physical properties is somewhat limited but has improved in the last few years with the advent of large earth-based radio astronomy facilities. Several authors have recently reviewed Mercury's physical properties: Kuiper (1970), Klopp, et al. (1971), and Divine, et al. (1972). A brief summary of our present knowledge of Mercury's physical properties is presented in the following paragraphs.

Pettingill and Dyce (1965) examined radar reflections from Mercury and deduced from the doppler spread in frequency that the period of rotation was not 88 days, as previously thought, but rather 59 days (a 3/2 spin orbit coupling). Dyce, et al. (1967) have concluded from radar measurements that Mercury's axis of rotation is within 28 degrees of the normal plane. Optical observations place the spin axis within 3^{o} of the normal to the orbital plane (Peale, 1972). In the absence of more definitive data, for this study the rotation axis has been taken as normal to the orbital plane (Sturms, 1971).

The mass of Mercury is determined primarily by Earth-Venus radar data through short-period perturbations introduced by Mercury on the orbit of Venus. Using the radar determined values for the radius and reciprocal mass of Mercury together with well-known solar and terrestial data, the ratio of the

density of Mercury to that of Earth may be calculated. Ash, et al. (1967) arrived at the value 0.995 ± .009 if a Newtonian model is used, and 0.986 ± 0.009 if a general relativity model is used. That is, the density of Mercury is very nearly equal to that of Earth (~5.52 gm/cm^3). Since Mercury has a small mass, there should be little gravitational compression; therefore, Mercury's observed density may be compared with the uncompressed density of the Earth (4.2), of Mars (4.0), and of the Moon (3.3). Mercury's unusually high density implies that it may be a metallic-rich planet, 65-70% by weight metal phase and only some 30% by weight silicate phase.

Little is known about Mercury's internal mass distribution, but the 3/2 spin-orbit coupling may be explained by making certain assumptions. The general method of approach is to assume that Mercury is subject to two types of solar torques: an orbital tidal torque and a torque about the spin axis arising from a postulated asymmetry in Mercury's equatorial shape. If Mercury's principle moments of inertia are represented by A, B, and C, where A and B are the moments around perpendicular axes lying in the equatorial plane and C is the moment about the spin axis, the asymmetry is measured by the quantity (B-A)/C, where B is traditionally larger than A. Goldreich and Peale (1966) estimate that the 3/2 resonance state will be stable if (B-A)/C is greater than 10^{-8}. For comparison, Kaula (1969) determined from satellite observations that the value of (B-A)/C for the Moon is about 2.3×10^{-4}.

Mercury's surface temperature distribution may be determined from microwave observations, assumed planetary absorption and emissivity values, and assumed values for the inverse thermal inertia. Models of Mercury's thermal properties are presented in Appendix 1 in which a 700°K subsolar hot pole and a 100°K night-side minimum temperature are assumed.

There is no conclusive experimental evidence that Mercury has an atmosphere. A number of searches for spectroscopic evidence of an atmosphere have been made since Moroz (1964) first reported detecting the 1.6 μ CO_2 band in the spectrum of Mercury. From observations near 0.8 μ, Spinrad, et al. (1965) set an upper limit of 57 m-atm to the CO_2 content. Binder and Cruikshank (1967) attempted to repeat the measurements of Moroz with negative results. An upper limit of 5 m-atm was set by Belton, et al. (1967) from observations

of the 1.05μ CO_2 band, and this limit was reduced another order of magnitude by Bergstralh, et al. (1967) from observations near 1.2μ. Since Mercury's photometric properties are almost identical with those of the moon, it would be expected that the surface of Mercury would also be exposed to darkening by the solar wind. If such darkening has occurred, an upper limit to the atmospheric surface pressure can be estimated; a value of about 10^{-5} mb has been suggested by Sagan (1966) and by O'Leary and Rea (1967). From calculations of the rate of escape of an atmosphere, Belton, et al. (1967) suggested 10^{-6} mb as an upper limit to the surface pressure. In light of these recent results, the assumption of an appreciable atmosphere appears unjustified for this study.

2. Science Return from MVM'73

Some of Mercury's physical properties will be known more accurately after the MVM'73 flyby results have been analyzed. Table IV-1 presents a list of science instruments to be included on the MVM mission. The imaging experiment will provide the first close-up pictures of the surface of Mercury.

Data from the magnetic and plasma probe experiments should indicate the type of interaction between the solar wind and the planet. If Mercury has an atmosphere surface pressure greater than about 10^{-10} mb, then it should be detected and compositionally analyzed with the UV spectrometer. The radio occultation experiment will also aid in determining the atmospheric properties along with planet size and shape information. An estimate of the planet's thermal inertia should be obtainable from the infrared radiometer measurements. A charged particle telescope is provided for learning more about the sun and the solar system environment.

The MVM'73 results should provide an adequate basis for a qualitative model of Mercury from which to design an orbiter mission. If MVM '73 detects an atmosphere, then detailed compositional analysis experiments will have high priority on an orbiter mission. Likewise, if MVM'73 detects an intrinsic magnetic field, high priority would be given for mapping the magnetic field on an orbiter mission. Orbiter and orbiter/lander missions are required for detailed quantitative models of Mercury from which inferences of the internal composition and structure can be made.

TABLE IV-1 MVM'73 SCIENCE INSTRUMENT PAYLOAD

INSTRUMENTS	OBJECTIVES
TV Camera	Planet appearance, size, and shape
Magnetometer	Intrinsic magnetic field, solar wind interaction, solar system environment.
Plasma Probe	Solar system environment, solar wind interaction with planet.
UV Spectrometer	Atmospheric composition
Radio Occultation	Atmospheric properties, planet size and shape.
IR Radiometer	Thermal conductivity, radiation balance
Charged Particle Telescope	Solar system environment.

3. Science Objectives and Instruments

The overall science objective for any Mercury mission will be to make measurements which will aid in understanding Mercury's composition and internal structure. Direct measurements of Mercury's internal structure will of course be impossible; but a combination of experiments such as imaging, S/C tracking, radar altimeter measurements, and radio occultation data will enable the determination of the size, shape, and gravity harmonics which will lead to a better understanding of Mercury's internal structure. Once the internal density distribution is known, some aspects of the internal composition can be inferred. A list of the science objectives and experiments for a Mercury Orbiter mission is presented in Table IV-2. The list is not intended to be a complete list of all possible instruments to meet each objective but is intended as a representative list of instruments which may be used to satisfy most science objectives.

Size, Shape, and Internal Properties - Full planet images and radar altimeter and radio occultation measurements are the proposed methods for determining the planet's size and shape. A global mapping imaging experiment is the primary experiment for determining if Mercury is presently or has been an active planet. Mariner 6 and 7 which flew by Mars indicated that Mars was an inactive planet similar to our Moon; but the pictures from the Mariner 9 orbiter indicated that Mars is definitely an active planet. The activity on Mars is limited to only one hemisphere implying that it may still be in the early stages of planetary evolution due to its small mass (Murray, 1973). This implies that, due to its small mass, Mercury may also be in an early stage of planetary evolution, but only by thorough mapping of the planet will we know for sure.

By tracking a transponder in a low near-circular orbit, the gravity harmonics can be determined. The planet's gravity harmonics along with its size and shape are essential for determining the internal mass distribution. Knowledge of the two parameters; (C-A)/C and J_2, will enable the calculation of the important radial mass distribution term, C/MR^2. Peal (1972) has shown that (C-A)/C can be determined from measuring the angle between the planet's spin axis and orbit normal to within $\pm$ 1 arc minute if all perturbing

TABLE IV-2 SCIENCE OBJECTIVES AND EXPERIMENTS FOR A MERCURY ORBITER MISSION

MISSION OBJECTIVES *	SCIENCE EXPERIMENTS																	
	Imaging	Radar Altimeter	Radio Occultation (Gravity Harmonics)	X-Ray Spectrometer Transponder	γ-Ray Spectrometer	IR Spectrometer	Magnetometer	UV Spectrometer	IR Limb Scanner	IR Radiometer	Plasma Probe	Photometer	Charged Particle Telescope	Meteoroid Detector	Plasma Wave Sensor	Neutron Monitor		
SIZE AND SHAPE	X	X	X															
INTERNAL PROPERTIES	X			X				X				X						
SURFACE PROPERTIES	X				X	X	X	X	X		X	X	X					
ATMOSPHERIC PROPERTIES			X				X	X	X	X		X	X					
SOLAR SYSTEM ENVIRONMENT	X		X		X	X	X	X	X			X	X	X	X	X	X	

* The primary mission objective is to determine Mercury's internal composition and structure. In order to accomplish this primary objective, measurements pertaining to the following are required: size and shape, internal properties, surface properties, and atmospheric properties. The solar system environment is a secondary mission objective.

gravitational affects (Venus, Jupiter, etc.) are taken into account. An orbit with a small eccentricity and semimajor axis is needed in order to enhance the gravitational harmonic effects and reduce solar perturbations.

A magnetometer, a plasma probe, and a plasma wave sensor are suggested for determining the interaction of the solar wind with the planet. Studying this interaction will provide information about Mercury's intrinsic magnetic field (if one is present), the electrical and magnetic conductivity properties of the surface and interior, and its upper-atmospheric properties (if one is present). The solar wind can interact with a planet in three categories: strong, moderate, weak. The strong interaction occurs when the solar wind interacts solely with the planet's intrinsic magnetic field. It is most unlikely however, that Mercury will have a stong enough intrinsic magnetic field to shield the planet from the solar wind. The moderate interaction can occur when the solar wind interacts with the upper ionized atmosphere, and a detached bow shock is produced; or when the solar wind produces electrical currents in the planet's interior of sufficient magnitude that significant magnetic fields are produced, again resulting in a detached bow shock. A moderate interaction of the solar wind with Mercury is possible if Mercury has an atmosphere or if Mercury's surface does not prevent the coupling between the conducting interior of the planet and the solar wind plasma. Ness and Wong (1971) have analyzed the critical conductivity of the surface layer necessary for such a coupling to occur as a function of core conductivity and surface thickness. They conclude that it is doubtful that the conductivity of the surface layer is sufficiently high to lead to the development of a secondary magnetic field strong enough to deflect the solar wind flow. However, they mention that the high average density of the planet indicates the possible existence of a core of sufficiently high conductivity and sufficiently large size to compensate for the low conductivity of the surface layer. Under these conditions, a moderate interaction of the solar wind could occur. A weak solar wind interaction will occur if Mercury has neither a magnetic field (intrinsic or induced) nor an atmosphere. In case of a weak interaction, the bow shock is attached to the surface.

Surface Properties - X-ray and γ-ray spectrometer experiments are ideal for elemental mapping of Mercury's surface due to Mercury's proximity to the Sun and the expected absence of atmospheric attenuation. Solar quiescent X rays are energetic enough to produce flourescent X rays in all elements with atomic numbers less than or equal to 14 (S_i). During solar flares the solar X rays are energetic enough to produce flourescent X rays in all elements with atomic numbers less than or equal to 26 (Fe). Current X-ray spectrometers cannot detect the soft flourescent X rays from elements with atomic numbers less than 12; therefore, only Mg, Al, and Si can be detected during solar quiescent times. The X-ray spectrometer has the advantage of good spatial resolution, easy data analysis, and a minimal background radiation problem. The γ-ray spectrometer can theoretically identify most elements since most elements will be activated from cosmic, solar, and galactic particle bombardment. The natural occuring radioactive elements can also be identified with a γ-ray spectrometer. The γ-ray spectrometer has the disadvantage of poor spatial resolution, complex data analysis, and possible background problems.

Other experiments which may be helpful in determining the surface properties are the IR spectrometer, UV spectrometer, IR radiometer, photometer, and the solar wind experiments discussed previously. The spectral signature of the IR radiation from the surface is dictated by the surface chemical composition; but, at present, the only currently unambiguous signature is that of SiO_2. The UV spectrometer may also be helpful in identifying the surface composition. Solar radiation will produce UV radiation from the planet's surface with a spectral signature characteristic of the surface material. Interpreting UV spectra data from surface material is ambiguous, however, and therefore, the primary purpose of a UV spectrometer would be for atmospheric analysis.

The purpose of the IR radiometer is to map the surface temperature distribution. If Mercury's spin axis is normal to its orbital plane, then the 3/2 spin-orbit coupling will produce the unusual effect of two hot and two warm poles on Mercury. (These "poles" are points on the equator.) An IR radiometer will provide the data needed to measure the surface temperature and thermal gradients, which will be indicative of the thermal conductivity in the surface layers, and which will aid in the detection of an internal heat

source if one is present.

The determination of Mercury's radiation balance from photometrically mapping the planet will provide information pertaining to Mercury's atmospheric and surface composition as well as its internal and surface thermal properties. Measuring the planet's albedo at different phase angles will provide data for determining the large scale surface roughness and/or atmospheric absorption properties if atmosphere is present. The particle size distribution and/or small scale surface roughness can be determined from using a photometer with polarizing filters. This combination of a photometer with polarizing filters can also be used for determining the particle size distribution of micrometeoroids which are responsible for the Zodiacal light.

Atmospheric Properties - Estimates of the upper limit of Mercury's atmospheric pressure range between 0.1 mb and 10^{-6} mb. A UV spectrometer is the most sensitive remote sensing instrument for determining the atmospheric composition. A UV spectrometer can determine the composition of atmospheres with pressures less than 10^{-6} mb and probably as small as 10^{-10} mb (Bowyer, et al, (1970). The atmospheric composition may be due to outgasing, and may therefore be indicative of Mercury's internal composition. If Mercury's atmosheric pressure is greater than about 2×10^{-3} mb, then the temperature profile can be measured with an IR limb scanner. Data from the S- and X-band occultation experiments may also be useful for determining the atmospheric properties. Other experiments which may aid in identifying atmospheric properties are the IR spectrometer, solar wind and photometer experiments. The IR spectrometer, for instance, should aid in the compositional analysis of the atmosphere. The other experiments have previously been described.

Solar System Environment - The geometry of Mercury's orbit enables solar environmental measurements to be made between .31 - .47 AU. There are many possible experiments to choose from, but only a few representative ones will be discussed. A charged particle telescope may be used for detecting solar charged particles. The γ-ray, X-ray, UV, and IR spectrometer can be used to monitor solar activity; but, the primary goal of these instruments is a determination of Mercury's surface and atmospheric properties. The radio occultation experiment can be used to make measurements of the solar corona

near superior conjunction. The magnetometer, plasma probe, and plasma wave sensor experiments can be used continuously throughout the mission to measure the solar wind properties from 1.0 to .31 AU. The solar neutron flux at Mercury may be 10 to 50 times greater than the solar neutron flux at 1 AU; thus, a solar neutron experiment for a Mercury Orbiter mission has a much greater probability of detecting solar neutrons than a similar experiment at 1 AU (see Appendix 1 for neutron environmental models at Mercury.) Since Mercury's orbit is located near the outer edge of the Zodiacal light region, a meteoroid detector would be useful for making in situ measurements of the meteoroid environment which is responsible for the Zodiacal light (see Appendix 1 for the meteoroid environmental models at Mercury). The particle size distribution of the Zodiacal light can be determined with a photometer or imaging system using polarizing filters.

An orbiter is limited in the amount of useful unambiguous data possible from remote sensing experiments for determining the internal, surface and atmospheric composition. In situ measurements of Mercury's surface and atmosphere will be needed to reduce the ambiguity in the remote sensing data; thus, a lander should follow a successful orbiter mission. A lander will also permit seismic experiments which will be extremely valuable for understanding the internal structure. Detecting planet wobble by accurately tracking the lander would aid in determining the mass distribution. Appendix 5 discusses the performance requirements for a small lander.

4. Science Considerations for Orbit Selection

The actual orbit selected will be determined from trade-offs dictated by thermal constraints, ΔV requirements, and science return. The science considerations are discussed for each science instrument below.

a. Imaging - The three objectives for an imaging experiment are complete regional mapping with ground resolution between 1. and 0.3 km, local imaging with ground resolution of 100 meters or better, and whole planet views. The complete regional mapping requirement requires a near-polar orbit. In order to accomplish all three objectives requires either three cameras in a near circular orbit, or two cameras in a highly eccentric orbit. The eccentric orbit has the disadvantage that only part of the planet will be accessible to

local imaging.

b. Radio Occultation - The only orbital requirement for this experiment is many Earth occultations. Figures IV-13 and IV-14 show the Earth occultation time histories as a function of orbit orientation. The radio occultation experiment provides the greatest quantity of data when in a near-equatorial orbit.

c. Transponder - The gravity harmonics are determined from spacecraft tracking data taken over many orbits; the best orbit for this purpose is a low, circular orbit. Trying to extract the gravity harmonics from spacecraft tracking data based on any other type of orbit results in a significant increase in the complexity of the analysis and a serious degredation of the resulting conclusions. If the spacecraft were to be in a highly eccentric orbit, then a subsatellite with a tracking transponder in a low, near-circular orbit would be necessary if the gravity harmonics are to be determined accurately. The sizing and deployment options for a subsatellite are discussed in Appendix 2.

d. Radar Altimeter, X-Ray Spectrometer, γ-Ray Spectrometer, IR Spectrometer, IR Radiometer, IR Limb Scanner - The resolution of all mapping instruments decreases as the altitude increases. The most advantageous orbit for these instruments would be a low, circular orbit. Since these are mapping instruments, a high inclination orbit is required for complete planet coverage.

e. Magnetometer, Plasma Probe, Plasma Wave Sensor - These instruments map the interaction of the solar wind with the planet; thus, measurements both close to and far from the planet are required. This indicates that a highly eccentric orbit is preferred. In order to make measurements of the solar wind cavity far from the planet, a low-inclination orbit is required, but this would preclude the possibility of mapping the bow shock at high latitudes. Plots of planetocentric radial distance versus phase angle for θ_{AIM} values in 30 degrees increments are provided in Figures IV-16 and 17.

f. UV Spectrometer - The primary purpose of the UV spectrometer is to observe the atmospheric UV absorption and emission lines. Since the signal strength of the emission lines diminishes with altitude, a low near-circular orbit is preferred. Since UV absorption measurements require solar occultation, a low inclination orbit is indicated; but measurements at many latitudes may be

desirable to check for atmospheric inhomogeneities, thus implying a high inclination orbit.

g. Photometer - The objective for this instrument is to make full planet and regional albedo measurements. If the field of view of this instrument is fixed, then an eccentric orbit is desirable. Since complete regional coverage is also an objective, a high inclination orbit is required.

h. Charged Particle Telescope, Meteoroid Detector, Neutron Monitor - The objective of these instruments is to make measurements pertaining to the solar system environment. The only orbital constraint is to be as far away from the planet as possible so that planetary perturbations will be minimized; thus, an orbit with a large semimajor axis is desirable.

i. Summary - A single orbit cannot be chosen which will maximize the return from all instruments individually. An eccentric and highly inclined orbit appears to be an adequate compromise, since planet coverage is assumed to take precedence over obtaining many occultations. Near apoapsis of such an orbit, the whole planet can be viewed with a wide-angle camera for size and shape measurements; the photometer can view the planet for whole planet albedo measurements, and regional mapping can be accomplished with the narrow-angle camera. When the S/C is near periapsis, all the resolution sensitive mapping instruments can make their measurements. For a high-inclination orbit, the periapsis is constrained to be in the vicinity of one of the poles (see Figures IV-1 and IV-3 through IV-6); therefore, high resolution will be restricted to one hemisphere. Although more occultations are available in near-equatorial orbits, all highly inclined orbits provide many earth and solar occultations during a 176-day mission. An inclined eccentric orbit appears to adequately satisfy most orbiter science objectives.

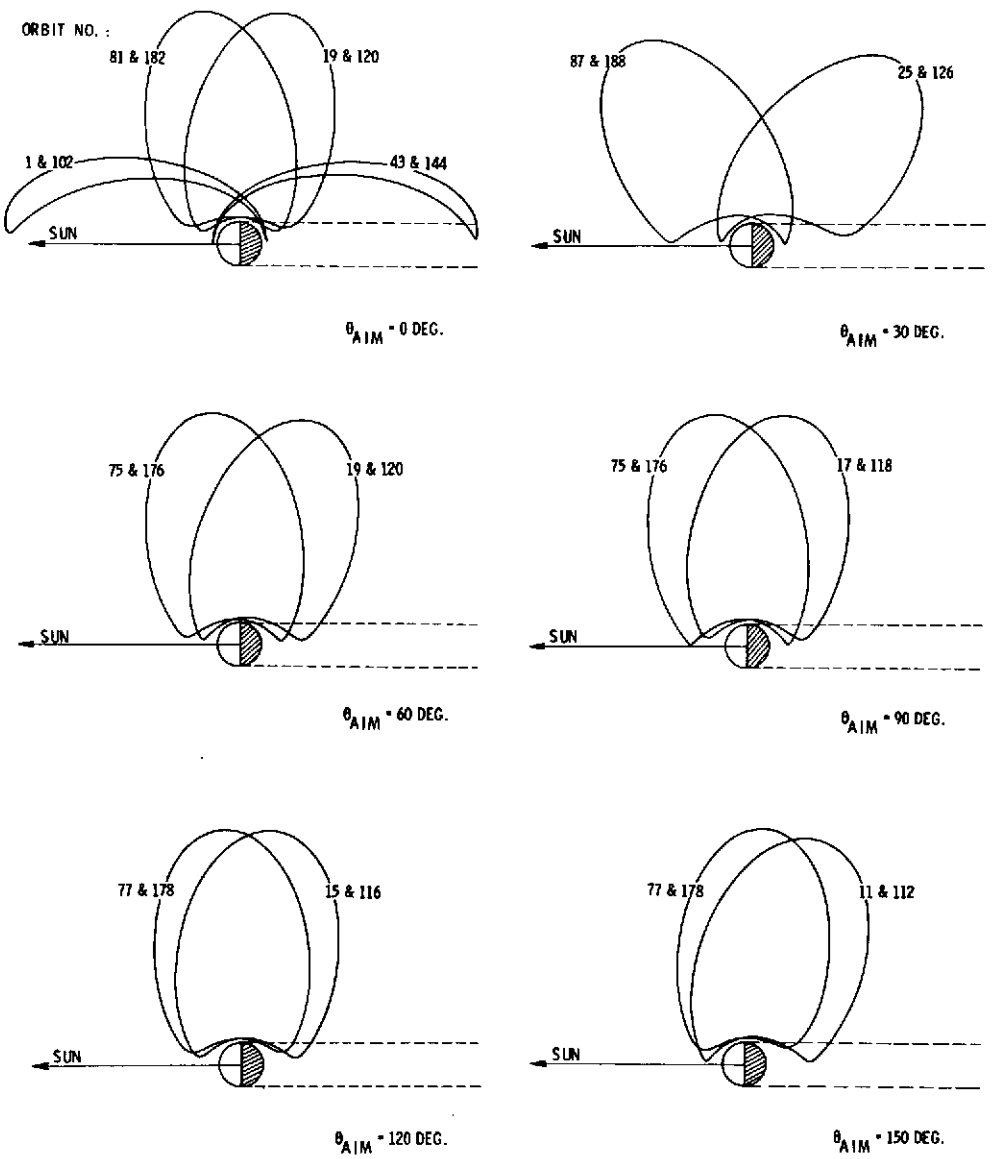

FIGURE IV-16 PLANETOCENTRIC RADIAL DISTANCE VS. PHASE ANGLE, θ_{AIM} 0 to 150 Degrees

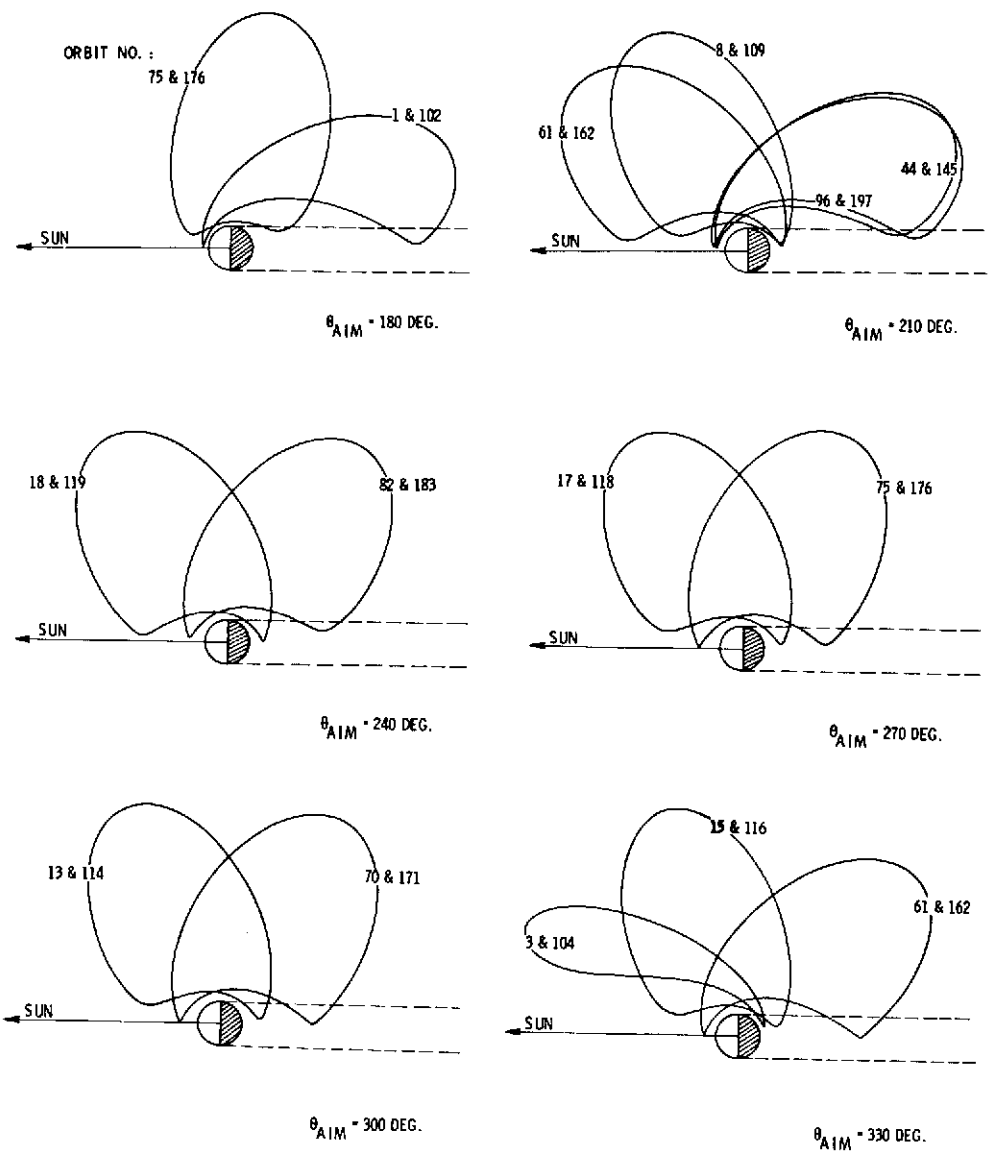

FIGURE IV-17 PLANETOCENTRIC RADIAL DISTANCE VS. PHASE ANGLE, θ_{AIM} 180 to 330 Degrees

V. REPRESENTATIVE ORBIT ANALYSIS

V. REPRESENTATIVE ORBIT ANALYSIS

The purpose of this section is to analyze the science return from a "nominal" orbit for the 1980 mission opportunity. Since imaging is a key experiment which monopolizes the data storage and transmission requirements, the science return is analyzed primarily on the basis of imagery. Arguments for selecting the nominal orbit are presented below. The nominal selected orbit is not intended to be the preferred, or best orbit for science return, but only a typical orbit from which the science return can be analyzed.

A. NOMINAL ORBIT SELECTION

Figures III-4 and III-5 illustrate that the ΔV requirements are minimized for orbits with a low periapsis and large eccentricity. Thermal requirements are minimized for orbits with high subsolar altitudes and large periapsis phase angles. The science orbit selection considerations discussed in Section IV-B imply that an eccentric orbit with a high inclination provides an adequate compromise for the overall science return. For these reasons, an orbit with a 500 km periapsis and 0.8 eccentricity has been chosen for the nominal size and shape. A summary of the orbit orientation considerations for all the θ_{AIM} values in 30 degree increments is presented in Table V-1. Assuming that mapping experiments requiring planet coverage take priority over occultation dependent experiments, the choice of θ_{AIM} values is reduced to 60^{o} through 120^{o} and 240^{o} through 300^{o} (see Table V-1).

Of the remaining θ_{AIM} values, those between 60^{o} and 120^{o} result in orbits having the periapsis in the southern hemisphere. For these θ_{AIM} values, the spacecraft impacts the planet before the end of the 176-day mission, unless there are trim maneuvers. Since θ_{AIM} values of 240^{o} through 300^{o} present similar planet coverage and viewing conditions, the θ_{AIM} values of 60^{o} through 120^{o} can be rejected unless MVM'73 discovers something of particular interest in the southern hemisphere which requires the periapsis to be in the southern hemisphere.

The remaining candidate θ_{AIM} values are 240^{o} to 300^{o}, and the remaining considerations are: should the initial periapsis be on the night or day side, and how critical are the thermal requirements. The latter question is beyond the scope of this contract. The near-polar orbit with $\theta_{AIM} = 270^{o}$

TABLE V-1 SUMMARY OF S/C ORBIT ORIENTATION CONSIDERATIONS

θ_{AIM} (deg)	INCLINATION (deg)	INITIAL PERIAPSIS# LOCATION (night/day)	MAX THERMAL FLUX FROM MERCURY (watts/cm^2)	ORBIT NUMBER FOR MAX. HEATING	SCIENCE EXPERIMENT CONSIDERATIONS**	TRIM MANEUVER REQUIRED (yes/no)
0	19	night	0.50	139	occultation	no
30	30	night	0.57	135	occultation	no
60	60	night	0.37*	27	planet coverage	yes
90	87	night	0.24*	15	planet coverage	yes
120	116	day	0.46*	3	planet coverage	yes
150	146	day	0.87	203	occultation	no
180	176	day	0.85	203	occultation	no
210	146	day	0.69	1	occultation	no
240	120	day	0.41	1	planet coverage	no
270	93	night	0.18	83	planet coverage	no
300	66	night	0.23	49	planet coverage	no
330	39	night	0.39	39	occultation	no

All orbits were assumed to have an initial 500 km periapsis and 0.8 eccentricity

* The maximum thermal flux for orbits requiring a trim maneuver was determined by assuming the periapsis altitude was kept constant at 500 km.

**Near equatorial orbits have more solar and earth occultations than near-polar orbits, whereas, near-polar orbits provide more planet coverage.

corresponding to an inclination of 93° has thermal advantages as well as good polar coverage. The disadvantages of a polar orbit are: smaller surface area coverage at lower altitudes than other θ_{AIM} values, initial night side periapsis, and less longitude coverage early in the mission. Since it is assumed desirable to accomplish as many science objectives as possible early in the mission, which implies a day-side periapsis for local imaging, a θ_{AIM} value of 240° was chosen for the reference orbit.

B. SCIENCE INSTRUMENT PAYLOAD

A representative science instrument payload for a Mercury Orbiter mission is presented in Table V-2. This list of instruments is not intended to be a complete list of all possible instruments to meet each objective, but is intended to present one or more instruments which may be used to satisfy most science objectives. No attempt has been made to size instruments other than imaging and the subsatellite for a Mercury Orbiter mission. Therefore, the weight and power estimates in Table V-2 for the instruments other than imaging and subsatellite are only representative.

C. MAPPING STRATEGIES

The imaging experiment is a key science experiment for a Mercury Orbiter mission and the data storage and transmission requirements of all the other science instruments combined are negligible compared with the imaging requirements. Figure V-1 compares the planet coverage possible from a Mercury Orbiter with that of the MVM'73 mission and early lunar observations. The plot in Figure V-1 for the Mercury Orbiter mission assumes imaging from wide and narrow angle MM'71 cameras and planet coverage from a high inclination orbit. A 176-day mission corresponds to one solar day on Mercury due to the 3/2 spin-orbit coupling. This permits complete mapping of the planet surface at all phase angles. If the images are carefully selected for regional mapping such that there is 20% overlap for images with phase angles greater than 30° and 60% overlap (stereo viewing) for images with phase angles less than 30° then complete regional mapping can be accomplished with about 850 pictures. High resolution local images can be taken of selected points of interest. The planet coverage from 1600 images presented in Figure V-1 for local imaging assumes that there was no image overlap. These 1600 high resolution images

TABLE V-2 REPRESENTATIVE SCIENCE INSTRUMENT PAYLOAD

FOR A MERCURY ORBITER MISSION

INSTRUMENTS	WEIGHT (kg)	POWER (watts)
o Imaging #	26	33
o Radar Altimeter Mapper	5	45
o Radio Occultation	*	*
o Subsatellite	15**	0***
o X-ray Spectrometer	9	5
o γ-ray Spectrometer	7	3
o UV Spectrometer	4	3
o Magnetometer	3	2
o IR Radiometer	3	5
o Photometer	3	4
o Plasma Probe	3	4
o Charged Particle Telescope	2	2
o Meteoroid Detector	1	1
o IR Spectrometer	9	12
o Plasma Wave Sensor	3	4
o IR Limb Scanner	5	15
o Neutron Monitor	3	4

The MM'71 camera system (including both a wide and narrow angle camera system)

* Radio (S-X) required for navigation.

**Assuming a 10 kg injected weight in a 500 km altitude circular coplanar orbit from the nominal (500 km periapsis and 0.8 eccentricity) orbit.

***If the subsatellite is tracked from the ground, there will be no extra power required from the S/C; but, if the subsatellite is tracked from the S/C, then extra power will be required from the S/C. The type of subsatellite tracking has not been defined in this study.

MM '71 PLANET COVERAGE
(MASURSKY, 1973)

PLANET COVERAGE	RESOLUTION (KM)
100%	1 - 3
1 - 2%	0.1 - 0.3

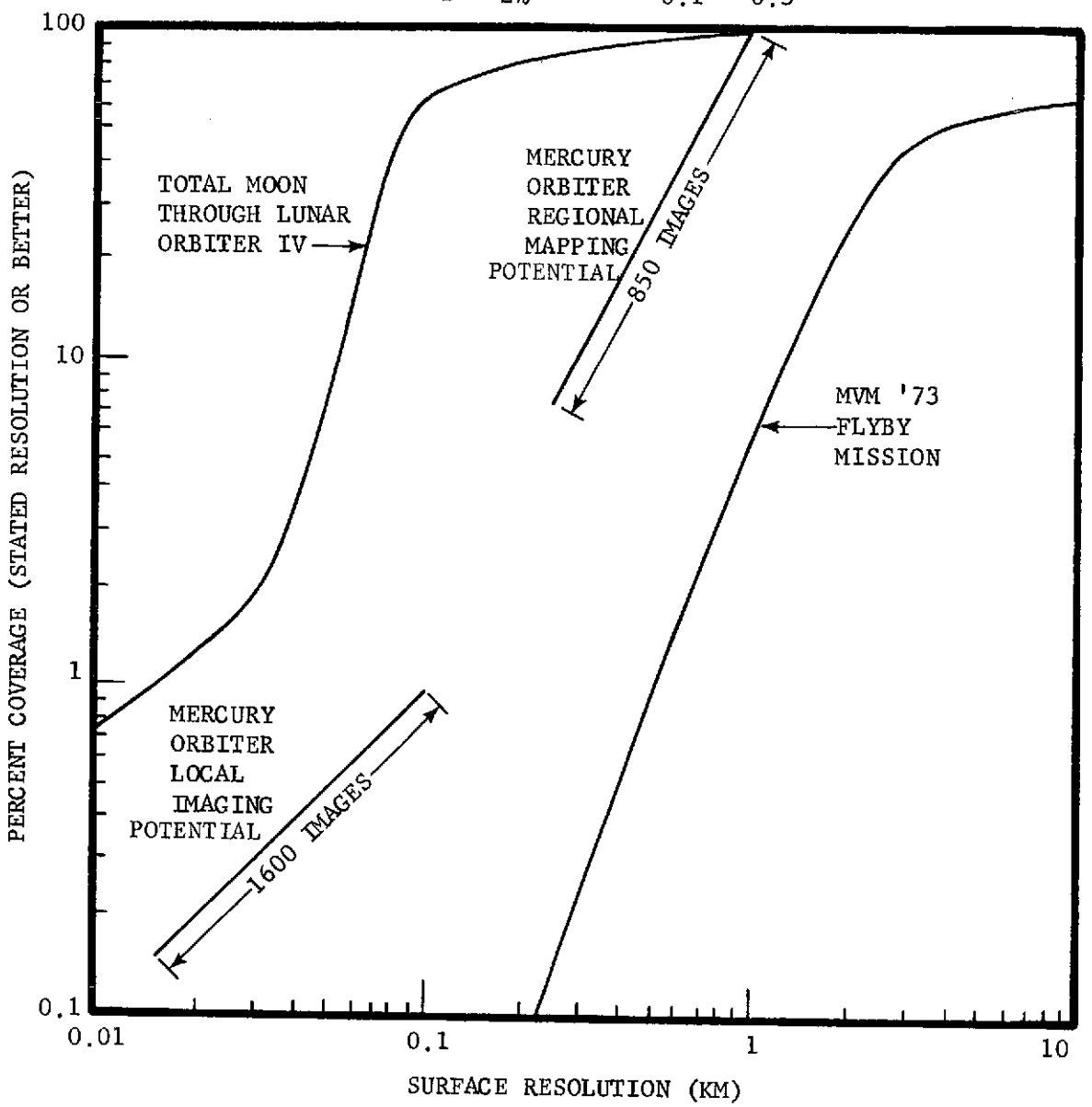

FIGURE V-1 PLANET COVERAGE COMPARISON OF A MERCURY ORBITER WITH THE MVM '73 FLYBY MISSION

represent a nominal number of pictures; the magnitude of this number is dependent upon the communications system. Figure V-1 indicates that if images are carefully selected, then a modest Mercury orbiter mission compares favorably with that of the MM'71 results.

Figures V-2 through V-7 present the planet coverage for the nominal orbit ($\theta_{AIM} = 240^{o}$, e = 0.8, and initial h_p = 500 km) of the 176-day 1980 mission. These figures illustrate the fact that complete planet coverage is feasible and at least one hemisphere is accessible for local imaging. Figure V-8 summarizes the total planet coverage possible from the nominal orbit. Since the mission duration lasts for one solar day, the latitudes in Fig. V-8 correspond to the minimum phase-angle values. The angle of reflectance in Fig. V-8 is defined as the angle that the viewing direction makes with the tangent to the planet's surface. The region from 60^{o} to -60^{o} latitude is the part of the planet accessible for radial imaging (angle of reflectance equal to 90 degrees). The polar regions cannot be viewed radially from an orbit with $\theta_{AIM} = 240^{o}$; thus, the maximum values for the angle of reflectance are: 34^{o} for the north pole, and 55^{o} for the south pole.

The imaging science objectives are to take full-planet views, regionally map the planet, and take as many high-resolution local images as possible. The purpose for taking full-planet images is to aid in determining the planet's size and shape; therefore, full-planet images every 5^{o} to 10^{o} degrees of planetocentric longitude should be sufficient. One of the objectives during the first part of the mission will be to map as much of the planet as possible in order to identify local regions of interest for high-resolution images. The regional mapping requirement can be accomplished within the first three months since 100% of the planet has at sometime been in the sunlight. There is also a need to take some high resolution images early in the mission since it is desirable to accomplish as many science objectives as possible early in the mission.

A typical mission design would involve 1600 high-resolution local images, 850 regional mapping images (see Fig. V-1), plus one other image per orbit corresponding to approximately 14 frames per orbit. The regional mapping and full-planet objectives can be accomplished during the first three months by

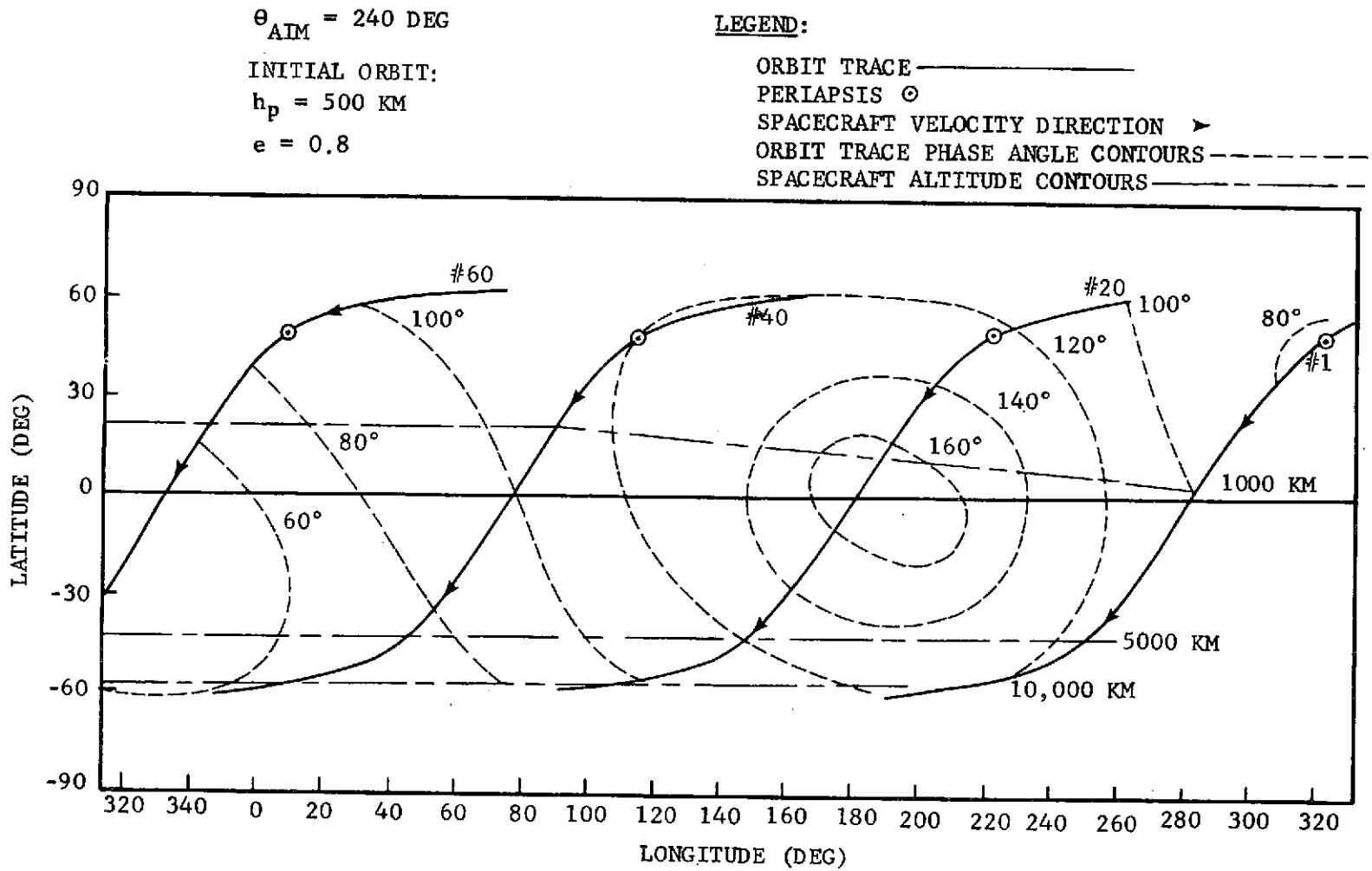

FIGURE V-2 PLANET COVERAGE, 1980 MISSION, ORBITS 1 TO 60, DESCENDING SEGMENT

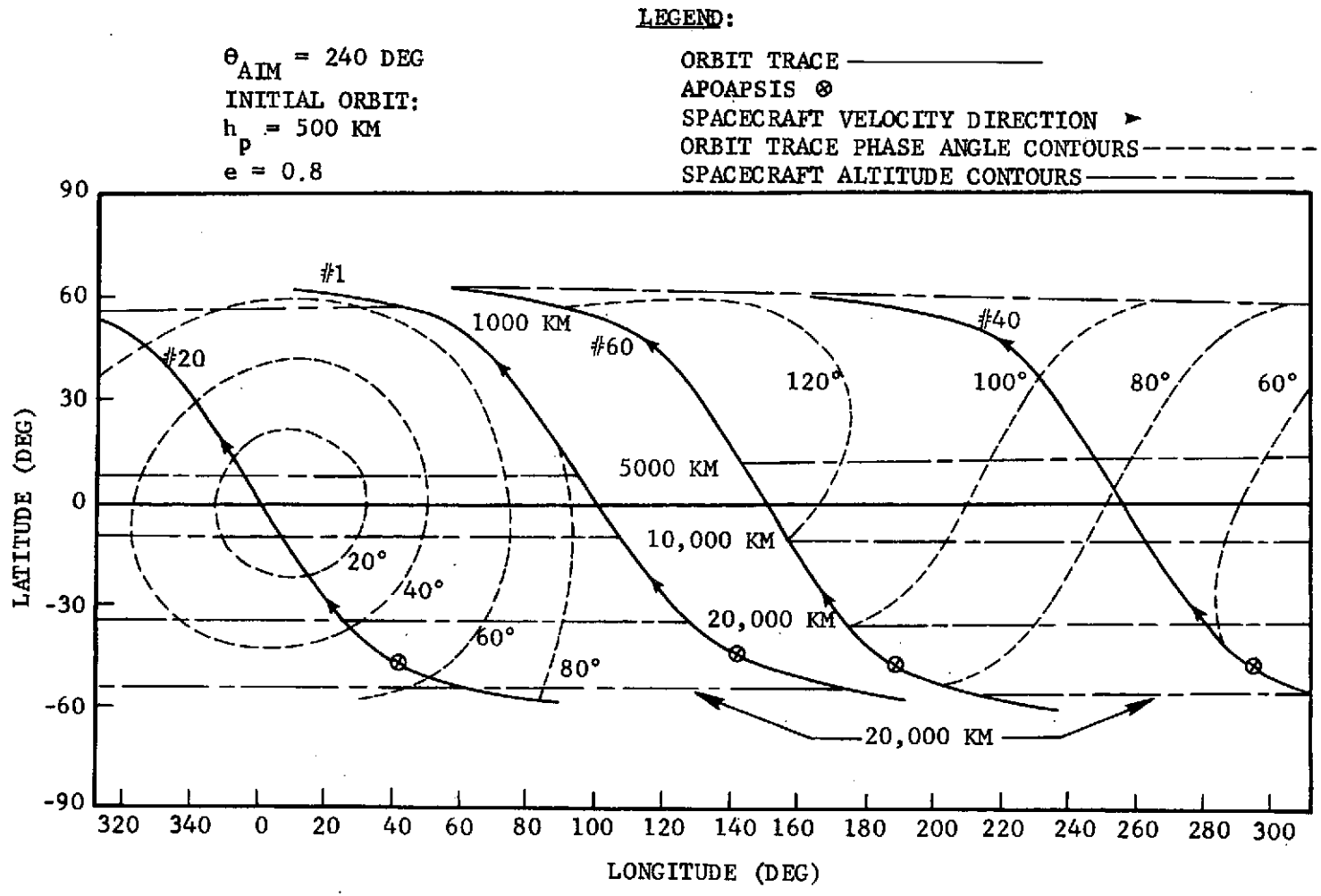

FIGURE V-3 PLANET COVERAGE, 1980 MISSION, ORBITS 1 TO 60, ASCENDING SEGMENT

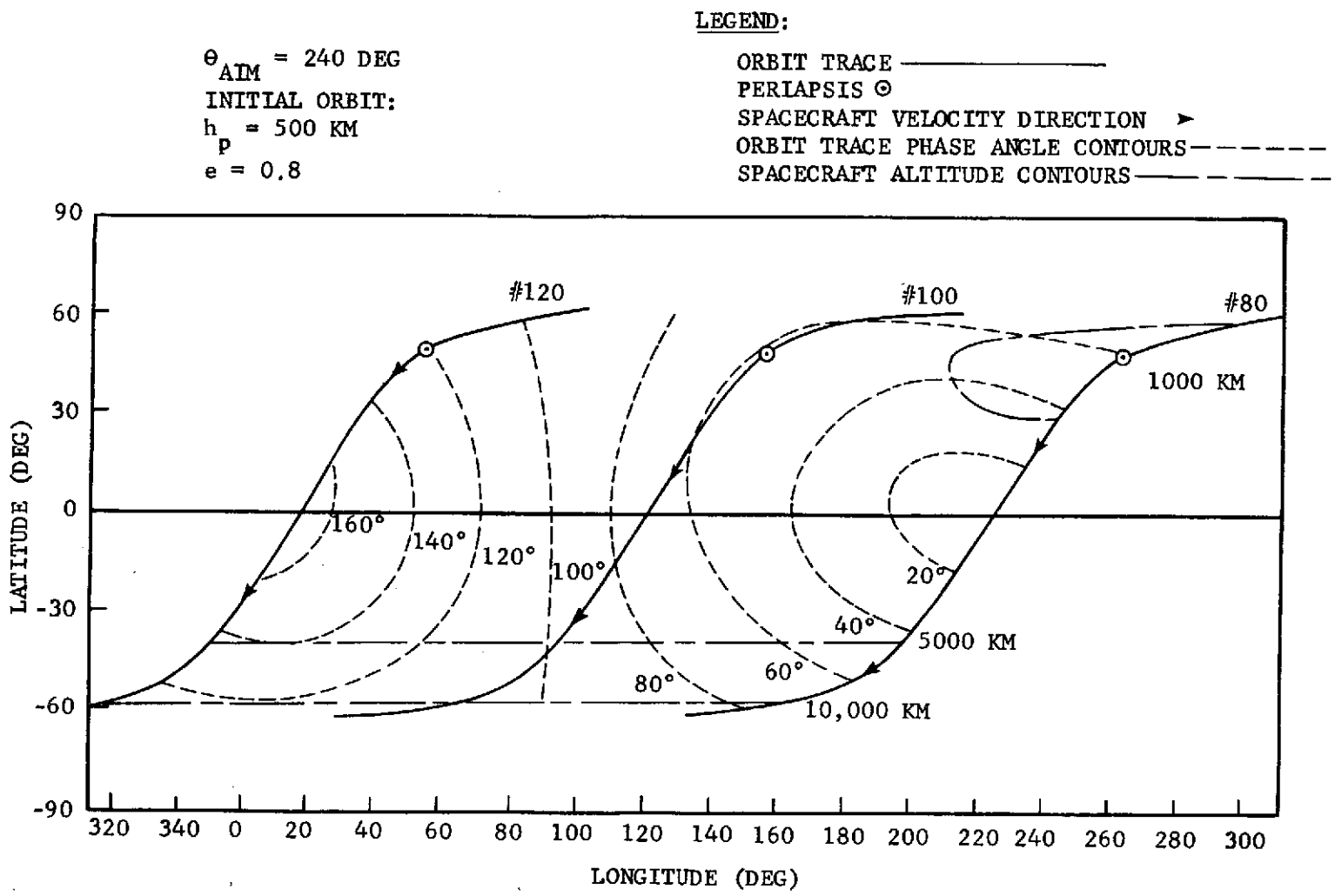

FIGURE V-4 PLANET COVERAGE, 1980 MISSION, ORBITS 80 TO 120, DESCENDING SEGMENT

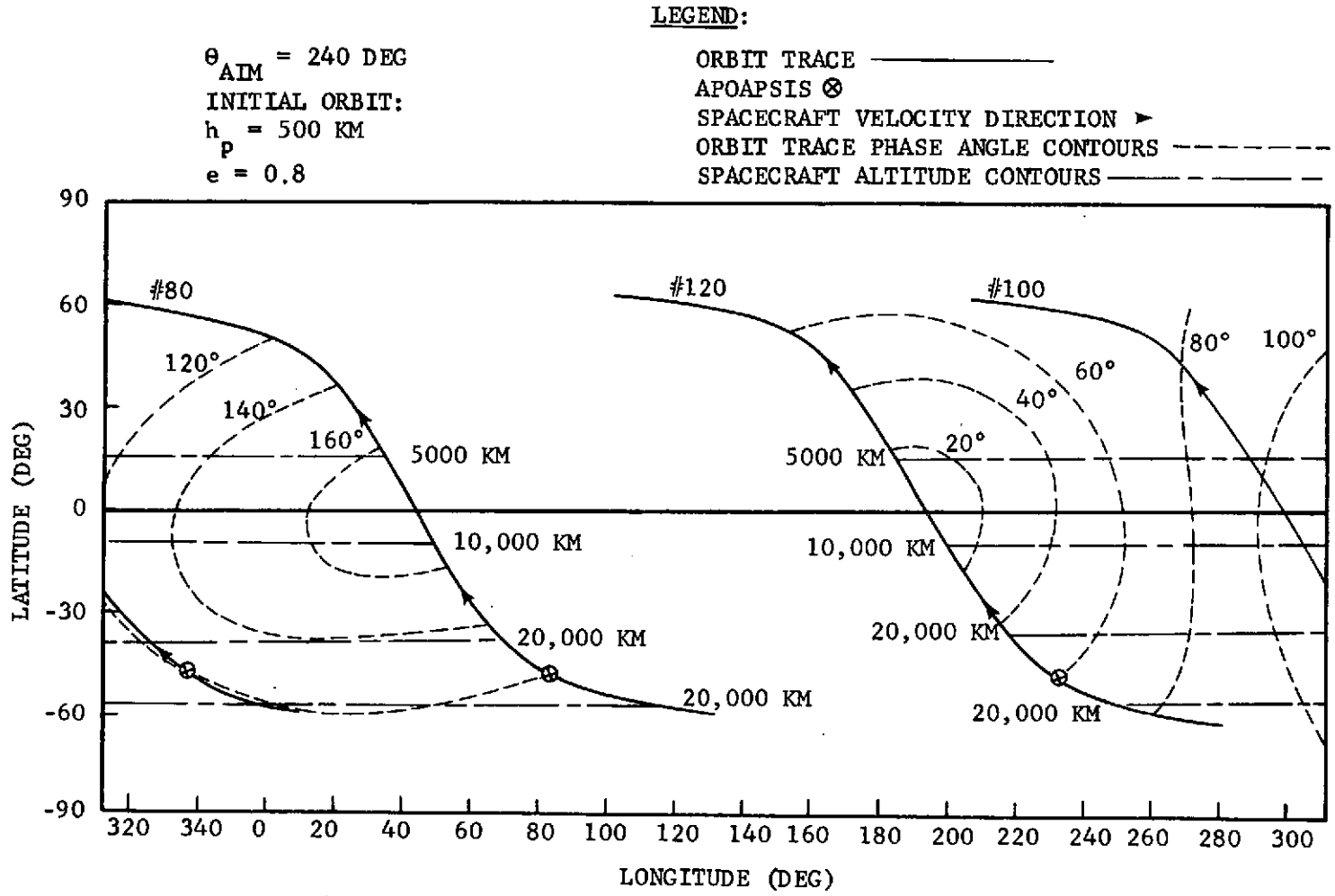

FIGURE V-5 PLANET COVERAGE, 1980 MISSION, ORBITS 80 TO 120, ASCENDING SEGMENT

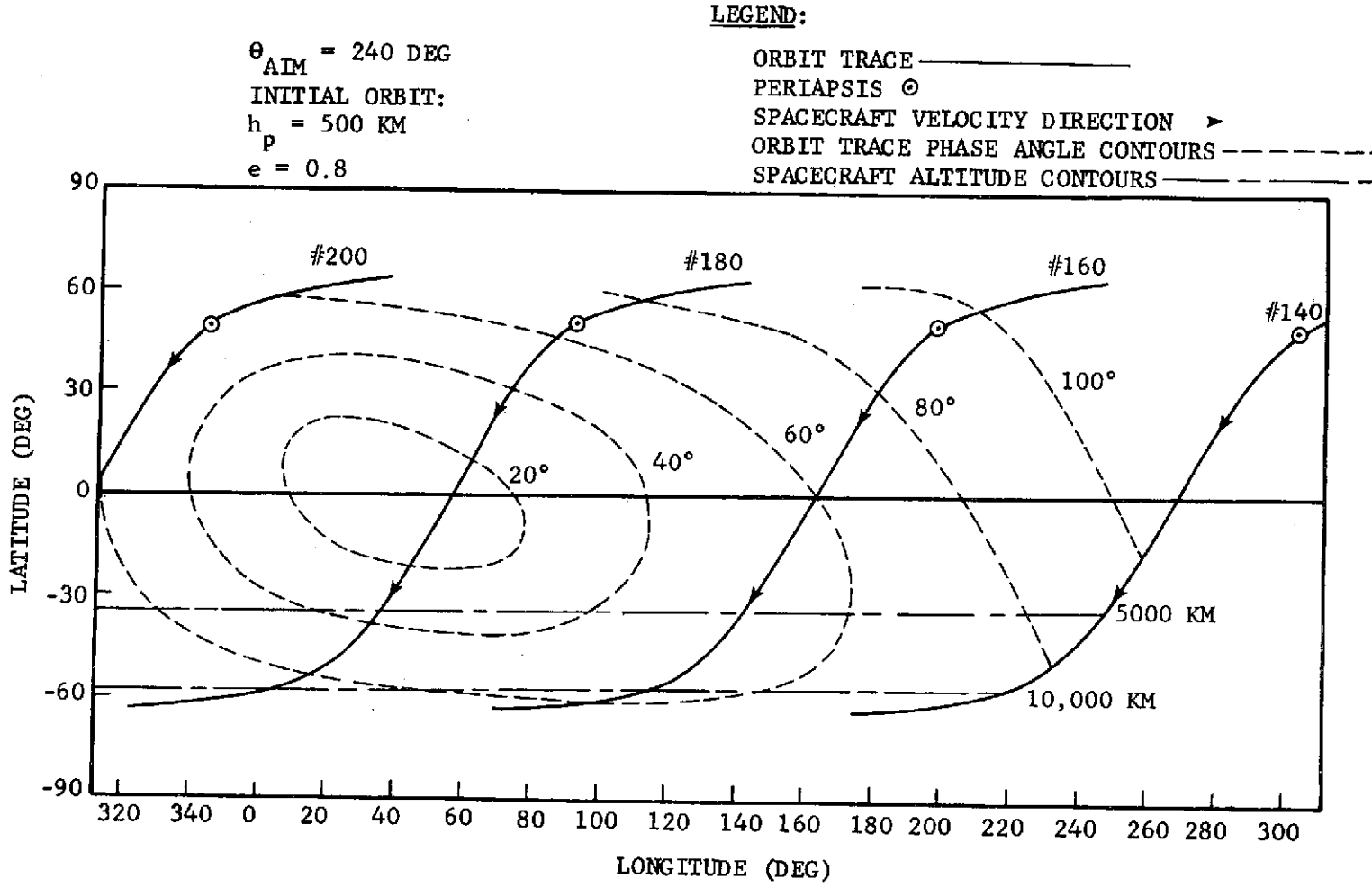

FIGURE V-6 PLANET COVERAGE, 1980 MISSION, ORBITS 140 TO 200, DESCENDING SEGMENT

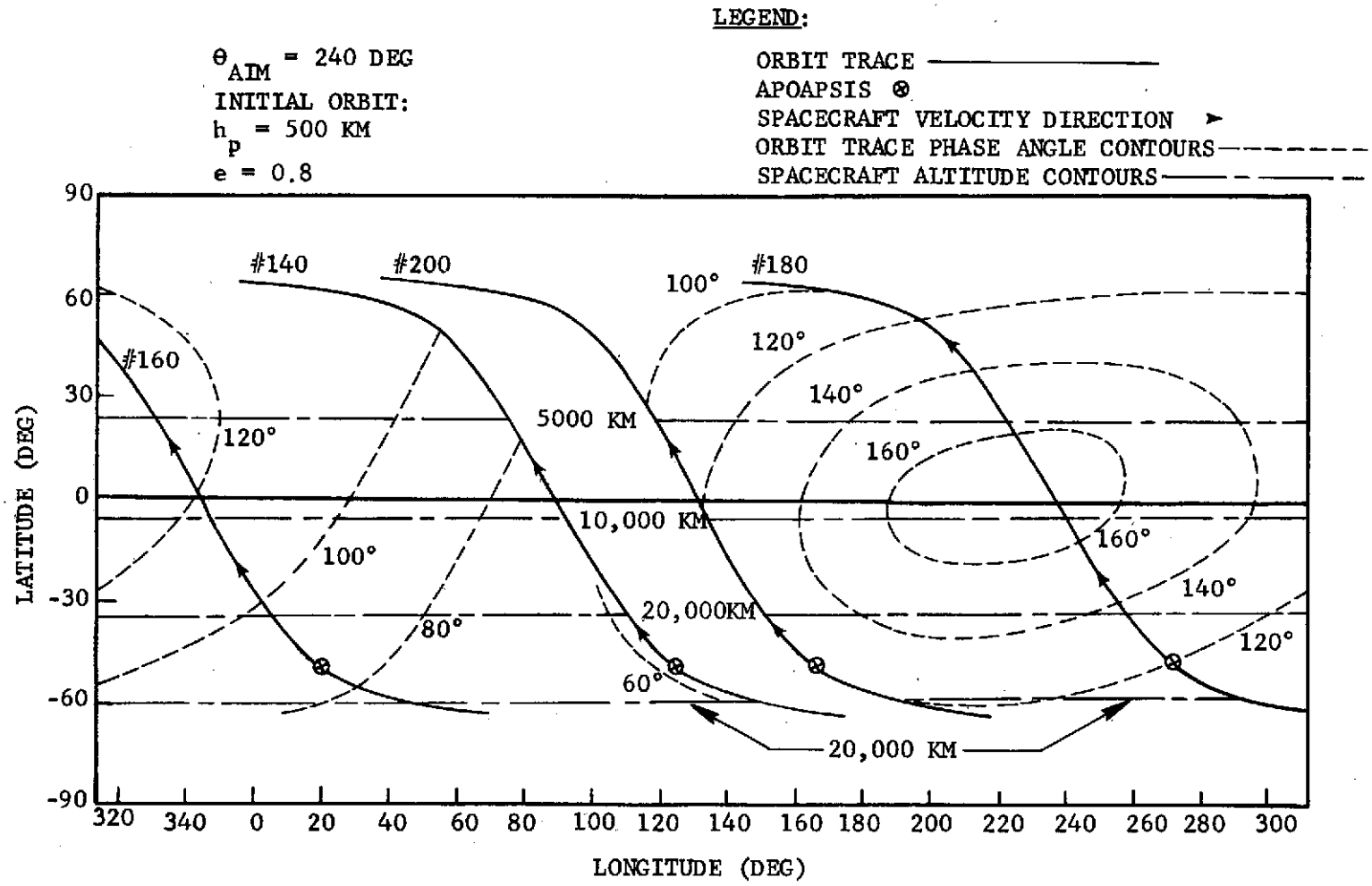

FIGURE V-7 PLANET COVERAGE, 1980 MISSION, ORBITS 140 TO 200, ASCENDING SEGMENT

MAPPING COVERAGE (RESOLUTION = .25 to 1. KM)

r = ANGLE OF REFLECTANCE, N = NUMBER OF IMAGES

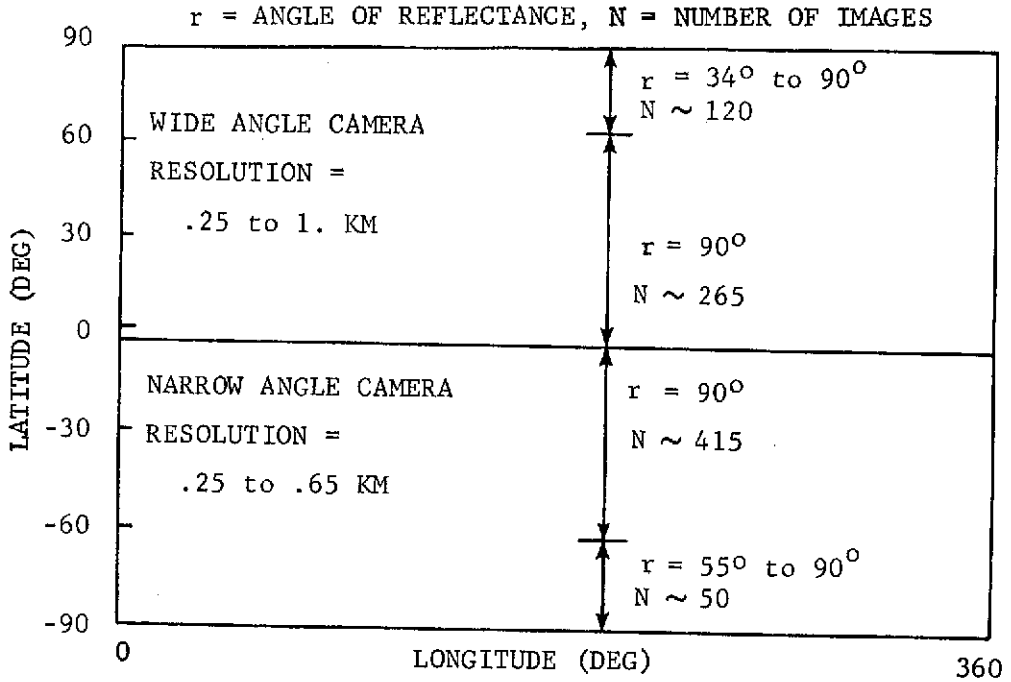

HIGH RESOLUTION IMAGING OPPORTUNITIES

(100 METER OR BETTER, 60% OF THE PLANET IS ACCESSIBLE)

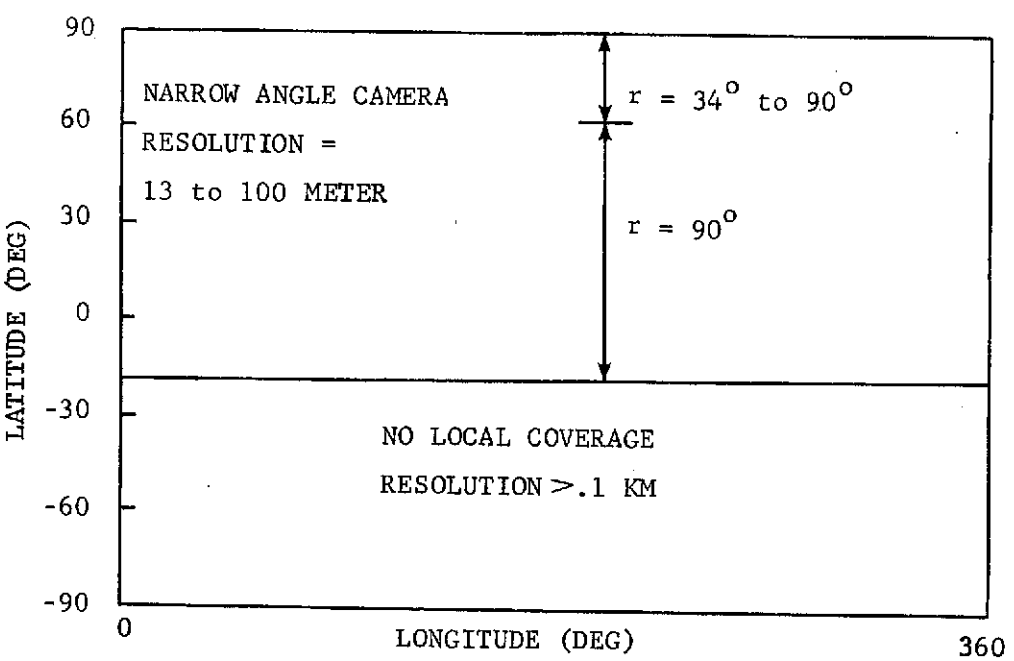

FIGURE V-8 PLANET COVERAGE SUMMARY

taking 8 regional mapping images per orbit and 1 full-planet image every other orbit, resulting in a full-planet picture every 7.2 degrees in planetocentric longitude. Therefore, in this scheme, 5 high-resolution pictures can be taken each orbit, and one picture every other orbit is available to take duplicate high-resolution or mapping scenes at different phase angles. During the second three months, 13 local images and 1 duplicate scene at different phase angles can be taken each orbit.

D. DATA MANAGEMENT

Since the data storage and transmission requirements of all the other science instruments combined are negligible compared with the imaging requirements, the data handling and communications systems should be sized according to the imaging requirements. The imaging data management requirement is about 14 images per orbit which amounts to 7.2×10^7 bits/orbit assuming an 800 x 800 pixel array and 8 bit encoding.

The data transmission and storage requirements are dependent upon: Earth-Mercury geometry, Solar and Earth occultations, and S/C antenna pointing. Each of these is discussed in the following paragraphs.

Earth Mercury Geometry - The important communication parameters upon which the size of the spacecraft communication system depends are the Earth-Mercury distance and the Sun-Earth-Mercury angle (Figure V-9). Worst case conditions are those associated with superior conjunction, at which point the signal to noise ratio is degraded by the increased distance and by the RF interference caused by solar radio emission and the transmission characteristics of the solar corona and the dense solar plasma in the vicinity of the Sun. A similar situation occurs at inferior conjunction, but signal degradation is much less severe in this case due to the decreased communication distance and no transmission attenuation through the coronal plasma. The effects of the solar interference which occurs during conjunctions (Figure V-9) can be minimized with the use of the Arecibo facilities. During the first 120 days after insertion of the 1980 mission, for instance, Arecibo can be in contact with the spacecraft each day (Appendix 3).

Solar and Earth Occultations - The S/C may not be capable of transmitting

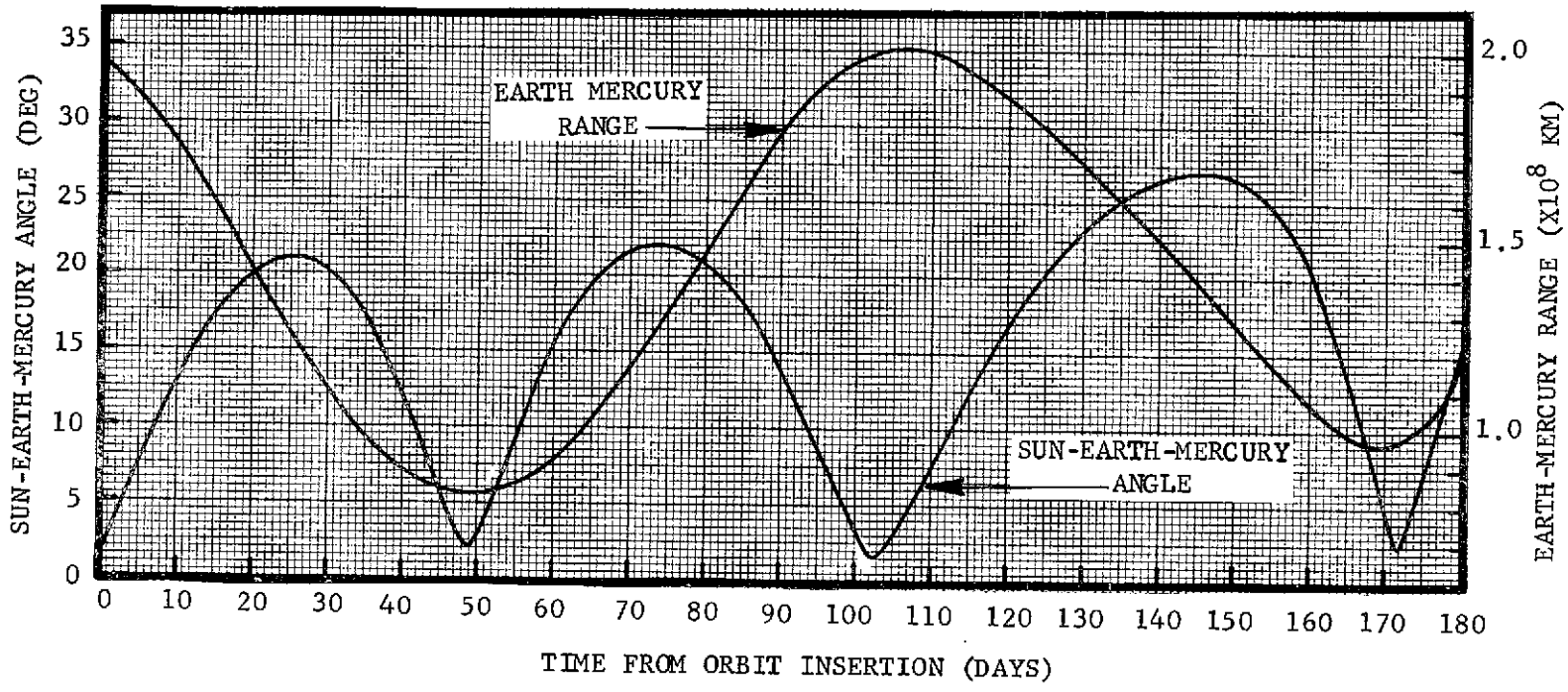

FIGURE V- 9 COMMUNICATION GEOMETRY, 1980 MISSION

during solar occultations if it operates on solar power and of course the S/C cannot transmit to Earth during Earth occultations. The only Earth occultations for the 1980 mission occur near superior conjunction when Earth and solar occultations occur simultaneously. Since there appears to be little demand for taking pictures during solar occultations, the data storage requirements will be minimum.

S/C Antenna Pointing - The antenna pointing requirements have not been analyzed because they depend on the S/C axis orientation, which is beyond the scope of this contract.

The minimum Sun-Earth-Mercury angle for the 1980 mission, which occurs on the 102^{nd} day of the mission is 1.62 degrees, corresponding to an apparent Sun-Mercury separation of about 6 solar radii as viewed from the Earth. Unless the transmitter signal is of sufficient strength to overcome these adverse conditions, there will probably be several days in which there will be little or no data transmission. The options would then be either to store the data, or else to reduce or stop taking data. The latter option seems preferable, since the 176-day mission allows ample opportunity for excellent planet coverage, even accounting for these interruptions. If this approach is followed, the data storage system can be sized according to normal orbit communication opportunities, which are dependent upon the antenna configuration and S/C axis orientation.

THIS
PAGE
BLANK

VI. TECHNOLOGY EVALUATION

VI. TECHNOLOGY EVALUATION

This part of the study report presents the results of investigations made to identify the technology requirements for implementation of a Mercury Orbiter Vehicle design, development and operation. The required vehicle systems are identified with their related technology evaluation and recommended design approaches. There were no technology areas identified which require research studies to substantiate feasibility of implementing a vehicle design.

Several approaches to vehicle configuration are possible. The stabilization mode, one of the most decisive influencing factors, may be designed for spin or three-axis stabilization. The reliability and functioning for the vehicle operating systems and science instruments are most affected by the natural solar environments, UV radiation, solar flare protons, solar wind, and in particular, solar thermal flux, which are high because of the small solar distance (.31 to .47 AU). These environments coupled with the IR flux experienced during subsolar Mercury periapsis transit imply that the main technological problems are in the area of thermal control and associated questions of subsystem environmental stability and protection.

For the purpose of this study, technology requirements were categorized for criticality based upon the state-of-the-art for each discipline involved and the technical study, design or developmental effort which may be necessary to provide operating systems which will satisfy the requirements of the Mercury Orbiter mission. The technology evaluation definitions used are as follows:

1) Non Critical (NC) - Similar requirements have been met with existing proven designs.
2) Low Criticality (LC) - Similar requirements have been met through design or development with prototype and/or model testing.
3) Medium Criticality (MC) - Similar requirements have been met through design studies and implementation of system level or conceptual design.
4) High Criticality (HC) - Specific design data satisfying the requirements is not available; related technology studies and supporting research provide direction for technical and design studies.

A. MISSION REQUIREMENTS

1. Mission Phases

Determination of spacecraft functional requirements must first be made in order to define the necessary vehicle subsystems. The subsystems defined must then be designed to perform their required functions for the life of the mission while subjected to the induced and natural environments which may occur. Functional requirements were determined by dividing the mission into specific phases, detailing the operations required during these phases, and subsequently, the systems required to perform these operations. Five mission phases were defined within which to categorize vehicle functions, these are the pre-launch phase, the launch, separation and acquisition phase, the cruise and encounter phase, the insertion phase and the post-insertion and orbit phase. Table VI-1 lists these phases and their related functional requirements and subsystems.

2. Mission Performance Requirements

During the prelaunch and launch, separation and acquisition phases, no mission peculiar requirements are encountered which necessitate functioning systems different from those common to most spacecraft launches. The cruise and encounter phase includes all vehicle activities required after separation from the launch vehicle and establishment of a communications link through encounter with Mercury. Vehicle performance parameters and maneuver requirements for this phase are reflected in Table III-2. Significant subsystem design requirements include environmental compatibility with the increasing affects of solar energy and adequate power generation for both near and far solar distances. Other functional requirements, although mission and design peculiar, are within proven system design technologies. The mission parameters and performance requirements for the orbit insertion and orbiting phases of the mission are also reflected in Table III-2, and, like those for the cruise and encounter phase, reflect functional requirements demanding more critical technological evaluation in the areas of environmental control and power generation.

TABLE VI-1

FUNCTIONAL REQUIREMENTS FOR A TYPICAL MERCURY ORBITER MISSION

MISSION PHASE	FUNCTIONAL REQUIREMENTS	FUNCTIONING SYSTEM
PRE-LAUNCH	Checkout	Power (Ground Supply) Data Management Telecomm. (Closed Loop)
LAUNCH SEPARATION & ACQUISITION	Communications Attitude Control Data Monitor	Power Data Management Telecommunications ACS Propulsion (ACS) Instrumentation Structural/Mechanical
CRUISE & ENCOUNTER	Communications Attitude Control Δ V Maneuvers Data Monitor & Storage Environmental Control (9 to 27 months)	Power Data Management Telecommunications ACS Propulsion Instrumentation Thermal Control Pyrotechnic Structural/Mechanical Science Instruments
ORBIT INSERTION	Communications Attitude Control Insertion Δ V Data Monitor & Storage Environmental Control Prop. Module Separation	Power Data Management Telecommunications ACS Propulsion Instrumentation Thermal Control Pyrotechnic Structural/Mechanical Science Instruments
POST INSERTION AND ORBIT	Communications Attitude Control Science Instr. Control Data Monitor & Storage Environmental Control Orbit Adjust (6 months typical)	Power Data Management Telecommunications ACS Propulsion Instrumentation Thermal Control Pyrotechnic Structural/Mechanical Science Instruments

3. Science Requirements

The major functional requirements peculiar to or impacted by the science requirements occur with the imaging system including, scan platform control and data management and telecommunications. As with the technology requirements for meeting the mission design, environmental control and power generation are of prime significance. Imaging system design must be peculiar to its specific application and consequently systems technology for design approach and application to Mercury mapping was evaluated. Imaging system requirements are reflected in Section V.C, Mapping Strategies.

B. SUBSYSTEM TECHNOLOGY OPTIONS

As indicated earlier, one of the most decisive factors influencing the overall vehicle configuration is the selection of the stabilization mode, either spin stabilized or three-axis stabilized. Since each of these design approaches can be defined for this study as non-critical, the disciplines investigated have been evaluated for application to both spin and three-axis stabilized vehicles.

1. Thermal Control System

Virtually all vehicle subsystems or components are affected by temperature variations and extremes. Consequently, the thermal control system design becomes a vital element in the spacecraft upon which most all other vehicle subsystems are to some degree dependent. Temperature control for sub-normal temperatures may be accommodated with relative ease through the use of super-insulation, controlled heating elements and the utilization of heat generated by on-board functioning subsystems. Likewise, systems for protection from and dissipation of excess thermal energy through the use of super-insulation, low absorptivity (α) and high emissivity (ϵ) coatings and louver systems have proven quite successful. However, thermal control system design for protection from the severe environment encountered at Mercury poses a greater challenge to this technology.

The Mercury orbit thermal environment is the most hostile of any of the known planets. The direct solar flux alone is formidable, ranging up to 11 times the Earth solar constant at Mercury perihelion. This flux is manageable however because its energy is concentrated in the visible light band. This

allows the use of surfaces on the spacecraft which are highly reflective (low absorptivity, α) to the solar flux, while at the same time possessing a high emissivity (ϵ) in the infra-red band, so that the non-reflected fraction of the solar flux can be efficiently radiated to deep space. Further, the solar radiation is from a specific direction so that spacecraft surface aspect angles can be chosen to reduce absorbed solar heat to small levels. Consequently, if direct solar flux alone is considered, spacecraft temperatures can be maintained within ranges normally required for operating equipment.

Planetary energy emission however imposes a significant addition to the thermal energy which the spacecraft design must withstand. Mercury's surface is primarily a solar absorber with a solar reflectivity = 0.07. (Reference VI-1.) This means that approximately 93% of the solar flux is absorbed and is emitted from the planet in the infra-red band. The planet's low rotation period causes the sunside surface temperature to reach essentially steady state values up to 705°K at perihelion. Under these conditions, a spacecraft at low altitude (500 km) at the subsolar point will encounter an infra-red flux from the planet surface equivalent to 9-10 "suns," in addition to the 11 "sun" direct solar flux. Since the planetary albedo is relatively small (average value .12) the radiant energy in the visible band is equivalent to less than 1 sun and therefore not considered a formidable contributor.

Of the radiant energy sources, the infra-red planetary radiation is the most troublesome. The reason for this is two-fold. First, the energy is diffusely emitted from the planet surface so that it arrives at the spacecraft surface from any direction that a line of sight exists to the planet. Second, gray body radiation characteristics are such that a surface possessing a high emissivity in a given wave band will also be a good absorber in that band. Thus, the surfaces which efficiently reflect visible band energy and emit infra-red will absorb a large portion of the incident infra-red flux.

Figure VI-1 reflects the radiant infra-red flux expected during the worst case Mercury orbit for the 1980 mission. Curves are shown for orbits with initial periapsis altitudes of 500, 1000, 1500, and 2000 kilometers.

Existing thermal control system design for spacecraft application which most closely approaches the environment and requirements of a Mercury orbiter

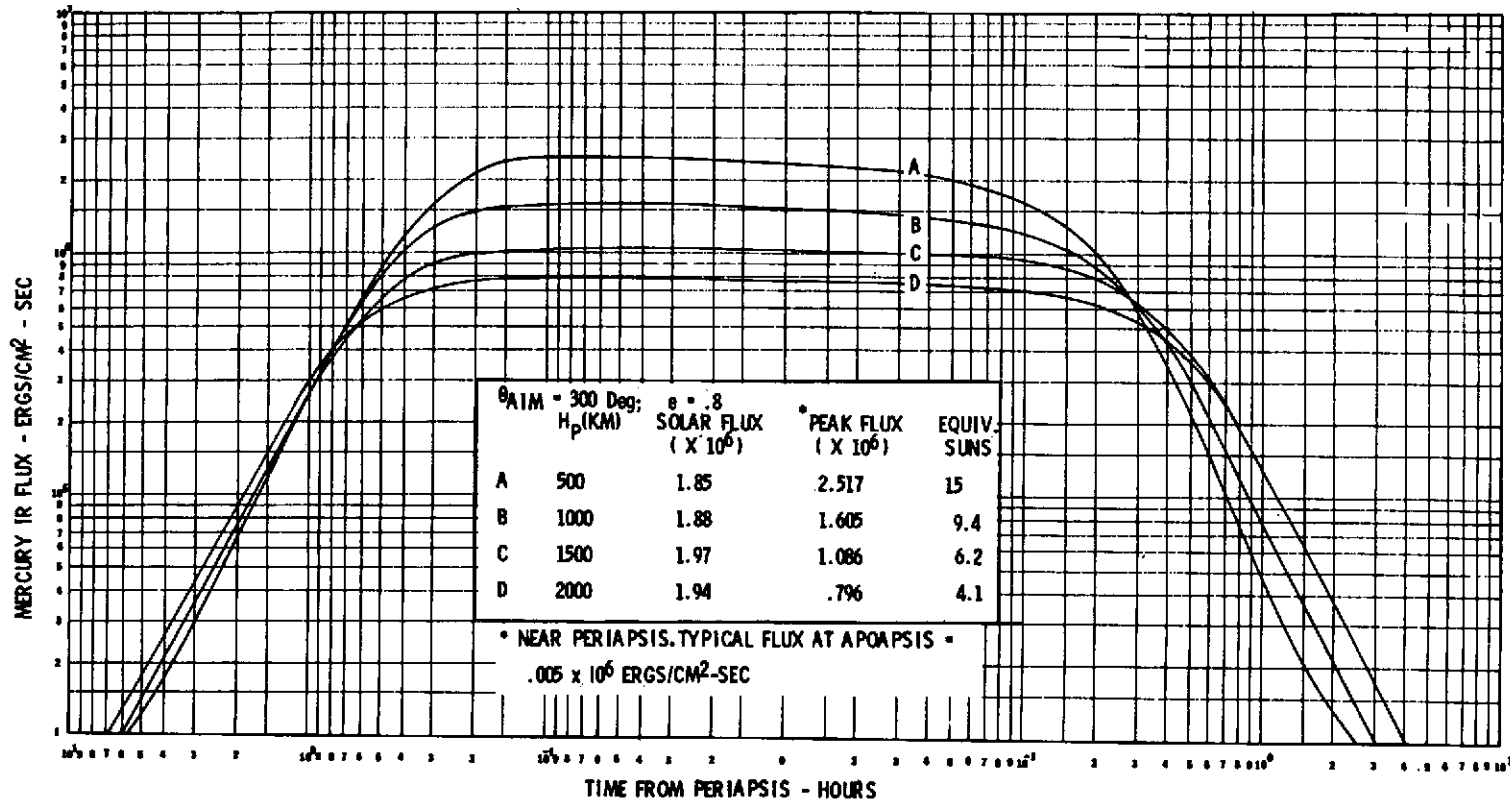

	H_p(KM)	SOLAR FLUX (X 10^6)	*PEAK FLUX (X 10^6)	EQUIV. SUNS
A	500	1.85	2.517	15
B	1000	1.88	1.605	9.4
C	1500	1.97	1.086	6.2
D	2000	1.94	.796	4.1

FIGURE VI - 1 Orbiter Thermal Environment, 1980 Mission

is that for the Helios vehicle, scheduled for launch in the fall of 1974 and designed for flyby of the sun at a solar distance of .25 AU. A review of the thermal control capabilities of this design (Ref. VI-2,3) reveals that the equipment bay is maintained between -10 and +30°C and the solar array panels between -65 and +180°C. The upper limits essentially reflect a maximum steady-state operating temperature that will be sustained during perihelion. The solar intensity at this time is equivalent to 16 "suns" for a duration of approximately three weeks. At a solar distance of .3 AU (approximately 11 "suns") this thermal control design will maintain a thermal balance at an array temperature of 120°C.

Figure VI-2 reflects a thermal balance curve for the Helios design showing a capability of 1.2×10^{11} ergs/sec at .25 AU; at .3 AU the system maintains a balance at an energy level of 9.5×10^{10} ergs/sec, while operating at 120°C. The dashed curve in Figure VI-2 reflects the allowable additional thermal energy the Helios system will accommodate as the temperature is increased, indicating an allowable change slightly in excess of 1×10^{6} ergs/sec-cm^2 at maximum operating temperature of 180°. Applying this allowable thermal flux delta level to Figure VI-1, it can be seen that the representative Mercury mission with (subsolar) periapsis altitudes of 1500 km or greater have thermal environments within current design capabilities. The (Helios) truncated cone type design would require modification to provide the necessary incidence to emission area ratio to balance the accommodation of added flux with loss of the heat sink in the anti-solar direction. This may be accomplished for a spinning spacecraft with spin axis normal to the incident flux by increasing the angle of the truncated cone thereby decreasing the effective incidence area and increasing the effective emittance area.

This design approach is peculiar to a spin stabilized spacecraft and would not be effective for a three-axis stabilization mode. Although existing or prototype design configurations are not available for a three-axis stabilized vehicle designed to an environment approaching that of the Mercury Orbiter, a Mariner type vehicle utilizing a super insulation heat shield to provide thermal "lag" protection during subsolar transit, and active incidence angle control (for solar cell panels) for reduction of exposure to planetary emission during close approach will survive the orbital environments. This type of

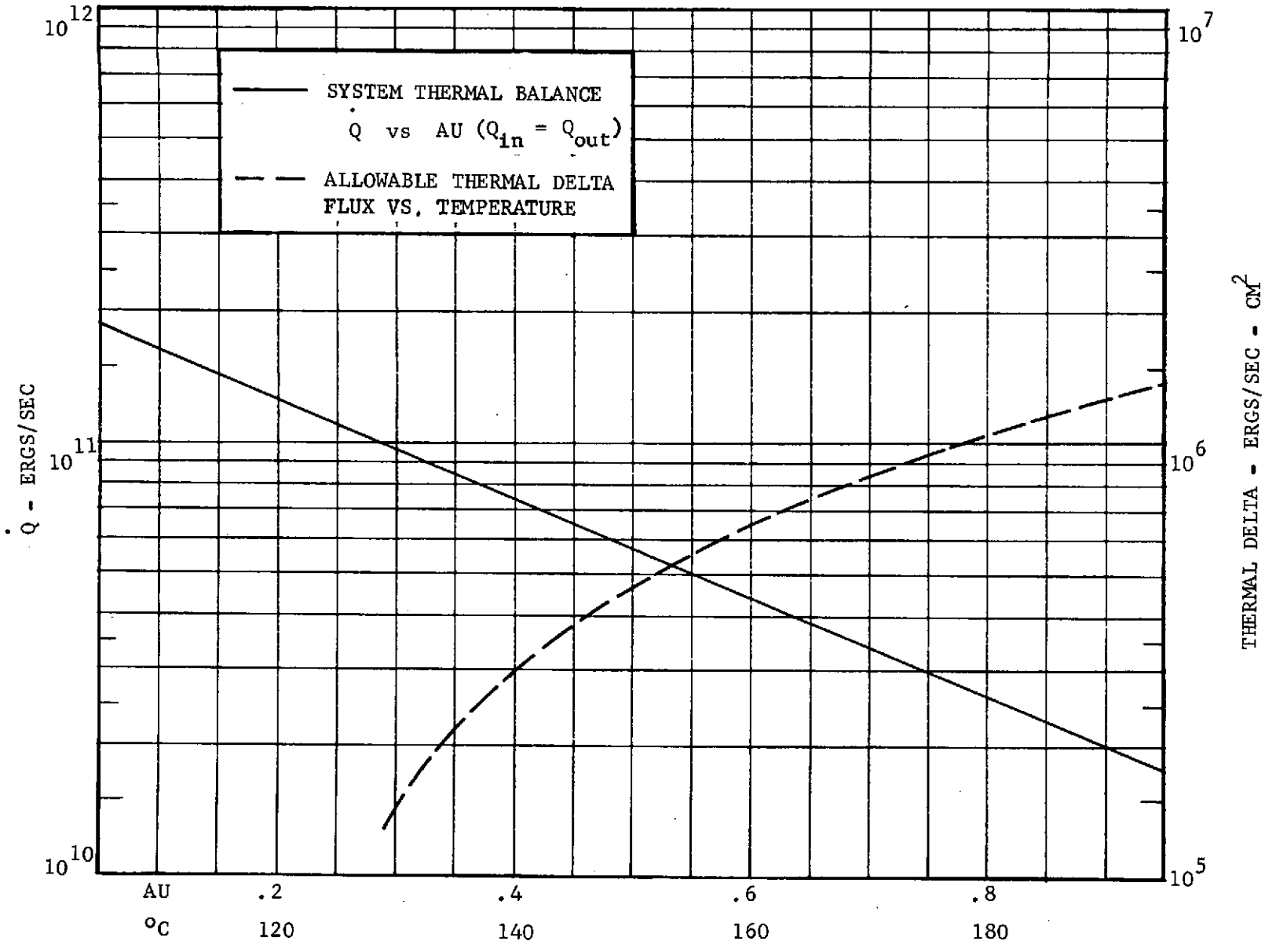

FIGURE VI-2 HELIOS MODELED THERMAL CONTROL SYSTEM

control will also degrade the optimum sun incidence angle for power generation. For the worst case condition, the period of concern is less than 2 hours.

An alternate thermal design approach for a three-axis stabilized vehicle utilizes a solar collector and thermoelectric power generation system which can operate effectively at higher temperatures and is less susceptible to degradation and damage from periodic temperature (thermal flux) increases. This approach would also require a thermal "lag" heat shield for protection during subsolar transit. Heat shield absorber coatings which remain stable up to temperatures of 1000°C are available (Ref. VI-4). These coatings coupled with insulation systems possessing mean thermal conductivity as low as 10^{-4} W/cm °K (Ref. VI-5) would provide protection to a thermally decoupled equipment bay located in the "shade" of the shield. Sun orientation for the solar collector and planet orientation for the heat shield are necessary for this approach.

It is expected that detailed thermal analysis may show temperature problems with individual equipment components which require insulation blanket or heat shield penetrations. These problems may be eliminated by thermal isolation in the structural design, coupled where necessary with phase change material (PCM) heat sinks which will provide energy storage during critical (high thermal flux) periods with release as the orbital thermal environment decreases. Candidate phase change materials reviewed (Ref. VI-6) showed the availability of hydrated salts with melting points within the required temperature range possessing latent heat properties ranging up to 160 BTU per lb ($\sim 17 \times 10^{11}$ ergs/lb). Utilizing the flux levels shown in Figure VI-1 for the 500 km periapsis altitude, incident planetary energy during transit is 5.85×10^{9} ergs/cm^2. Assuming 50% effectivity in the PCM absorber due to requirements for thermal conductors, packaging, etc., a one pound PCM absorber package with a latent heat property of 160 BTU per lb will accommodate a "hot" spot area of approximately 140 cm^2.

The following conclusions are drawn from the thermal control system technology evaluation:

a) The first consideration for approach to thermal control system design should be selection of orbit geometry for minimum exposure to the thermal

environment consistent with science objectives and selected instrumentation.

b) Equipment bay thermal control while in Mercury orbit may be accomplished through the use of low absorptivity thermal coatings (Optical Solar Reflectors) coupled with super insulation and a thermally controlled louver system.

c) For a spin-stabilized vehicle, the Helios TCS design proves the feasibility of providing a system which will function within severe thermal environments similar to those anticipated for a Mercury Orbiter.

d) Solar panel thermal control must be achieved through incidence angle control and restriction on periapsis altitude.

e) For a three-axis stabilized vehicle utilization of a solar powered thermoelectric generator will eliminate the need for a mechanical control system for solar arrays, and relax overall temperature constraints.

f) Phase change materials offer a reasonable means for accommodating "hot" spots.

Table VI-2 reflects the thermal control system approaches evaluated and their assessed criticalities.

2. Electrical Power System

Power system alternatives investigated included those systems which utilize solar and thermal energy for conversion to electrical power; specifically, photovoltaic systems (solar cells), thermoelectric systems and thermionic systems. Of these three, the thermionic system was found to be the most critical technology application for a planet orbiting spacecraft, with the greatest impact on other vehicle systems.

Recent developments in lithium doping of solar cells have improved cell survivability and efficiency of operation in solar proton flux. Additionally, development of a welding process for panel interconnections has allowed design and development of a solar array system (Helios Vehicle) that will satisfactorily perform at 180°C rather than the customary constraint of 160°C imposed by soldered interconnections (Ref. VI-7). These improvements in solar cell technology enhance the adaptation of this type system for a space-

TABLE VI-2 Thermal Control System Options

TCS ELEMENTS / VEHICLE STABILIZATION MODE	THERMAL COATINGS	OPTICAL SOLAR REFLECTORS	THERMAL INSULATION	HEAT SHIELD	PHASE CHANGE MAT'L	THERMAL LOUVERS	REMARKS
Spin	LC	NC	LC	--	MC	LC	Minimum impact on ACS
Three-Axis W/Solar Cell Power System	LC	NC	LC	MC	MC	LC	Requires active Panel Control System; Requires Sun Pointing
Three-Axis W/Thermo-electric Power System	MC	--	LC	MC	MC	LC	Requires Sun Pointing

Technology Assessment:

NC - Non Critical

LC - Low Criticality

MC - Medium Criticality

HC - High Criticality

craft designed for operation at Mercury's distance from the sun (.31 to .47 AU). At 200°C, cell efficiency has declined to approximately 50%, see Figure VI-3(a), reaching 0 at approximately 235°C. As the distance to the sun decreases, however, solar panel tilting can maintain temperature levels for almost constant power output since the solar illuminance is increasing. Figure VI-3(b) shows the solar cell temperature that can be expected for panel tilt angles of 60, 70, and 80°. For an average Mercury sun distance of .38 AU, maximum power output corresponds to a tilt angle of about 70 deg. (Ref. VI-8).

As indicated in the discussion on thermal system techniques, if solar thermal energy alone is considered, the design problems are well within the capability of existing systems; the solar cell limiting operating temperature of 180°C is reached rapidly however when Mercury's thermal flux is encountered.

Solar cell arrays utilized on a three-axis stabilized vehicle require mounting normal to a sun oriented vehicle axis and installation on movable panels that may provide exposure to solar radiation at 90° in the vicinity of the earth with rotation (or folding) as the vehicle approaches the sun in order to prevent excessive heating. Additionally, as the vehicle orbits Mercury, the periodic (at periapsis) exposure to planetary flux emission, concurrent with the solar radiation, will require rotaton to a thermally compromising position (approaching panel-edge-only exposure to the sun), or folding to a protected area, precluding effective power generation during this period. This configuration incorporates a step motor to provide the rotational or folding force and a bimetallic mechanism for panel mounting to provide positioning control.

For spin stabilized vehicles (spin axis vertical to the ecliptic) the solar cells may be installed on a truncated cone surface designed to a cone angle that will assure required power at Mercury solar distance with maximum panel backside exposure to deep space for cooling. Effective near-earth operation could be accomplished by spin axis orientation so that the solar radiation incidence angle approaches 0°.

Each of these design approaches is within current state-of-the-art. In that the most significant limiting factor is the allowable temperature for solar cell operation, design studies cannot be conducted independently of those for the thermal control system.

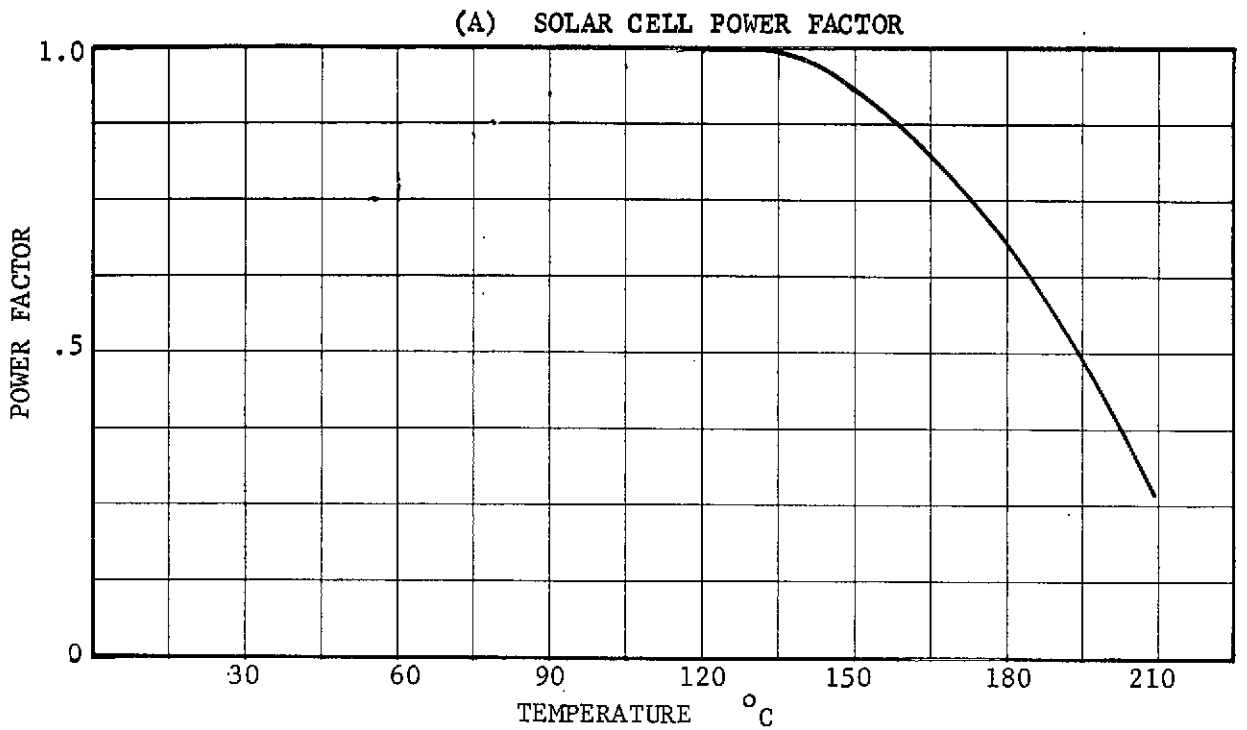

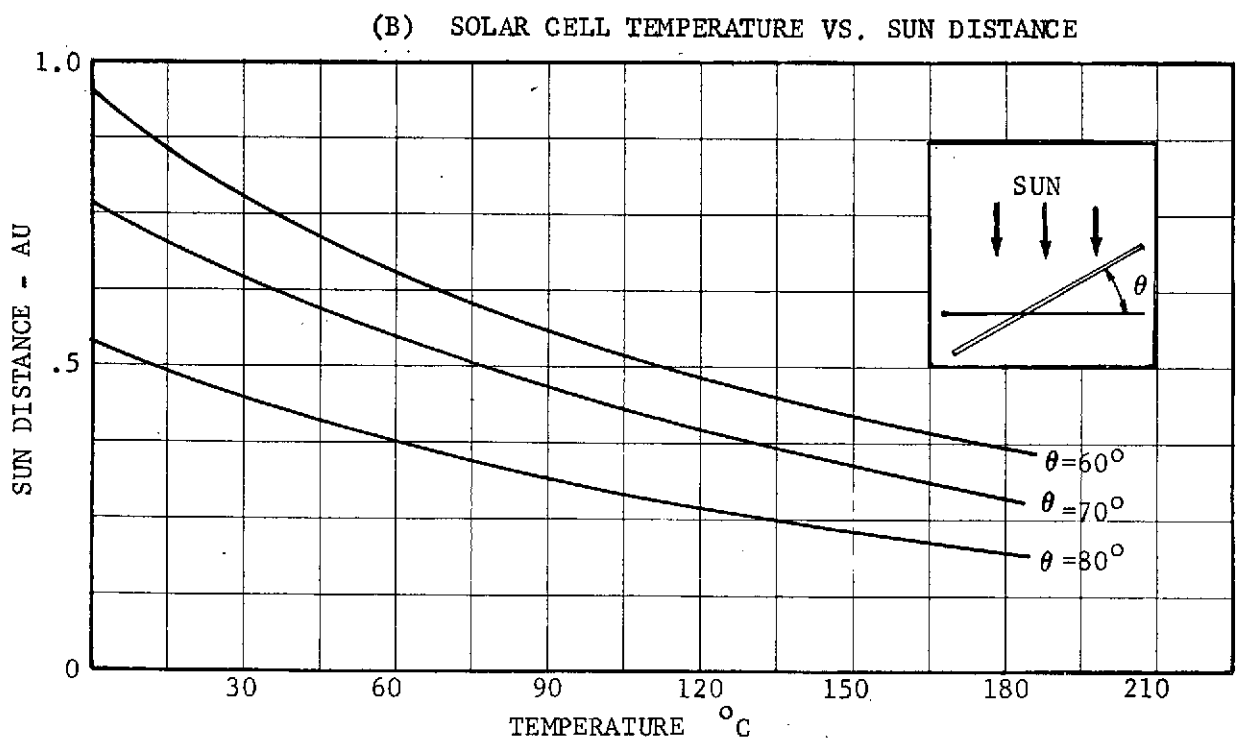

FIGURE VI-3 SOLAR POWER GENERATOR PERFORMANCE

The alternate approach considered for a power generation system is a solar powered thermoelectric (thermopile) system utilizing a flat plate solar collector (Ref. VI-9). An advantage of this approach is that the system requires a significant amount of thermal energy to operate effectively, thereby allowing higher operating temperatures and requiring a less complex thermal control design. Figure VI-4 reflects performance efficiency for the two principal thermoelectric technologies sufficiently advanced for application to space use. The operating voltage at maximum efficiency ranges from 15 to 30 V for the silicon germanium (Si-Ge) system and 2.8-5V for the lead telluride (Pb-Te) system; additionally, as indicated in Figure VI-4 the Si-Ge system maintains a higher performance level as temperature is increased making it a preferable system for the Mercury orbit environment.

Thermoelectric generator systems were found to be a little more than twice the weight of equivalent power solar cell systems, however, this weight is not considered prohibitive and current projections indicate efficiency improvements resulting in weight reductions up to 30%. Sizing for a nominal 200 watt system for operation at a mean solar distance of .38 AU and collector/radiator temperature of 800/200°C, resulted in a collector area of approximately .75 sq. meter and a radiator area of approximately .25 sq. meter, with collector/radiator weight less than 12 lbs.

Since the solar collector must take full advantage of the available solar radiation, sun orientation must be maintained. At Mercury sun distance, the collector absorptivity to emissivity ratio (α_s/ϵ) will approach 5.0 in order to achieve a "hot shoe" temperature approaching 900°C. Employment of this type system designed for operation at a mean solar distance of .38 AU, would require that near-earth and midcourse power demands be satisfied either by battery or through utilization of an auxiliary solar cell system which may be ejected upon Mercury encounter.

Application of the thermoelectric system can be made to both spin and three-axis stabilized vehicles. For a spin-stabilized vehicle, the spin axis must be sun oriented with a concentric solar collector. This type configuration will require greater complexity in orientation and control of an instrument scanning platform and a despun antenna. Adaptation to a three-axis stabilized vehicle has a minimal impact on other vehicle systems. Maintenance

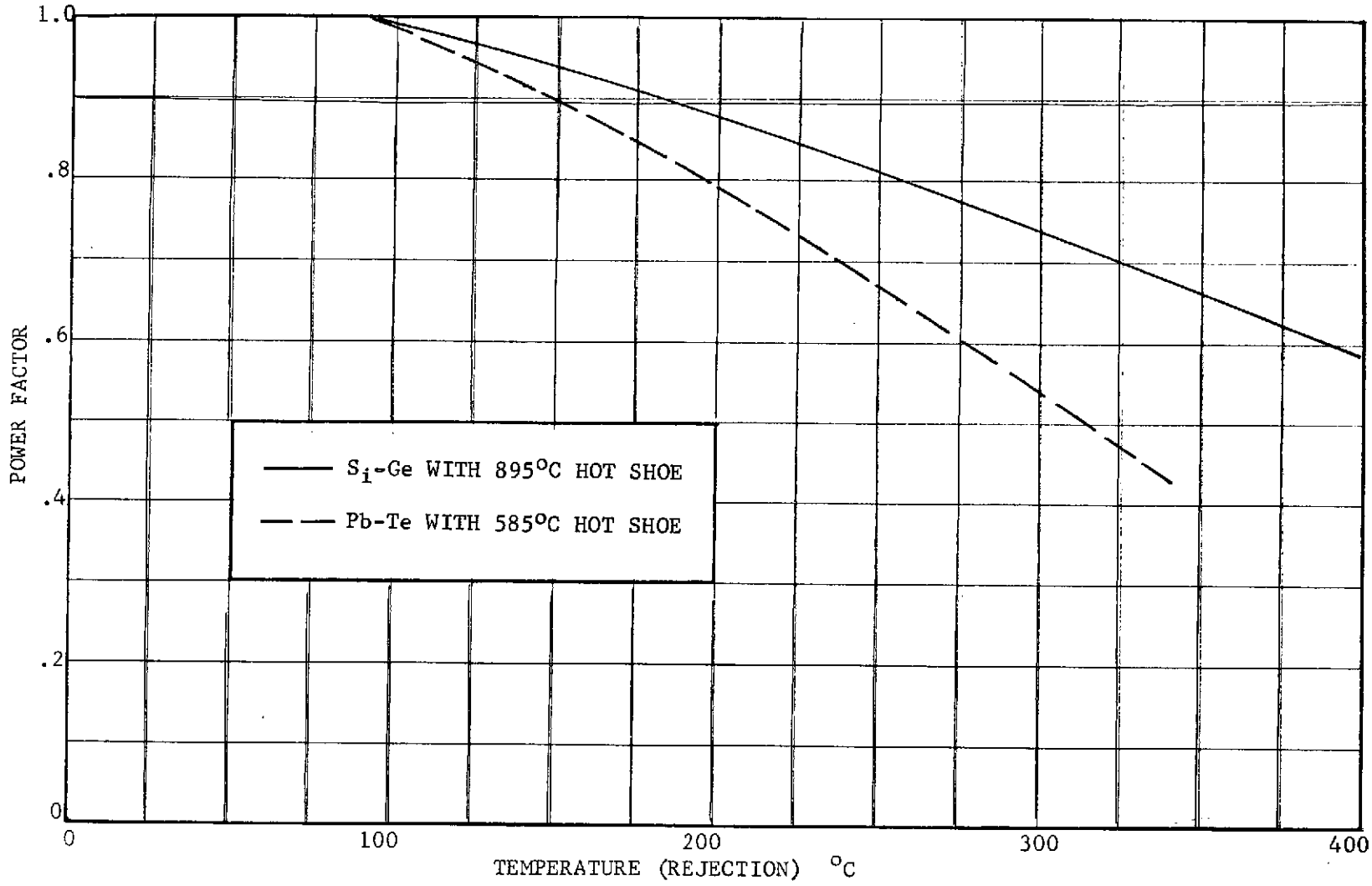

FIGURE VI-4 THERMOELECTRIC SOLAR GENERATOR POWER FACTOR

of sun orientation may be accomplished through the vehicle attitude control system or a collector step motor drive system.

Review of a thermionic system (Ref. VI-8) as an alternate for a power source did not indicate any advantages over solar cell or thermoelectric systems, although current technology should support design of a system for a Mercury Orbiter. The pointing accuracy required for the solar concentrator imposes mechanical and attitude control design requirements on the vehicle not otherwise required, increasing costs and reducing reliability and life in these areas.

The following conclusions are drawn from the electrical power system technology evaluation:

a) For a spin stabilized vehicle, the Helios power system design proves the feasibility of providing a system which will function within severe thermal environments similar to those anticipated for a Mercury Orbiter.

b) Solar thermoelectric power system technology is sufficiently developed to support design studies for a Mercury Orbiter application.

c) At Mercury's solar distance, a solar cell power system is more readily adaptable to a spin stabilized vehicle.

d) A solar thermoelectric power system requiring a solar collector is more readily adaptable to a three axis stabilized vehicle.

e) Thermionic power generator systems current technology is not competitive with solar cell or thermoelectric systems for space applications.

Table VI-3 reflects the electric power generator design approaches evaluated and their assessed criticalities.

3. Imaging System Options

A major science experiment for any planetary exploration mission is a visual imaging system. Pictures obtained from planetary surfaces and clouds can be a paramount contribution to the understanding of planetology, and provide an immediate two-dimensional understanding of the surface features and characteristics of the planet.

The imaging requirements postulated for the Mercury orbiter mission are reflected in Section V of this report. As referenced there, the type system

TABLE VI-3 Power Generator System Options

GENERATOR SYSTEM	VEHICLE STABILIZATION MODE	TECHNOLOGY ASSESSMENT	REMARKS
Solar Cell Array	Spin	LC	Most proven design technique.
	Three Axis	MC	Requires active panel tilt system
Thermo-electric Element	Spin	MC	Increases despin system requirements; requires auxiliary system for near Earth
	Three Axis	MC	Requires auxiliary system for near Earth
Therm-ionic	Spin	HC	Not competitive for spacecraft application.
	Three Axis	HC	

Technology Assessment:

LC - Low Criticality

MC - Medium Criticality

HC - High Criticality

modeled for science return estimates for this study was the MM'71 frame camera system (Ref. VI-10). Evaluation of potential use for a spin scan system was also made.

Most experience to date for spin scan imaging systems has come from geostationary satellites in near earth orbit, conditions under which relative motion between the spacecraft and the surface being viewed is small; for the Mercury Orbiter spacecraft - surface relative motion will be large. Studies are being conducted at Santa Barbara Research Laboratories for development of a scan imaging system, to operate from a spinning platform, for application to outer planet missions, where illuminance factors are inferior to Earth and relative spacecraft surface motions large. Utilization of this design concept for the Mercury Orbiter is feasible (Ref. VI-11); however, the low and constantly changing altitude experienced during the imaging sequence will increase the difficulty of matching scan line to scan line, necessitating a design providing sufficient detectors so that a large number of lines may be scanned per spin cycle. A percentage of these lines would allow for overlap matching.

The frame camera imaging system has been more widely used in space application to date. Camera characteristics critical to effective picture return are discussed in Section V of this report. As mentioned above, the MM'71 camera system was used as a model for a feasible Mercury Orbiter system. Because of the high camera to surface relative motion, the exposure time for the camera was reduced to assist in image motion compensation and reduce smear. The higher planet illuminance at Mercury in turn allows the shorter exposure. Picture taking rates, also discussed in Section V, are not a constraint on the imaging system for the mapping conditions considered. Assuming supporting subsystem design of sufficient capacity to record, store and transmit the camera system data output, the frame camera system then becomes a promising candidate for the Mercury Orbiter.

Camera control is required for mapping using either system, scan or frame, and control techniques for mounting on a spinning platform or a stable platform are represented in established systems. No critical technology problems are anticipated for camera control, either for a spin stabilized or three axis stabilized vehicle. Control on a spin stabilized vehicle, however, will

require a more complex system for viewing flexibility such as compound mirrors or a despun science platform.

A low criticality technology assessment has been assigned for a frame camera imaging system and medium criticality for a scan type imaging system.

4. Other Vehicle Systems

The technology evaluation for the remaining Mercury Orbiter vehicle subsystems has led to a non-critical or low criticality assessment in all cases. This assessment is based upon the determination that existing systems or system designs are available to satisfy functional requirements similar to those necessary for the Mercury Orbiter mission during the cruise and encounter, insertion, and orbit phases. Detailed study to determine the most appropriate design approach and subsequently the respective system elements for this approach was not a part of this contract. Certain major functional requirements however, which are key elements to the mission and science requirements, were evaluated for alternate approaches, the feasibility of these approaches, and past or current programs whose subsystems were designed to similar functional criteria.

As mentioned earlier, the stabilization mode is one of the most decisive influencing factors controlling the spacecraft configuration. The two candidate approaches, spin stabilization and three axis stabilization are both flight proven systems, either of which can be used for a Mercury Orbiter. The spin stabilization mode offers an advantage in accommodation of a solar array power generation system within the severe near-planet thermal environment, however, it may require a despun antenna system and more complex science instrument pointing control. The three-axis stabilization mode offers a more stable platform for pointing accuracy for both science and antenna systems; however it requires a control system for a solar array power generator and is more limiting with respect to thermal constraints. Present technology will allow system design for either approach. Since orbiter attitude maneuvers and on-orbit attitude adjustments will call for very low thrust impulses and, for a six month orbit mission with approximately 200 orbits, a large number of these impulses, a gas system would appear most feasible for the ACS impulse propulsion, augmented by a momentum flywheel (Stabilite) system for on-orbit control. Cold gas systems have been proven on the Mariner vehicles and have

been designed for use on the Helios, MVM'73 and VO'75 vehicles. Based upon existing designs, the technology for both attitude determination and reaction control are considered non-critical for application to a Mercury Orbiter vehicle design.

Midcourse correction maneuver requirements, as reflected in Section III of this report, will require a liquid vehicle propulsion system which allows the ability to vary total applied thrust and permits engine restart for additional thrust maneuvers, either midcourse or orbital. The high total thrust required to complete the orbit insertion maneuver promptly suggests the use of a solid rocket motor system which has a decided mass fraction advantage. The mission performance requirements show the need for the more favorable characteristics of each of these propulsion systems, indicating separate propulsion systems for maneuver operations (liquid) and orbit insertion (solid). Present technology for liquid propulsion system design for spacecraft application, both monopropellant and bi-propellant, will support design of a Mercury Orbiter system. The most significant design problem indicated is the environmental control of the liquid propellants and engine thruster assemblies, to maintain thrust levels within predictable margins. Current state of the art solid rocket motor technology will support the design of a motor to meet the Mercury Orbiter insertion requirements. Preliminary investigations indicate the possibility of scaled-up versions of existing (off-the-shelf) configurations that will satisfy the design requirements. Core design modification and development will be required to assure burn time and thrust levels within "g" load criteria established for the vehicle subsystems. Operation of a solid motor after prolonged storage in space environments has not been demonstrated as a part of an actual planetary mission conducted to date, however results of design development studies and vacuum chamber testing indicate current technology supports such design criteria.

Proven spacecraft monopropellant (Pioneer, MVM'73) and bipropellant (MM'71, VO'75) liquid propulsion systems support a non-critical technology evaluation for these systems. A low criticality evaluation has been determined for solid rocket motor technology since motor development requirements are indicated for physical characteristics not previously flight proven.

Telecommunication design for S-band uplink/downlink systems is state-of-

the-art technology, utilized in design of flight proven and currently planned spacecraft systems; current technology will support design of a communications system for a Mercury Orbiter. The most significant design constraint indicated is operation and survivability of the antenna system within the severe thermal environment. A similar antenna problem encountered in the design of the Helios communications system has resulted in the design and development of a high gain S-band antenna configuration for operation during and after prolonged exposure to an environment equivalent to 16 solar constants (Ref. VI-12). A review of this design approach indicates that it will support the design for a Mercury Orbiter system. This antenna system is mechanically despun for the Helios vehicle. The high gain antenna itself however may be accommodated to either a three-axis (with platform pointing) or a spin-stabilized vehicle.

The anticipated data rate of 16 KBPS for the desired science data return (Ref. Section V of this report) will require transmission system sizing and power requirements to allow this capability. The high rate however, results not only from the high science requirement but also from the periods of RF occultation and the approximately 20 hours orbit period of recurring observations. Accommodation of data storage, either analog or digital, is within the capability of proven data management systems.

The technology evaluation for both telecommunications and data management is considered non-critical with respect to support of system design for a Mercury Orbiter.

Table VI-4 summarizes the vehicle subsystems considered for technology evaluation and the assessments made. Current state-of-the-art design practices will support design of other subsystems.

5. Other Environmental Considerations

The thermal environment has been considered the most severe in the technology evaluations made for the vehicle subsystems; however, the solar proton environment may be the most severe of any proton fluence yet encountered in space missions. More substantive bases from which to model the solar proton environment in the Mercury regime are expected from the data to be obtained from both the MVM'73 and Helios missions. For this evaluation, the results of a study performed for the MVM'73 mission (Ref. VI-13) (which derived the

TABLE VI-4 SPACECRAFT SYSTEMS SUMMARY

VEHICLE SUBSYSTEM	TECHNOLOGY EVALUATED	RELATED DESIGNS	TECHNOLOGY ASSESSMENT	REMARKS
Attitude Control System	Spin Stabil-ization	Pioneer/ Venus Helios ITOS	NC	Low spin rate with effective nutation damping Proven sensing devices and tracking techniques Momentum wheel trim control (ITOS) Minimizes expendables Eases thermal control design May require despun antenna More complex science pointing control
	Three Axis Stabil-ization	Mariner Series MVM'73 VO'75	NC	Proven sensing devices & tracking techniques Accurate drift control Most stable platform Less complex science pointing control Requires solar array control More sensitive to solar wind
Attitude Control Propulsion	Liquid	Pioneer Pioneer/ Venus	NC	Proven system design (monopropellant hydrazine) Greatest specific impulse Lightweight system Requires close propellant & thruster temp. control
	Gas	MVM'73 Helios VO'75	NC	Proven system design Minute thrust increment capability Less costly

Technology Assessment: NC - Non-critical, LC - Low Criticality,
MC - Medium Criticality, HC - High Criticality

TABLE VI-4 SPACRAFT SYSTEMS SUMMARY (CONT.)

VEHICLE SUBSYSTEM	TECHNOLOGY EVALUATED	RELATED DESIGNS	TECHNOLOGY ASSESSMENT	REMARKS
Auxiliary Propulsion System	Liquid Mono-propellant	Pioneer MVM'73	NC	Proven system design Impulse duration controllable Multi-start capability Propellant management/blowdown system requirements
	Bi-propellant	MM'71 VO'75	NC	Propellant & thruster temperature control required
Retro Propulsion System	Solid	Pioneer/ Venus	LC	Mass fraction benefit for high thrust requirement Simplified hardware design Engine development required
Telecom-muni-cations	S-Band Uplink/ Down-link	Pioneer Helios	NC	Proven system design May require despun antenna for spin stabilized vehicle

Technology Assessment: NC - Non-critical, LC - Low Criticality
MC - Medium Criticality, HC - High Criticality

TABLE VI-4 SPACECRAFT SYSTEMS SUMMARY (CONT.)

VEHICLE SUBSYSTEM	TECHNOLOGY EVALUATED	RELATED DESIGNS	TECHNOLOGY ASSESSMENT	REMARKS
Imaging System	Frame	MM'71 Viking Hi-Resol. Imager	LC	Proven system design Requires high data rate processor
	Spin Scan	--	MC	Greater gray level detector ability Data matching (image reconstruction) more complex Less resolution (smaller data processor)
Power Generator	Photo-voltaic	Mariner Series Helios VO'75	LC	Proven system design Requires array panel control for three axis stabilized vehicle Upper limit temperature critical at Mercury
	Thermo-electric		MC	Reduces thermal design constraint Requires auxiliary system for near earth System development program required
	Therm-ionic		HC	Not considered competitive for spacecraft application
Thermal Control System	Passive & Semi-Passive	Helios	LC	Most critical design requirement System development program required Phase change material assessed as high criticality item

Technology Assessment: NC - Non-critical, LC - Low Criticality,
MC - Medium Criticality, HC - High Criticality

solar proton fluence induced by the solar wind and probabilistic high energy components from discrete solar events for its flyby mission to Mercury) were scaled to the Mercury Orbiter 1980 mission duration indicating that for energy levels $E \geq 1$ KeV a total fluence of 8.4×10^{16} protons/cm^2 can be anticipated. Sensitivity levels for electronic components show a threshold of light to moderate damage for silicon controlled rectifiers of 2.4×10^{10} protons at 20 MeV (Ref. VI-14). Other semi-conductor devices and electronic components have higher damage thresholds; most all will suffer severe damage in a total fluence range of 10^{12} to 10^{14} protons/cm^2. Radiation shielding for components will be a requirement. The degree of shielding in g/cm^2 will be a design determination, however, current data shows that effective shielding may be obtained for a shielding density (aluminum) of .75 to 1.0 g/cm^2.

Radiation shielding for solid rocket propellants and pyrotechnic devices will also be required to insure a total proton fluence level below 10^{10} per cm^2, since irradiation tends to make these devices more sensitive to ignition, operate at lower temperatures and release more energy; premature operation could be expected as a result of too severe a radiation environment.

Recent development and tests of lithium-doped radiation resistant solar cells shows that they may be advantageously used in radiation environments of up to 3×10^{15} (1 MeV) equivalent electrons per cm^2 per year if the cells are maintained at a temperature of 50^{o}C or greater (Ref. VI-15). The advantage is even greater for radiation environments consisting of high-energy protons, neutrons, and electrons existing in damage clusters rather than simple point defects.

Shielding for micrometeroid protection should not present a design problem for a Mercury Orbiter vehicle, since the spatial density varies as the inverse of the radial distance from the Sun in AU's ($1/R$ to $1R^{1.5}$)(Ref. VI-16). The micrometeroid model for a spacecraft at Mercury solar distance should be less severe and show a much greater probability of no penetrations than those for spacecraft designed to date. The thermal protection offered by multilayer insulation may also effectively serve as a micrometeroid bumper.

Protection for solar particle bombardment will be required for the Mercury Orbiter vehicle sensitive components. This protection is within current state-of-the-art design practices, the degree of protection, however, depends

upon the fluence model established. Current available data shows that protection may be obtained at a shielding weight penalty of approximately 10 kg/m^2; a more accurate determination may be made after analyses of solar flux data recieved from MVM'73 and Helios. Current technology however will support design of protective systems.

C. TECHNOLOGY SUMMARY

The area identied which imposes the most critical constraints on a Mercury orbiter vehicle design is the thermal environment experienced by the vehicle. Accommodating this environment is possible through design of an adequate thermal control system coupled with an orbit selection which will allow the desired science return while providing a thermally acceptable orbit. Technology for design of most other vehicle systems was found critical only as affected by the thermal environment.

Table VI-5 summarizes the technology evaluations determined during the study. It should be noted that those disciplines with criticality designations of medium and high, while possibly desirable, were not found to be mandatory to a Mercury Orbiter vehicle design.

TABLE VI-5 TECHNOLOGY SUMMARY

VEHICLE SYSTEM	CRITICALITY NON	LOW	MED	HIGH
Thermal Control System				
Thermal Coatings		X		
Solar Reflectors	X			
Thermal Insulation		X		
Thermal Louvers		X		
Heat Shield			X	
Phase Change Material			X	
Power Generator System				
Solar Cell Array		X		
Thermoelectric			X	
Thermionic				X
Imaging System				
Frame		X		
Spin Scan			X	
Attitude Control System				
Spin Stabilized	X			
Three Axis Stabilized	X			
Attitude Control Propulsion				
Liquid	X			
Gas	X			
Auxiliary Propulsion System				
Monopropellant	X			
Bipropellant	X			
Retro Propulsion System				
Solid		X		
Telecommunication System	X			

VII. CONCLUSIONS

VII. CONCLUSIONS

Four Mercury orbiter mission opportunities in 1977, 1980, 1985, and 1988, predicated on ballistic mode flight with Venus gravity-assist, have been thoroughly analyzed in terms of transfer trajectory characteristics and navigation requirements. Performance requirements have been verified to be compatible with launch by the Titan IIIE/Centaur launch vehicle and orbit insertion by chemical propulsion. Feasibility of navigation for the complex flight geometries has been demonstrated analytically.

Investigations of alternate flight techniques established the performance improvement potential of midcourse maneuvers and the utilization of multiple Venus swingbys. These techniques provided additional spacecraft weight for the 1977, 1985 and 1988 missions, and identified a new mission opportunity in 1983. An extension of the study contract has been awarded to complete the analysis of these cases as well as to conduct further search for opportunities in the 90's.

Parametric study of orbits about Mercury have defined significant characteristics relevant to orbit selection criteria. In particular, orbit stability and exposure to the Mercury thermal environment have been correlated with access to primary science observables. Science objectives and corresponding instrumentation were postulated and assessed for compatabilities and conflicts relating to selection of orbit geometry. These latter considerations were necessarily parametric to encompass the contingencies of the MVM'73 flyby experience and findings.

Analysis of expected science return for a typical mission and orbit geometry was conducted to illustrate the potential of primary experiments such as imaging. From these assessments, it was concluded that even a modest Mercury orbiter mission would substantially advance the state of knowledge beyond that expected from the MVM mission.

Subsystem technologies for a Mercury orbiter spacecraft were evaluated to isolate any requirements for expensive new developments. No such areas were identified. However, since this study did not include spacecraft design effort, the best balance of conflicting requirements and constraints has not been postulated. Resolution of design feasibility will be more readily accomplished when the MVM flyby has clarified science objectives for an orbiter mission and

updated critical environmental data.

The primary conclusions drawn from this six-month study effort can be summarized as follows:

1) Ballistic mode Mercury orbiter missions offer adequate performance for effective follow-up of the MVM'73 science findings and an orderly program of advanced Mercury exploration.

2) The existing and programmed technology base is adequate for implementation of Mercury orbiter spacecraft design.

3) When the pending MVM flyby has been accomplished and the results analyzed, the data base will be adequate to support detailed orbiter spacecraft design efforts.

Items of significance to advanced Mercury mission planning which were not resolved in the course of this study, but warrent consideration for future effort, include the following:

1) Determination of Mercury orbit geometries comensurate with unambiguous isolation of gravity field harmonics and asymmetries.

2) Assessment of science potential and systems requirements for a small Mercury lander.

THIS

PAGE

BLANK

REFERENCES

REFERENCES

SECTION IV

Ash, M.E., Shapiro, I.I., and Smith, W.B., "Astronomical Constants and Planetary Ephemerides Deduced from Radar and Optical Observations," Astron, J., 74, 338, (1967).

Belton, M.J.S., Hunten, D.M., and McElroy, M.B., "A Search for an Atmosphere on Mercury," Astrophys. J, 150, 1111 (1967).

Bergstralh, J.T., Gray, L.D., and Smith, H.J., "An Upper Limit for Atmospheric Carbon Dioxide on Mercury," Astrophys. J., 149, L137 (1967).

Binder, A.B. and Cruikshank, D.P., "Mercury: New Observations of the Infrared Bands of Carbon Dioxide," Science, 155, 1135 (1967).

Bowyer, C.S., et.al., "A Strategy for Ultraviolet Observations on the 1973 Mariner Venus/Mercury Mission," Final Report of the UV-Spectrometer/ Photometer Science Advisory Team for the 1973 Mercury/Venus Mission Design (1970).

Divine, Neil, et.al., "The Planet Mercury (1971)," NASA SP-8085 (1972).

Dyce, R.B., Pettingill, G.H., and Shapiro, I.I., "Radar Determination of the Rotations of Venus and Mercury," Astron, J., 72, 351 (1967).

Goldreich, P. and Peale, S., "Spin-Orbit Coupling in the Solar System," Astron. J., 71, 425 (1966).

Kaula, W.M., "The Gravitational Field of the Moon," Science, 166, 1581 (1969)

Klopp, D.A. and Wells, W.C., "Mercury Orbiter Mission Study," IITRI Report No. M-26 (1971).

Kuiper, G.P., "The Planet Mercury: Summary of Present Knowledge," Communications of the Lunar and Planetary Laboratory, 8, 165 (1970).

Moroz, V.I., "Infrared Spectrum of Mercury (λ = 1.0 - 3.9μ) Soviet Astron. - AJ8, 882 (1965).

Murray, B.C., "Mars from Mariner 9," Scientific American, 228, 49 (1973).

Ness, N.F. and Whang, Y.C., "Solar Wind Interaction with Mercury," J.G.R., 76, 3136 (1971).

O'Leary, B.T. and Rea, D.G., "On the Polarimetric Evidence for an Atmosphere on Mercury," Astrophys. J., 148, 249 (1967).

Peale, S.J., "Determination of Parameters Related to the Interior of Mercury," Icarus, 17, 168 (1972).

Pettingill, G.H. and Dyce, P.B., "A Radar Determination of the Rotation of the Planet Mercury," Nature, 206, 1240 (1965).

Sagan, C., "The Photometric Properties of Mercury," Astrophys. J., 144, 1218 (1966).

Spinrad, H., Field, G.B., and Hodge, D.W., "Spectronscopic Observations of Mercury," Astrophys. J. 141, 1155 (1967).

Sturms, Francis M., "Polynomial Expressions for Planetary Equators and Orbit Elements with Respect to the Mean 1950.0 Coordinate System," Jet Propulsion Laboratory Technical Report 32-1508 (1971).

SECTION VI

1. The Planet Mercury (1971), NASA SP-8085, JPL, Pasadena, California, March 1972.

2. Critical Design Review Minutes, Helios Thermal Subsystem, prepared by Messerschmidt - Bölkow - Blohm GmbH, Munich, West Germany, October 16-20, 1972.

3. Analysis Notes - Helios Thermal Control Design, prepared by Messerschmidt - Bölkow - Blohm GmbH, Munich, West Germany, undated.

4. Siegel, Robert and Howell, John R., Thermal Radiation Heat Transfer, NASA SP-14, Volume I, The Blackbody, Electromagnetic Theory, and Material Properties, Lewis Research Center, Cleveland, Ohio, 1968.

5. Thermal Insulation Systems, NASA SP-5027, NASA Office of Technology Utilization, 1967.

6. NASA Tech Brief, B72-10464, Phase-Change Materials Handbook, Marshall Space Flight Center, Alabama, August 1972.

7. Critical Design Review Minutes, Helios Solar Array, prepared by Messerschmidt - Bölkow - Blohm GmbH, Munich, West Germany - October 1972.

8. Bifano, William J. and Scudder, Larry R., NASA TN D-3788, Comparison of Solar Direct-Energy Conversion Systems Operating Between 1.0 and 0.1 Astronomical Unit, Lewis Research Center, Cleveland, Ohio, February 1967.

9. Gurnee, Mark N., Thermoelectric Convertors for Integration with Solar Collectors, Unpublished Report, Honeywell, St. Paul Minnesota, 4 Jan. 1973

10. Development and Testing of the Television Instrument for the Mariner Mars 1971 Spacecraft, Technical Memorandum 33-505, JPL, Pasadena, Calif., November 1, 1971.

11. Dr. E. Russell, Santa Barbara Research Laboratories, Santa Barbara, Calif. Private Communication, April 1973.

12. Helios Spacecraft Requirements Document, GfW TN 70/14, Revision 6, Gesellschaft für Weltraumforschung, mbH, Bonn, West Germany, August 1970.

13. Thomas, J. R., Mariner Venus-Mercury 1973 Mission Solar Proton Environment: Fluence and Dose, JPL Quarterly Technical Review, Volume 2, No. 1, JPL Pasadena, California, April 1972.

14. Radiation Effects Design Handbook, NASA CR-1785, July 1971.

15. Berman, Paul A., Development of Lithium-Doped Radiation-Resistant Solar Cells, Technical Report 32-1574, JPL, Pasadena, California, November 15, 1972.

16. Meteroid Environment Model - 1970 (Interplanetary and Planetary) NASA SP-8038, NASA Space Vehicle Design Criteria (Environment), October 1970.

APPENDIX 1

Berg, Otto E. and Swamy, K. S. K., "Orbital Elements of Micrometeorites Derived from Pioneer 8 Measurements," GSFC (1969).

Dohnanyi, J. S., "Collisional Model of Asteroids and Their Debris," J. G. R., 74, 2531 (1969).

Kessler, D. J., et.al., "Meteoroid Environment Model - 1970," NASA SP-8038 (1970).

Ligenfelter, R. E. and Ramaty, R., "High Energy Nuclear Reactions in Solar Flares," published in High-Energy Nuclear Reactions in Astrophysics (New York: W. A. Benjamin, Inc., 1967).

Ligenfelter, R. E., "Solar Flare Optical Neutron and Gamma-Ray Emission," Solar Physics, 8, 341 (1969).

Morrison, David, "Thermophysics of the Planet Mercury," Space Science Reviews, 11, 271 (1970).

Öpik, E. J., "Collision Probabilities with the Planets and the Distribution of Interplanetary Matter," Royal Irish Academy Proceedings, 54, 165 (1951).

Öpik, E. J., "Strong Bodies in the Solar System; Part I. Survival of Cometary Nuclei and Asteroids." Advances in Astronomy and Astrophysics, 2, 219 (1963).

Ramaty, R. and Ligenfelter, R. E., "Nuclear Gamma-Rays from Solar Flares," to be published in NASA Symposium on High Energy Phenomonen on the Sun.

Whipple, Fred L., "On Maintaining the Meteorites Complex," Smithsonian Astrophysical Observatory Special Report, 239, (1967).

THIS
PAGE
BLANK

APPENDIX

APPENDIX

1. Mission Environment Models

Science experiments and spacecraft design require mission environment models. Three mission environment models are presented in this document: meteoroid, neutron, and thermal. The meteoroid and neutron environment models may aid in both designing science experiments for detecting meteoroid and solar neutrons as well as designing the required spacecraft protection. The thermal environment model presented here is inadequate for science experiment design purposes since it does not include detail thermal intertia considerations. The thermal model is primarily intended to be used for evaluating orbital constraints based upon thermal input from the planet. The effects of these models on detailed spacecraft design have not been determined.

Meteoroid - The meteoroid environment at Mercury will be treated as two sets: the large meteoroid (asteroid) environment, and the small meteoroid (micro-meteoroid) environment. There is a concensus among space scientists that the origin of the large meteoroids which occupy the region of the terrestrial planets is the Asteroid Belt. This theory is primarily based on Öpik's (1951) calculations of the mean lifetime of large meteoroids with respect to planetary capture. Since the mean lifetime of these meteoroids is much less than the expected age of the solar system, then for these large meteoroids to exist today in the region of the terrestrial planets indicates the existence of a source for these large meteoroids; the Asteroid Belt is the most likely candidate. If the meteoroids originate in the Asteroid belt then there should be more large meteoroids in the vicinity of the Earth and Moon today than in the vicinity of Mercury. If this theory is correct, then Mercury would be expected to have fewer "fresh" craters than the Moon.

The small meteoroids are thought to be responsible for the Zodiacal light as they spiral toward the Sun due to the Poynting-Robertson effect. The micro-meteoroids range in size from 0.2 μ to 5 cm. The lower limit was determined from equating the radiation pressure with gravitational attraction. The upper limit was determined from the fact that the larger the particle's radius, the slower it spirals in toward the Sun, and thus the higher the probability that it will be captured by a planet (Öpik, 1963).

The interaction between solar radiation and these orbiting micro-meteorites produces a drag, which causes them to lose angular momentum, and thus spiral in toward the Sun. This is called the Poynting-Robertson effect. The spiral time in years is given as:

$$t = C(e) \rho \, r_o \, r_p^2 \times 10^7 \tag{1}$$

(Whipple, 1967) where C(e) depends solely upon the orbital eccentricity, e (C(e)= 0.7 for e = 0, 1.9 for e = 0.5, and 7.3 for e = 0.9), r_o is the particle's radius, ρ is the particle's density, and r_p is the perihelion distance in AU.

In predicting the spatial density of micro-meteoroids for the vicinity of Mercury, circular orbits were assumed. The radial velocity is given as:

$$V_r = \frac{3 \, IR^2}{2 \, c^2 \rho \, r_o \, r} \tag{2}$$

where I is the solar constant, R is 1 AU in proper units, c is the velocity of light. Using equation 2 with the steady-state continuity equation ($\nabla \cdot \vec{NV} = 0$), the micro-meteoroid spatial density varies as:

$$N = N_e / r \tag{3}$$

where r is measured in AU, and N_e is the spatial density at 1 AU.

The data from the Berg and Swamy's (1969) experiment on the Pioneer 8 heliocentric spacecraft which had a perihelion of 0.99 AU and an aphelion of 1.088 AU detected a particle density of about 6×10^{-8} particle/m^3. From this data, the meteoroid distribution of Figure A1-1 was constructed.

Dohnanyi (1969) has predicted the steady-state mass distribution of meteoroids to be $Am^{-\alpha}dm$ (meteoroids/m^3) where $\alpha = 11/6$ and A is an experimentally determined quantity. The probability per unit time for a collision is proportional to A, and if A is too small, then the steady-state condition probably does not exist. Dohnanyi's theoretically predicted value for α was used in the NASA SP-8038 document for the engineering model of the Asteroid Belt to be used for space vehicle design criteria (Kessler, et al., 1970). Figure A1-2 was reconstructed from the NASA SP-8038 document.

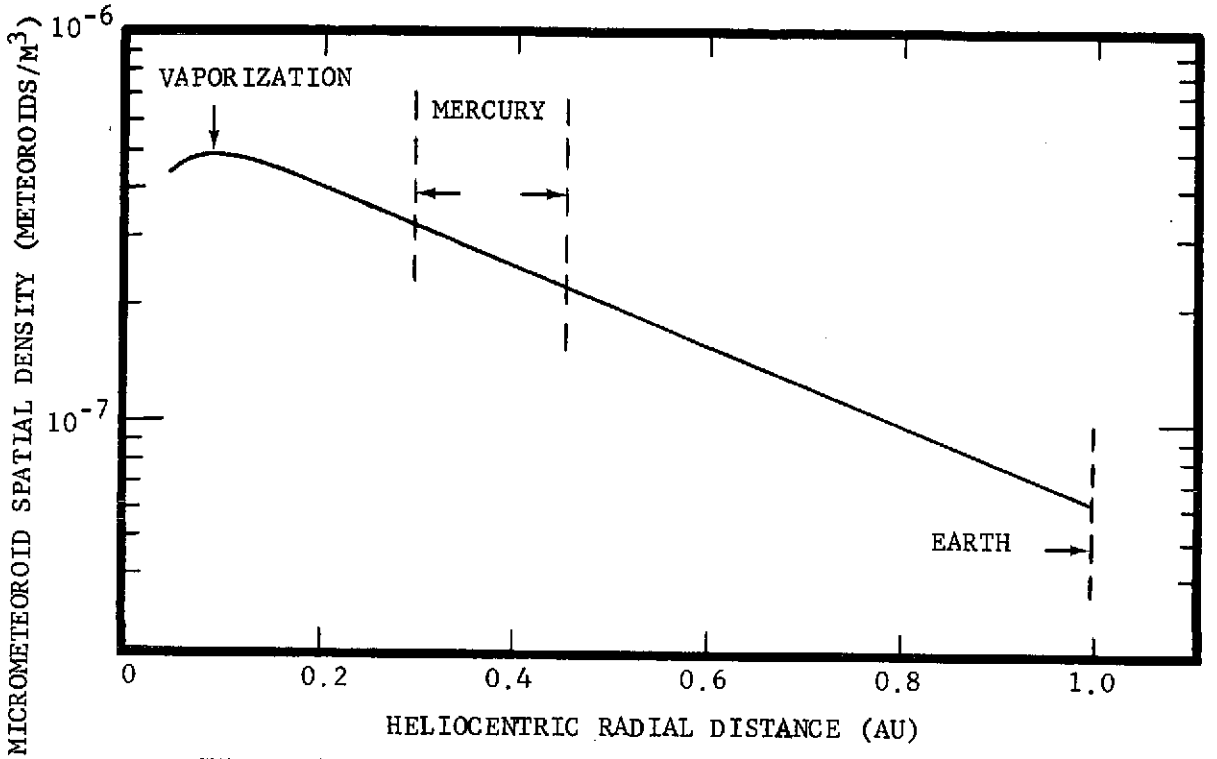

FIGURE A1-1 MICROMETEOROID SPATIAL DENSITY VERSUS AU

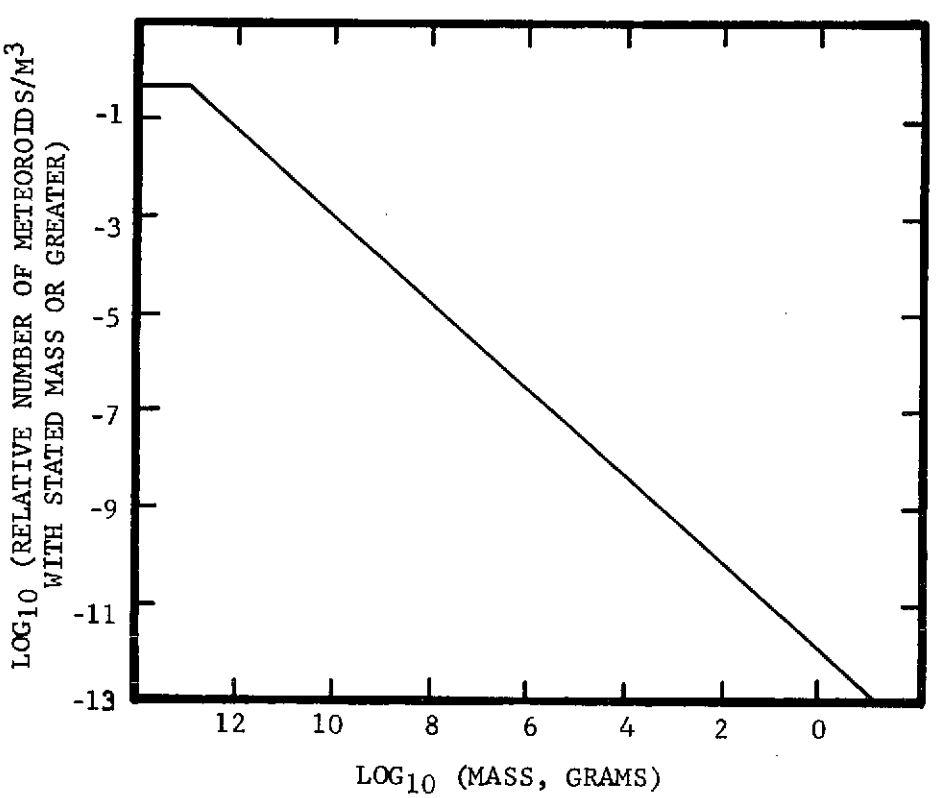

FIGURE A1-2 METEOROID MASS DISTRIBUTION

Neutron - It is expected that solar protons and alpha particles will interact with other solar nuclei to produce free neutrons which have a 12-minute half life. The solar neutrons that may be produced during the solar quiet times have energies less than 1 KeV. These neutrons seldom reach Mercury and will not be considered in this study. Only the neturons produced during large solar flares (>1 MeV) will be discussed.

The estimate presented here of the neutron flux at Mercury is based on the models of Ligenfelter and Ramaty (1967, 1969, to be published), in which two types of observations are needed to define the characteristics of a solar flare: the optical brightness of the flare and the gamma-ray intensity. The optical brightness is characteristic of the energy dissipated in ionization losses for short duration flares; whereas the gamma-ray flux is characteristic of the solar proton energy spectrum.

Figure A1-3 shows the predicted neutron flux per erg of ionization energy loss for short duration flares. This figure was determined from Figure 24, Ligenfelter and Ramaty (1967). H-alpha observations of the 4 August 1972 flare (Ramaty and Ligenfelter, to be published) indicated a total ionization energy loss of about 2×10^{30} ergs.

For long duration flares (long duration implies that the flare exists longer than the neutron flight time) the brightness of the flare is assumed to be a function of the power dissipated in the ionization processes. The neutron flux/erg$(\text{sec})^{-1}$ at Mercury from long duration flares is presented in Table A1-1. This table was determined from Figure 1, Ligenfelter (1969). Table A1-2 compares the peak neutron flux at Mercury with that at Earth for the different types of flares.

TABLE A1-1 PEAK NEUTRON FLUX AT MERCURY FROM LONG DURATION FLARES

Particle Rigidity (MV)	Neutrons $(\text{cm}^2\text{-sec})^{-1}/\text{ergs } (\text{sec})^{-1}$
60	3.6×10^{-28}
125	4×10^{-27}
200	4×10^{-26}

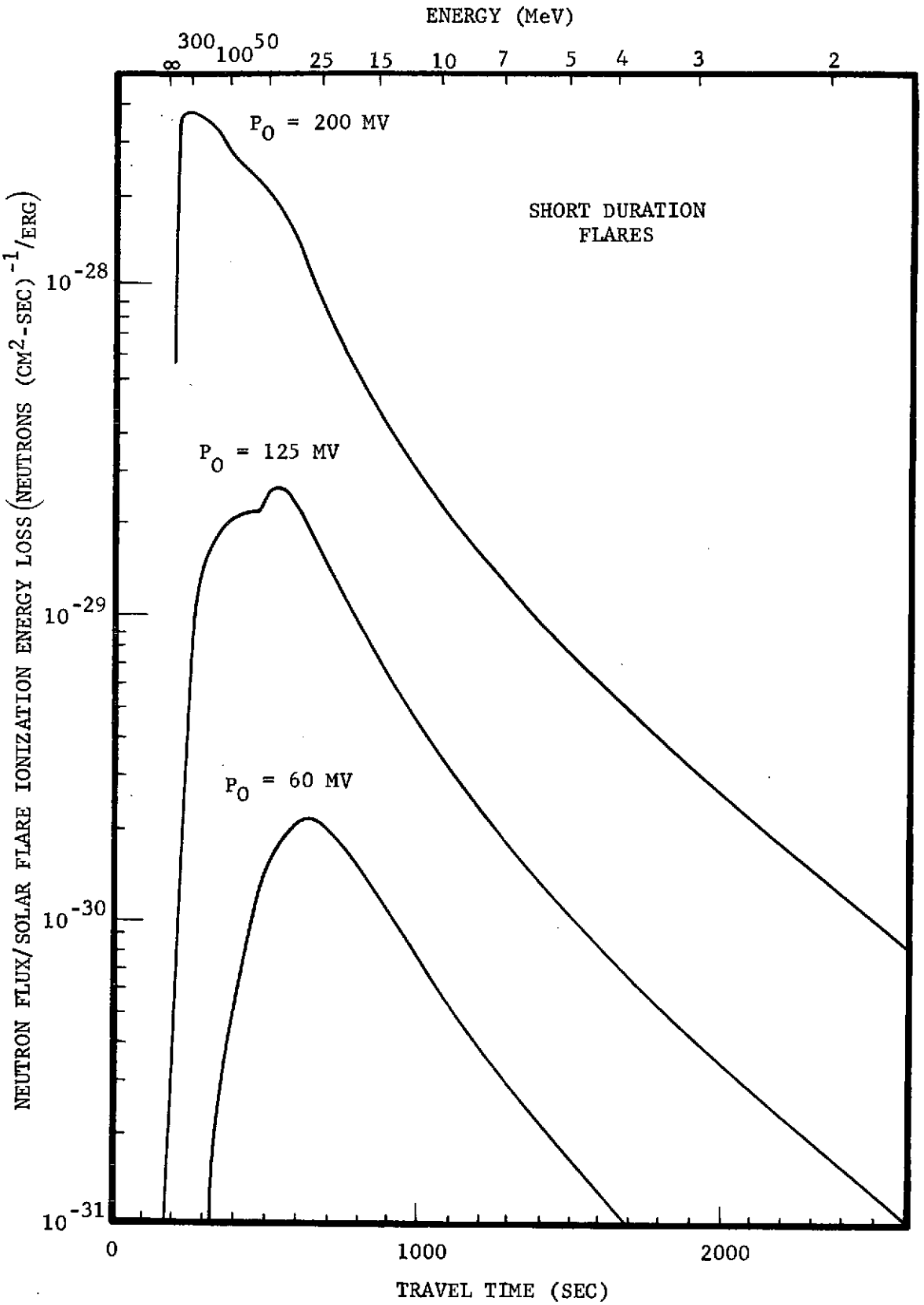

FIGURE A1-3 SOLAR FLARE NEUTRON FLUX AT MERCURY

TABLE A1-2 RATIOS OF THE PEAK NEUTRON FLUX AT MERCURY TO THOSE AT EARTH

Type of Flare	Proton Rigidity (MV)	Neutron Flux at Mercury / Neutron Flux at Earth
Short	60	38
Duration	125	24
	200	16
Long	60	50
Duration	125	40
	200	27

Thermal - Mercury's surface temperature distribution is based on the following assumptions:

(1) Mercury's rotation rate is slow enough so that the sunlit surface is in radiative equilibrium at all times.

(2) Mercury's surface is a non-conductor so that large temperature gradients can exist.

(3) The subsolar point is at 700°K, the evening terminator is at 150°K and the morning terminator is 100°K (Morrison, 1970).

Mercury's 3/2 spin-orbit coupling, assuming the spin axis is normal to the orbital plane, results in two "hot" and two "warm" poles. Because of Mercury's appreciable orbital eccentricity, a different total energy flux falls on each equatorial longitude. The orbital angular velocity slightly exceeds the constant rotational angular velocity whenever Mercury is within 26 degrees of perihelion, leading to a highly non-uniform motion of the Sun as viewed from Mercury (Figure A1-4). The hot poles, defined with longitudes of 0° and 180°, are the equatorial surface points which will alternately be the perihelion subsolar points; whereas, the warm poles, defined with longitudes of 90° and 180°, are the equatorial surface points which will alternately be the aphelion subsolar points (Figures A1-5 and A1-6).

The behavior of the Sun, as seen from one of the warm poles is most unconventional. The Sun rises in the East and then sets again (taking about nine Earth days). The Sun then rises for the second time, and subsequently sets twice about 88 Earth days later. This unusual behavior is responsible for the

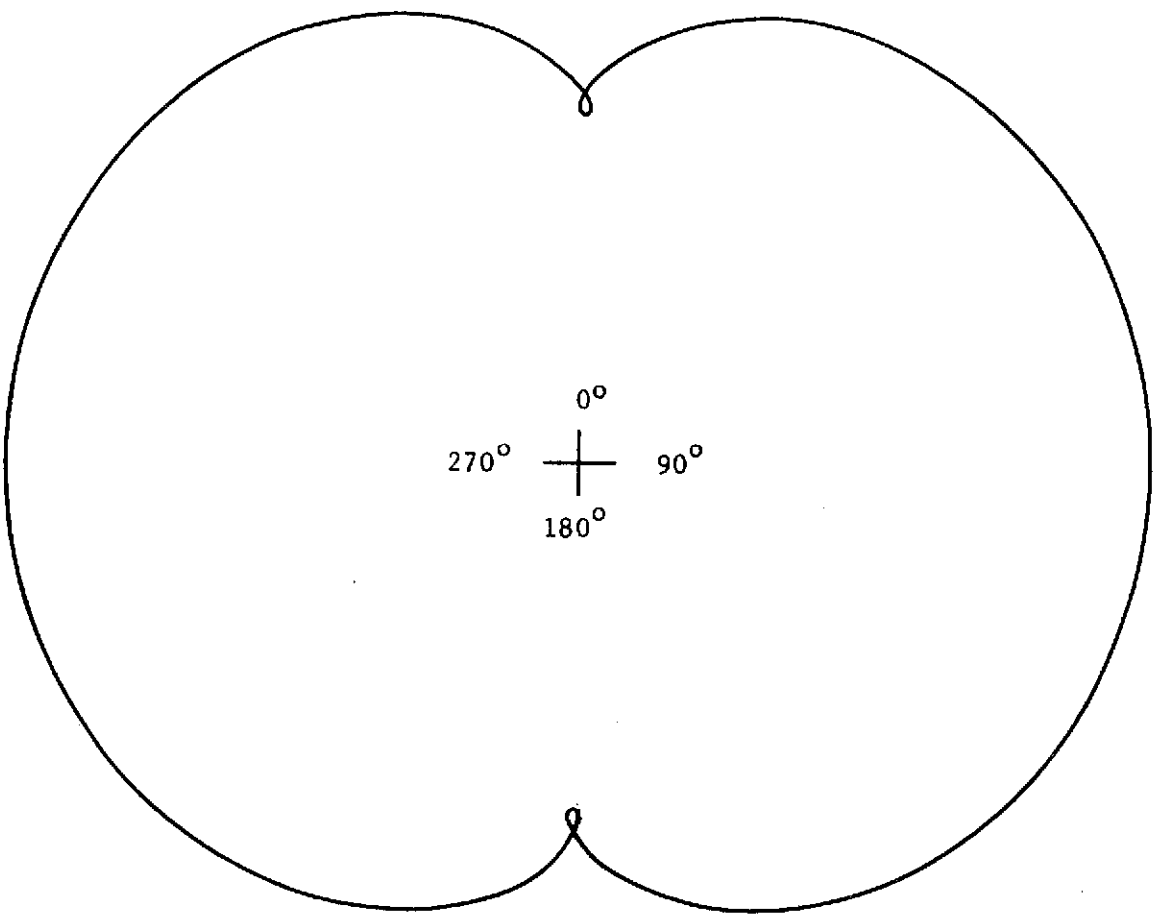

FIGURE A1-4 MOTION OF THE SUN AS VIEWED FROM MERCURY

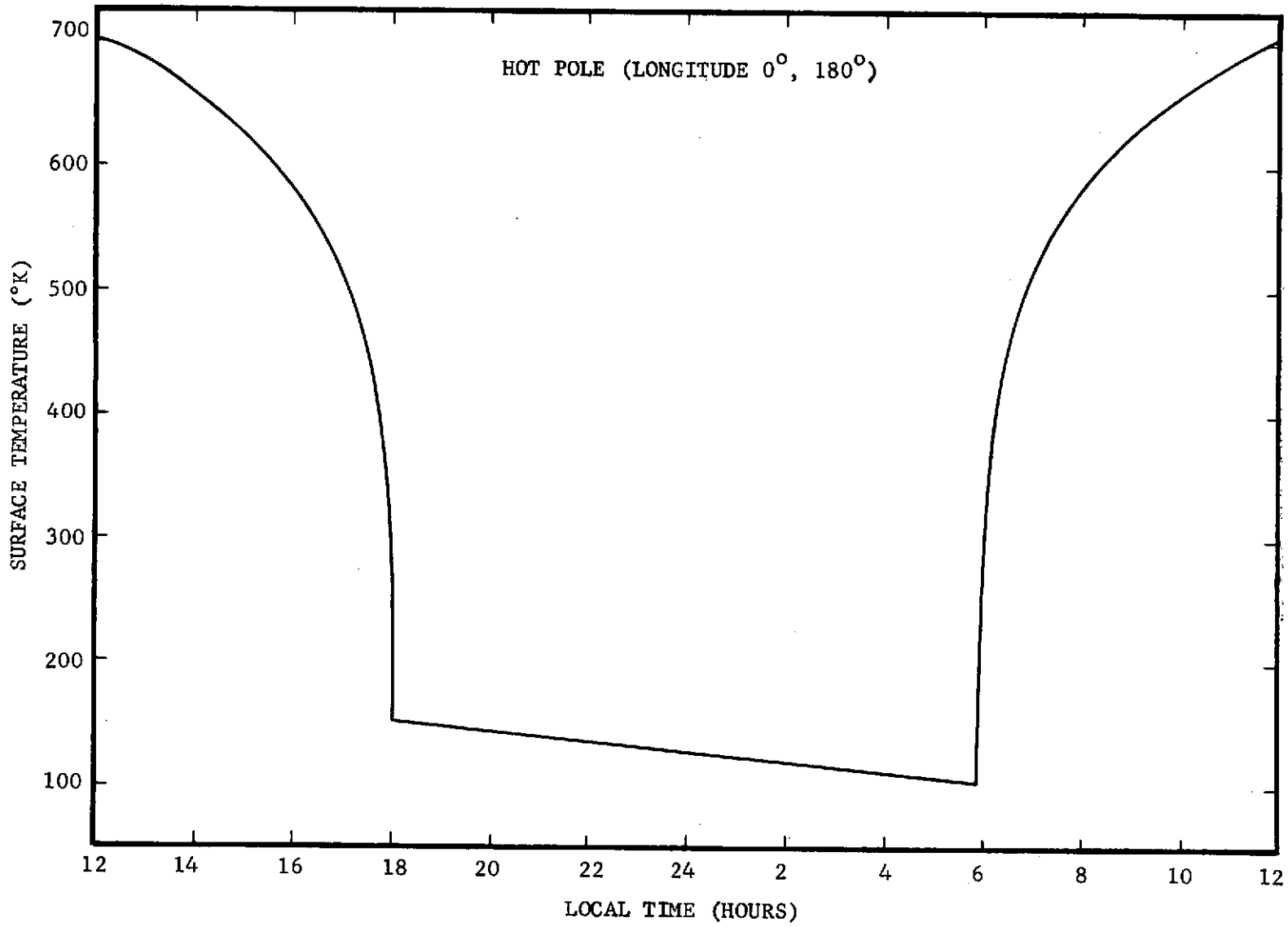

FIGURE A1-5 HOT POLE SURFACE TEMPERATURE MODEL

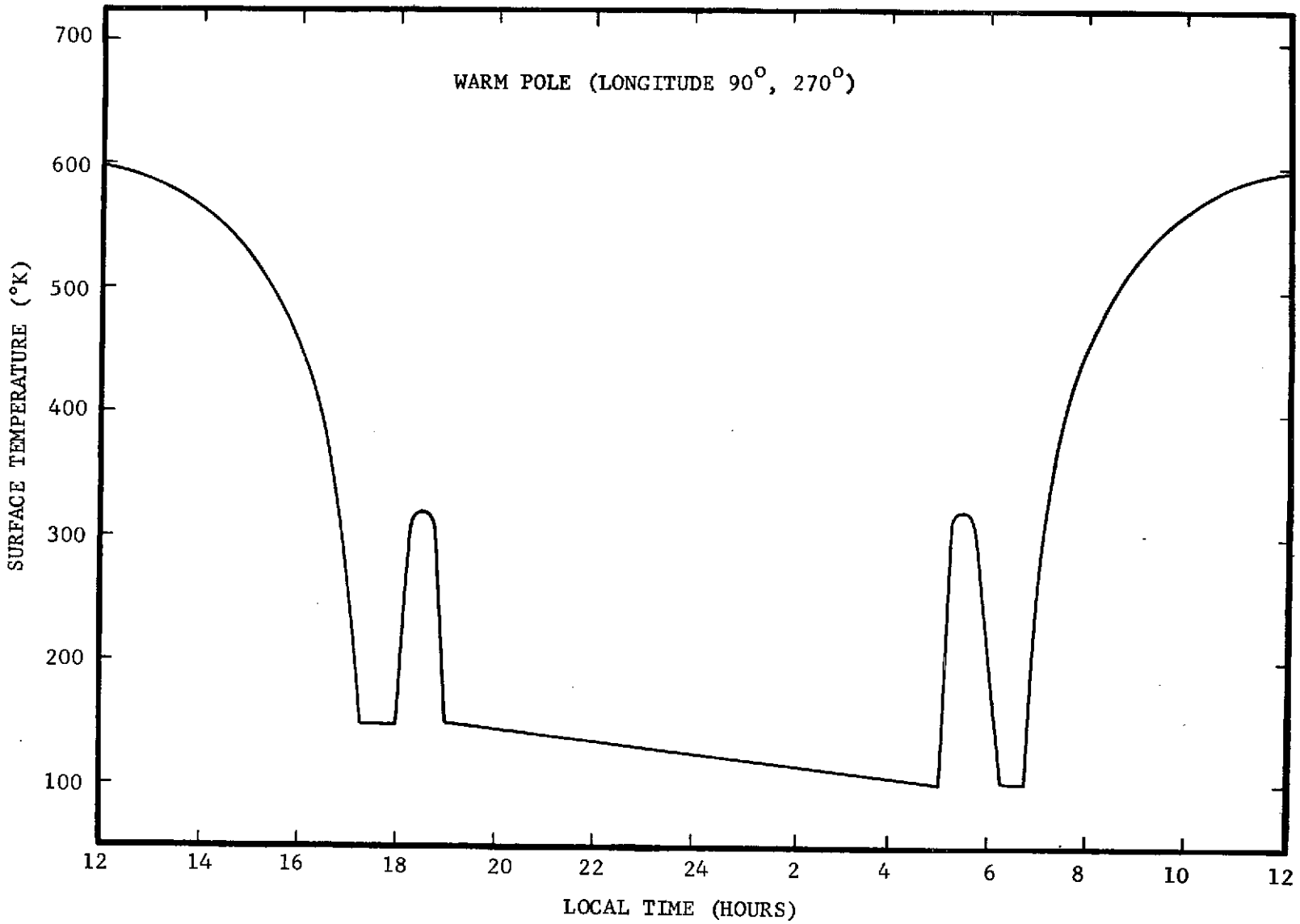

FIGURE A1-6 WARM POLE SURFACE TEMPERATURE MODEL

two thermal spikes illustrated in Figure A1-6.

Figure A1-7 presents a model of thermal contours on Mercury's surface corresponding to a Mercury "hot" pole. The contours on the sunlit side of the planet follow concentric circles about the subsolar point, whereas, the contours on the night side of the planet follow the longitudinal lines.

The flux of IR radiation incident on a spacecraft orbiting Mercury is important for determining thermal designs and orbital constraints. A spacecraft is usually designed to be an excellent reflector of visible radiation and an excellent emitter in the IR region, since most of the solar energy is in the visible. An excellent emitter of IR is unfortunately an excellent absorber of IR. This will impose subsolar altitude constraints due to the resulting thermal control problems.

Figures A1-8 and A1-9 illustrate the IR radiation from Mercury that an orbiting spacecraft would experience. As an aid to interpreting the data, consider that at 1 AU the solar IR flux is 41.3 mW/cm^2 and that at Mercury's perihelion (0.307 AU) the solar IR flux is 442 mW/cm^2. Table A1-3 is provided as an aid for comparing Mercury's thermal flux (Figures A1-8 and A1-9) with the solar flux.

TABLE A1-3 COMPARISON OF MERCURY'S THERMAL FLUX WITH THE SOLAR THERMAL FLUX

Subsolar Altitude (km)	IR Flux from Mercury (mW/cm^2)	Ratio Flux from ☿/Solar IR Flux @ 1.0 AU	Ratio Flux from ☿/Solar IR Flux @ 0.307 AU
500	930	22.5	2.1
1000	644	15.5	1.5
2000	351	8.5	0.8
4000	150	3.6	0.3
8000	51	1.2	0.1
16000	15	0.4	0.03
20000	4	0.1	0.009

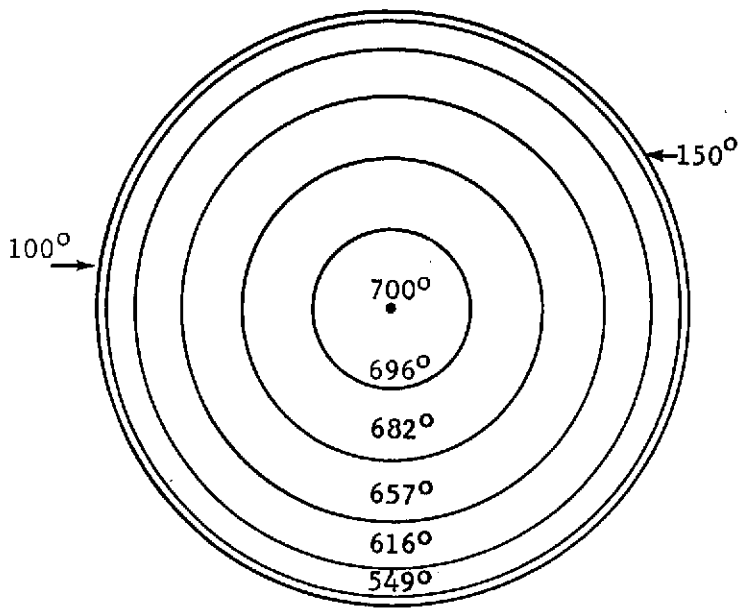

SUBSOLAR VIEW

NOTE: MERCURY AT PERIHELION (HOT POLE)

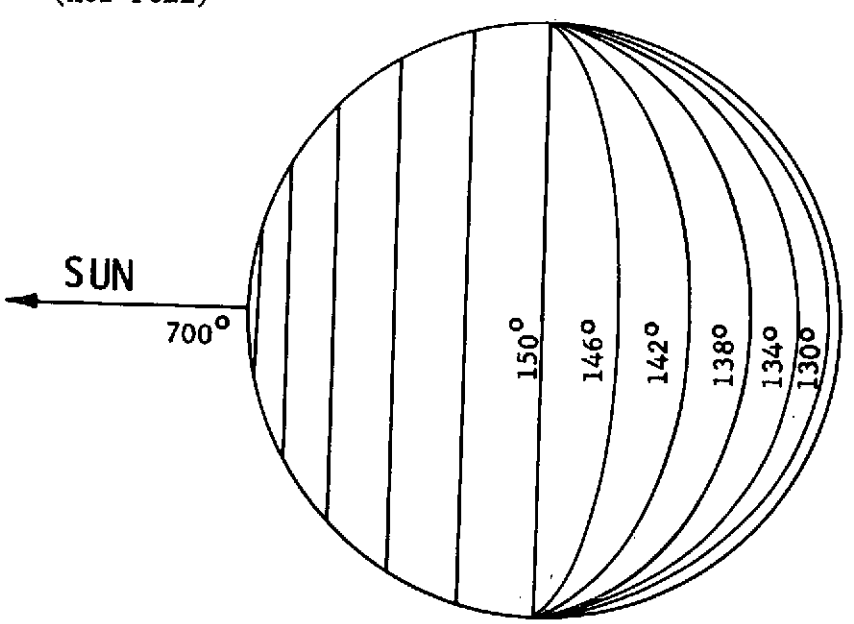

TERMINATOR VIEW

FIGURE A1-7 THERMAL CONTOURS ON MERCURY'S SURFACE

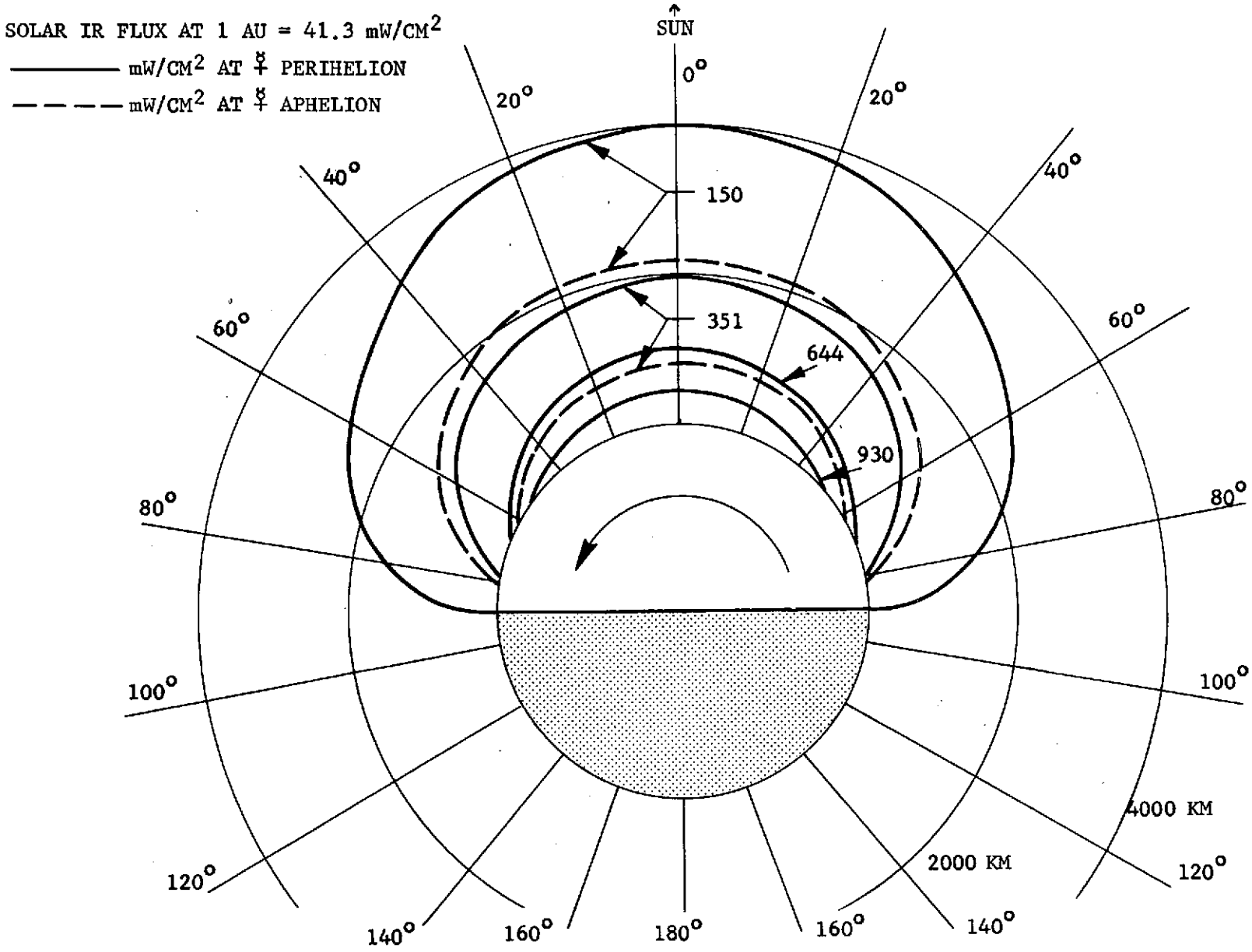

FIGURE A1-8 IR RADIATION CONTOURS, SURFACE TO 4000 KM ALTITUDE

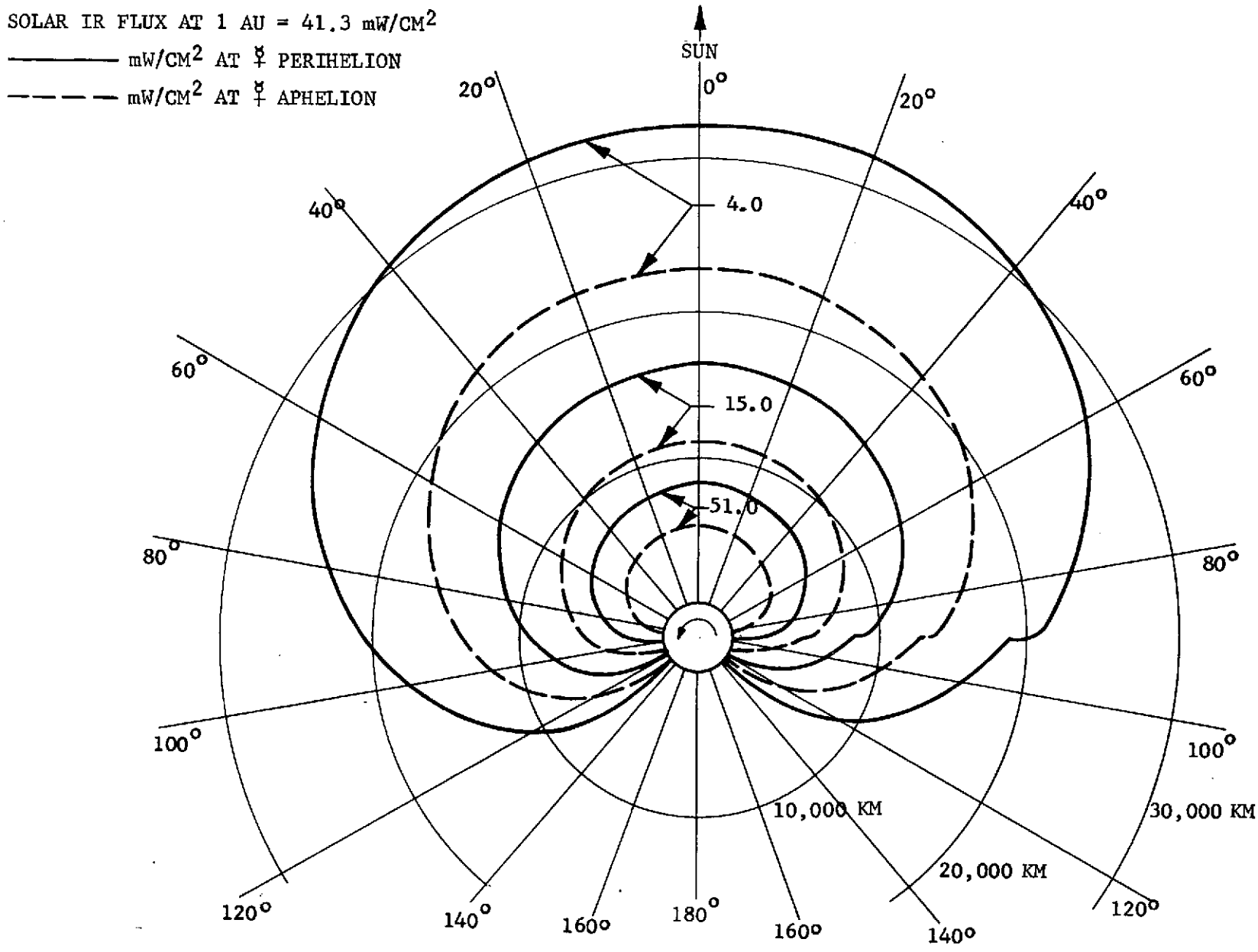

FIGURE A1-9 IR RADIATION CONTOURS, SURFACE TO 30,000 KM ALTITUDE

2. Subsatellite Sizing

A primary science objective for advanced Mercury missions involves determination of the gravity field harmonics and asymetries. This information would permit interpretation of density distribution, spin-coupling mechanics, etc.

Orbit selection for a single Mercury orbiter spacecraft involves a number of considerations consistent with high eccentricity and conservative periapsis altitude. This type of orbit is expected to preclude significant gravity measurements, especially in view of the solar influences perturbing such orbits. A subsatellite deployed to a lower orbit from the main orbiter spacecraft offers prospects of obtaining useful gravity measurements with modest investment of orbiter payload capabilities. This concept is depicted schematically in Figure A2-1.

An orbiter spacecraft established on a specific initial orbit will experience solar influences affecting periapsis altitude without modifying semi-major axis. These effects are dependent on B-plane targeting which will be established by a variety of considerations including science observables, thermal environment, etc. In general, orbit conditions at a time in the mission appropriate to deployment of a subsatellite cover a wide range of periapsis altitudes. Accordingly, subsatellite deployment has been addressed parametrically as shown in Figure A2-2.

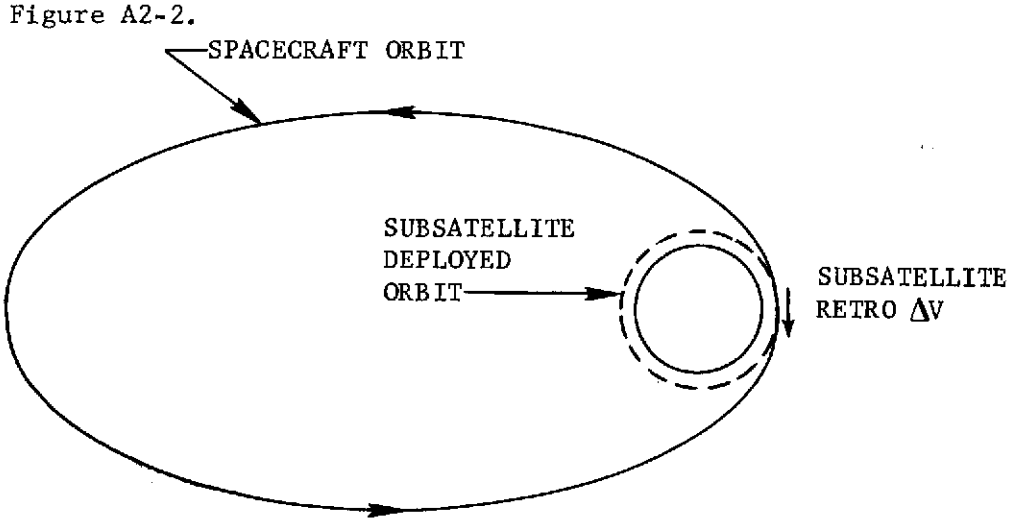

FIGURE A2-1 ORBITER/SUBSATELLITE GEOMETRY

Retro velocity increments for subsatellite deployment are on the order of 1 km/sec for typical initial orbits and no deflection of the orbit plane. The data of Figure A2-2 displays the variation of maneuver requirements for a range of retro altitude values and deployed subsatellite orbits. Options are shown

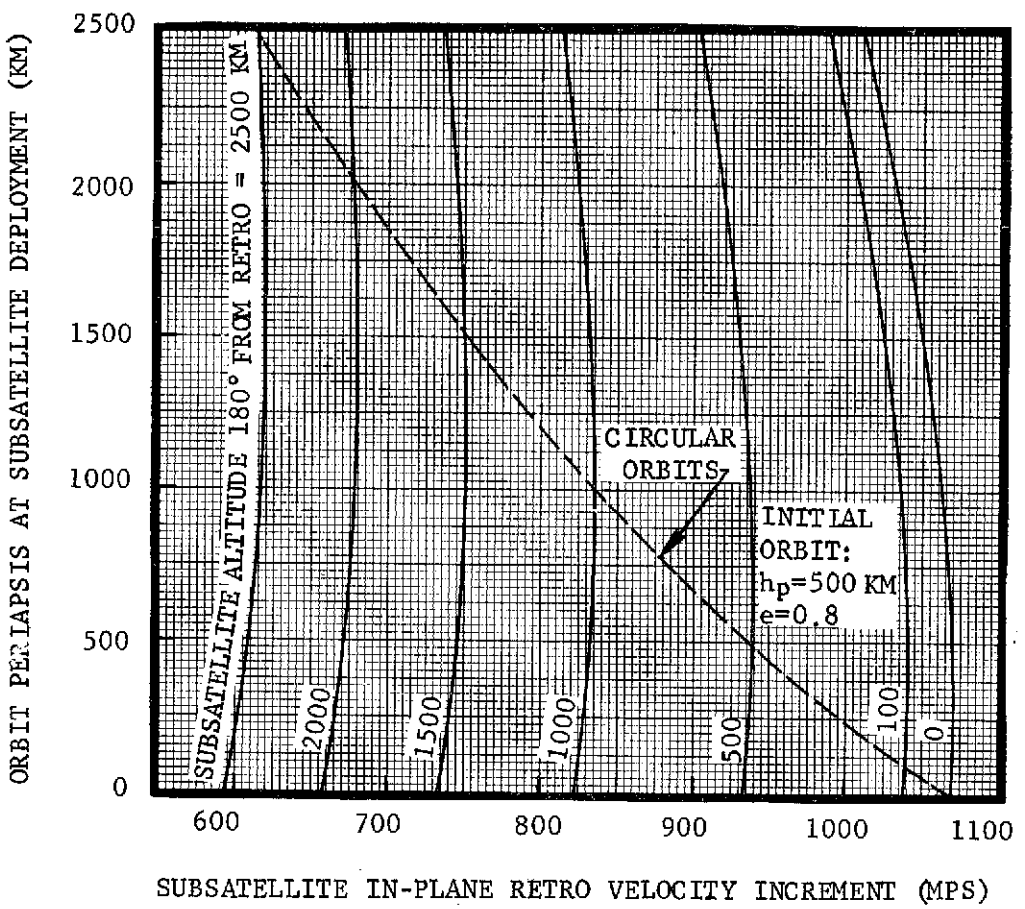

FIGURE A2-2 SUBSATELLITE DEPLOYMENT OPTIONS

for subsatellites with close approach to the planet surface. For example, if the orbiter periapsis has lowered to 100 km (implying night side location for thermal considerations), the subsatellite can be deployed with a conservative apoapsis (e.g. 1500 km) for a retro maneuver of about 740 mps. Alternatively, a high value of orbiter periapsis (e.g. 1500 km, appropriate to day side location) would require a subsatellite retro of 1025 mps to achieve 100 km periapsis on the planet night side. The figure shows the sensitivity of altitude to maneuver execution accuracy. For example, the latter case would impact the surface if overperformed by 25 mps.

Subsatellites with very low periapsis altitudes on the planet night side could be expected to operate for a period of a few weeks. However, when periapsis moves to the day side, the thermal environment would probably be prohibitive.

A method of sizing a simple subsatellite retro propulsion system (e.g. a

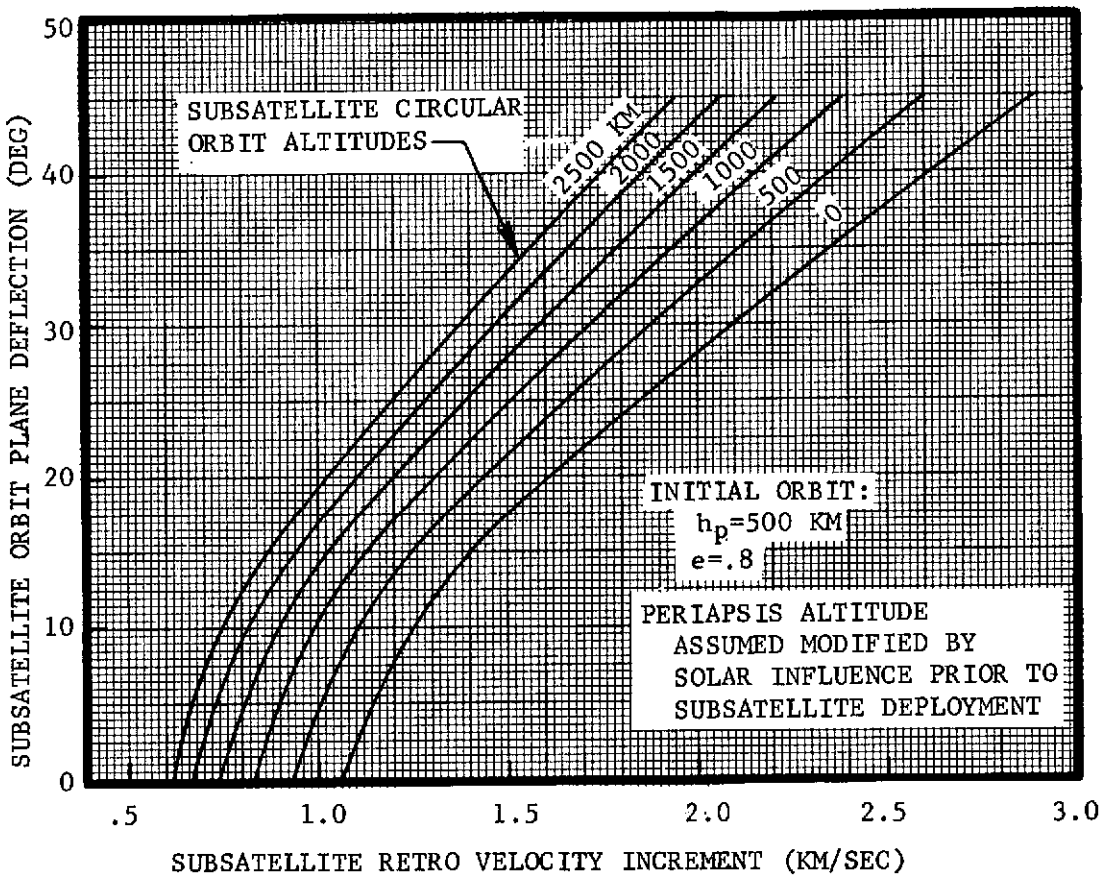

FIGURE A2-3 SUBSATELLITE ORBIT PLANE DEFLECTION

solid rocket motor) for a range of deployment conditions would involve sizing for the largest maneuver anticipated and, for actual conditions at deployment, pointing out-of-plane to achieve the desired degree of propulsion loss. The resultant plane deflections can be derived from Figure A2-3 for circular subsatellite orbits.

Figure A2-3 also presents the larger maneuver magnitudes associated with intentional plane deflections up to 45 deg. This option may be of interest if evaluation of the gravity field requires multiple subsatellites with differing orbits.

The weight of a subsatellite equipped with no functional instruments except cooperative tracking aids would depend on the method of tracking. Orbit determination from Earth may be feasible with low power output if Arecibo could be employed. (Appendix 3 presents data on Arecibo accessibility.) Alternatively, the subsatellite could be tracked from the main orbiter spacecraft if the compound orbit determination problem can be solved with sufficient accuracy.

Other candidate instruments for a subsatellite include the γ-ray spectrometer and the magnetometer (for close surface approach and to obviate magnetic cleanliness requirements for the orbiter spacecraft). A subsatellite including such systems would be considerably heavier and more complex than a minimum gravity field experiment.

Figure A2-4 presents representative weight factors for subsatellites deployed spin-stabilized with solid retro motors. For example, in-plane deployment on a 500 km circular orbit, which requires a retro maneuver of about 940 mps, corresponds to an initial weight 160% of the actual subsatellite net weight. Equivalent values for 45 degree plane deflection are 2600 mps and 400%.

For the case of in-plane deployment, a minimum subsatellite (estimated at about 10 kg) and a more ambitious subsatellite (e.g. 50 kg) would require allocations of orbiter spacecraft payload of 16 and 80 kg respectively. If 45^{o} orbit plane deflection is desired, only a minimum subsatellite (at 40 kg) seems practical.

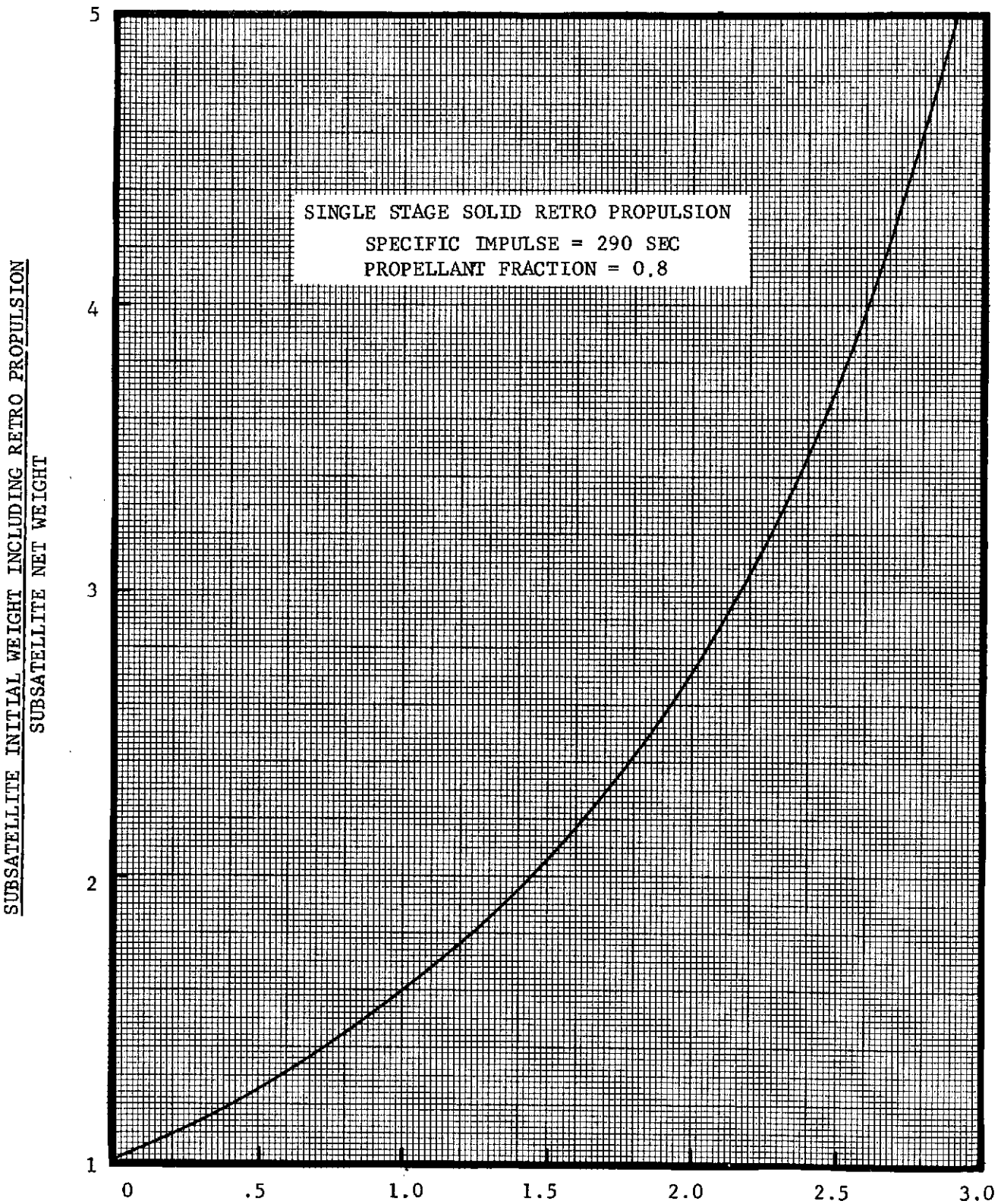

FIGURE A2-4 SUBSATELLITE SIZING

3. Arecibo Access

Side investigation of Arecibo viewing possibilities during S/C orbit about Mercury is shown for the four baseline and two multiple-Venus mission opportunities. The Arecibo antenna is capable of receiving the amount of data in about an hour that the DSN could receive all day (this is dependent upon the availability of sufficient data handling and storage hardware at Arecibo). At this time, the Arecibo antenna is undergoing changes to enable it to receive S-Band data in the near future. It is expected to be able to achieve 71 db gain while the DSN capability is 61 db for its 64 m antennas.

Time in view per day for 6 months after Mercury orbit insertion is shown for the six cases in Figure A3-1. These data show that receiving from Arecibo may be useful for the 1977, 1980, and both multiple-Venus missions (1983, 1988). In 1977, Arecibo is in view of the S/C during part of each day and for part of 135 days of that period in 1980. The 1988 double-Venus mission is in view of Arecibo for part of all except 20 days of the mission while the 1983 case would be without coverage for approximately 50 days early in the mission. Dots on the figures denote times of solar interference when communications problems would occur.

If Arecibo was available, it would enhance data return for a Mercury orbiter mission. However, it might be critical for a subsatellite or a lander (discussed in Appendices 2 and 5).

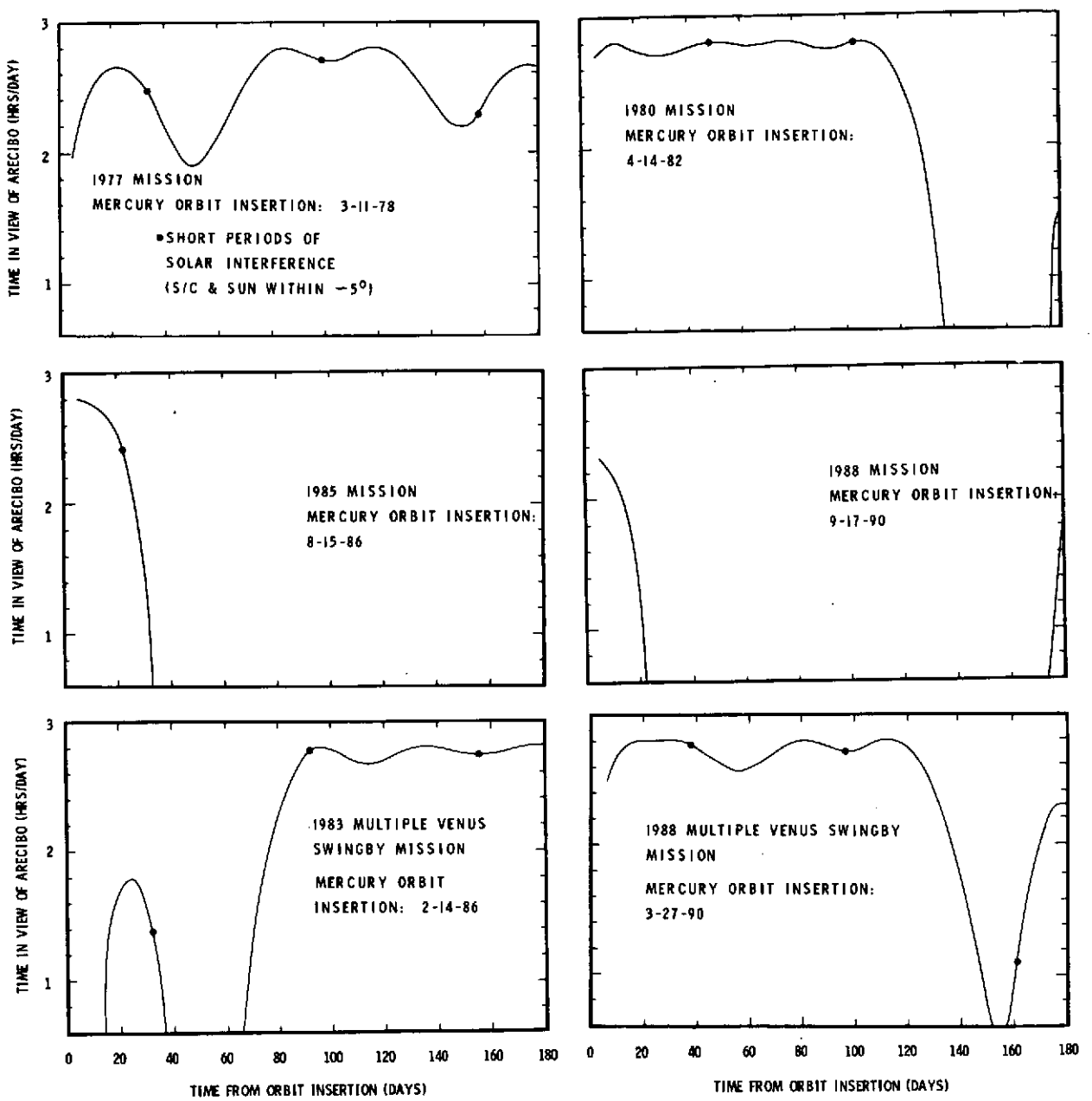

FIGURE A3-1 Arecibo Accessibility

4. Comet Viewing Opportunities

A side activity for a Mercury Orbiter during its interplanetary cruise phase could be comet observation. Two significant comets pass reasonably close to three of the Mercury orbiter trajectories. A 1980 mission would be able to view Encke during the comet's post-perihelion phase while Earth viewing of the post-perihelion will be poor for the 1980 apparition. During the Earth-Venus leg of the trajectory, closest approach to the comet occurs at .39 AU twelve days after Encke perihelion passage. An ecliptic projection of the spacecraft path and the Encke orbit is shown in Figure A4-1 with closest approach indicated. Actual S/C-comet range is shown below on the same figure for one month either side of closest approach since the inclination of a comet's orbit is not apparent on such a projection.

The 1986 perihelion passage of Halley will occur on the opposite side of the Sun from Earth giving poor Earth-based observation. A Mercury Orbiter with either a 1985 or 1983 (multiple-Venus swingby) launch would be able to observe the comet much better than anything on Earth or any Earth satellite. The Halley orbit and the S/C path are shown in the same manner as the Encke case in Figure A4-2 for the 1985 mission with closest S/C-Halley range at .18 AU. The 1983 mission is closest to Halley on 2-5-86, just before the comet goes through perihelion. Figure A4-3 shows the geometry for the 1983 opportunity and gives minimum distance from the comet as .29 AU. (No data is shown past 2-14-86 because that is the Mercury encounter date.) Both of these missions would approach Halley during the Venus-Mercury trajectory leg.

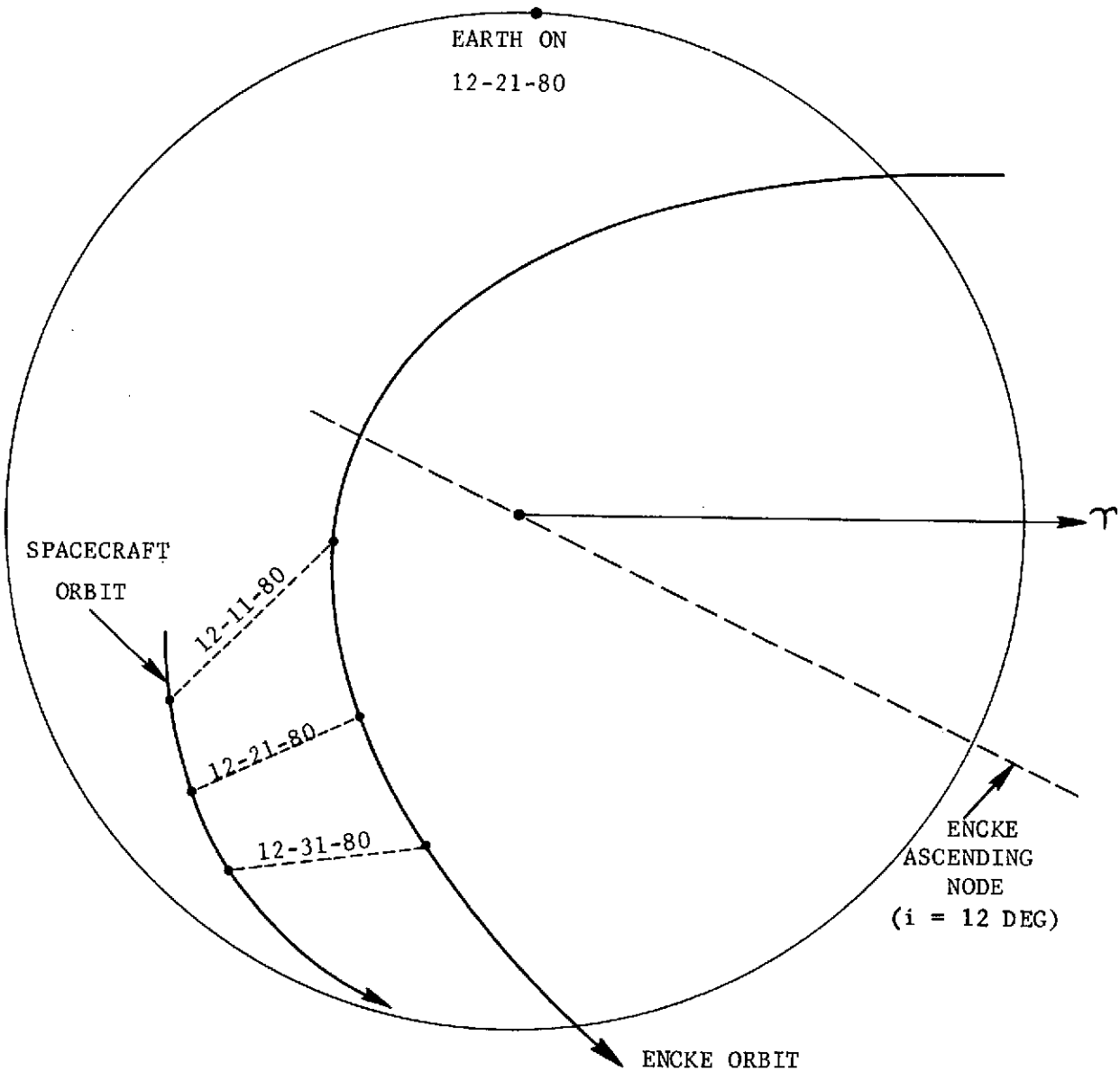

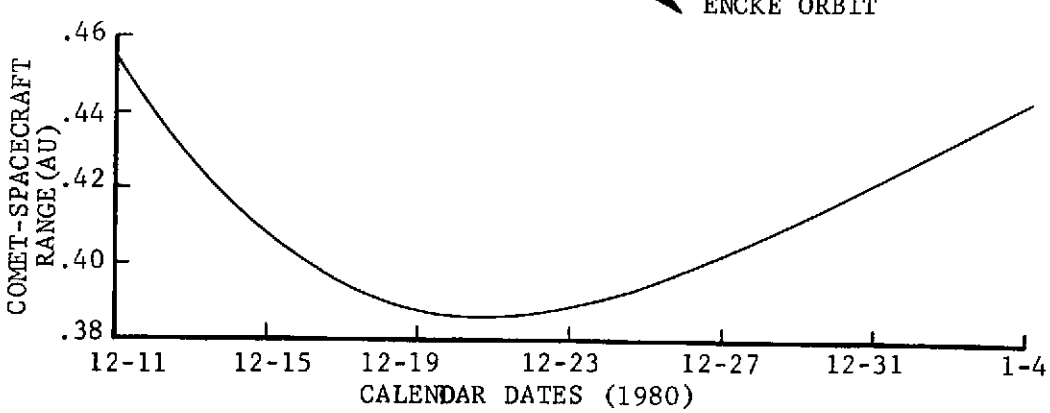

FIGURE A4-1 COMET ENCKE VIEWING FROM 1980 MISSION

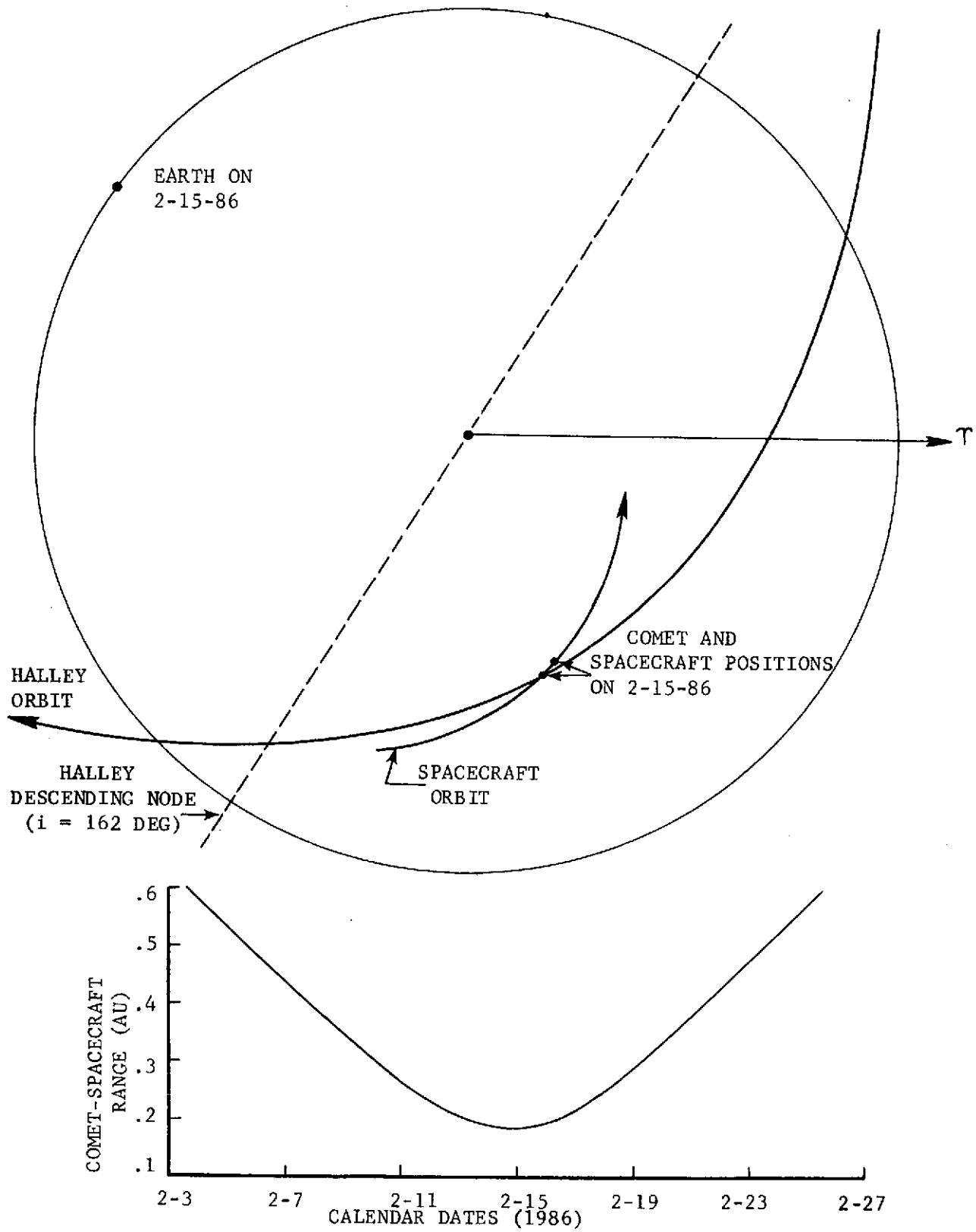

FIGURE A4-2 COMET HALLEY VIEWING FROM 1985 MISSION

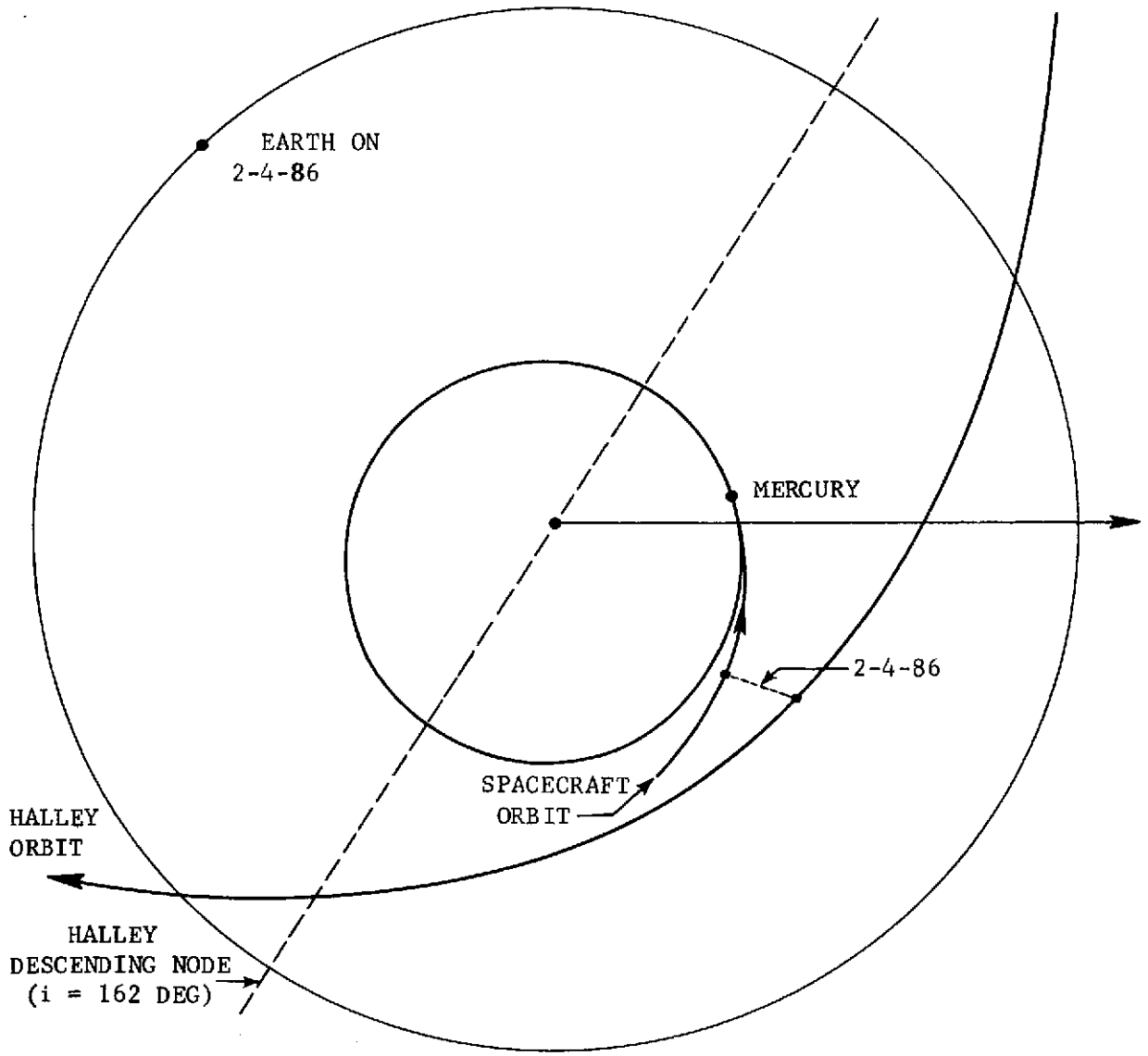

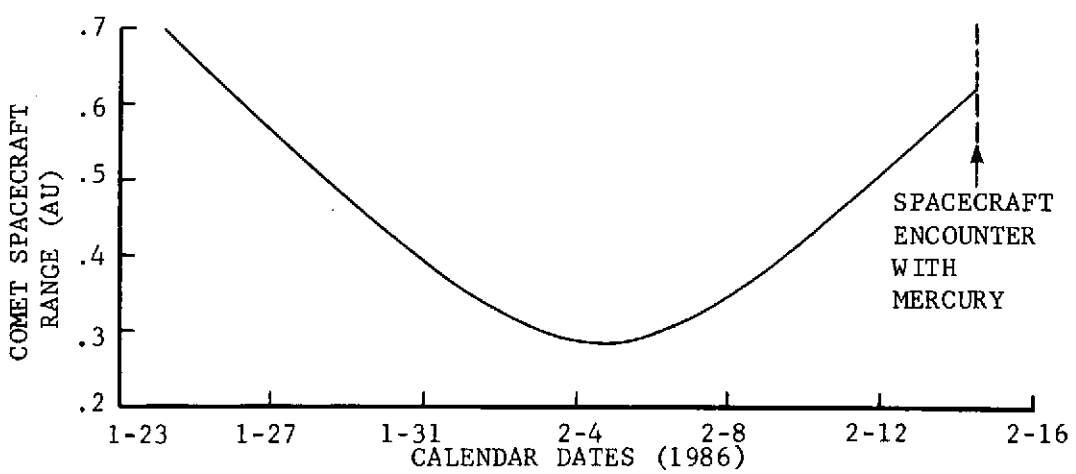

FIGURE A4-3 COMET HALLEY VIEWING FROM 1983 MISSION

5. Lander Sizing

Preliminary investigations have been conducted to evaluate the prospects that ballistic mode missions could accommodate a modest Mercury lander. It was assumed that a lander would be deployed from Mercury orbit and supported by an orbiter spacecraft for initial attitude reference, communication relay, etc. Further, it was judged that a minimum lander would be constrained by thermal considerations to the planet night-side (permitting up to 3 months operation) or, possibly, near-polar latitudes if the planet equator is confirmed close to the planet orbit plane.

Figure A5-1 illustrates two landing techniques assessed for general performance requirements and sensitivity to maneuver execution errors. Both techniques are predicated on simple thrust attitude programs. Horizontal attitude for velocity maneuvers to achieve vertical free-fall conditions would be established by the orbiter spacecraft and retained by the spin-stabilized lander vehicle through maneuver execution. Vertical attitude reference for arrest of free-fall velocity would require planet oriented sensors such as doppler radar.

The 3-impulse landing technique depicted involves two maneuvers in the local horizontal to lower periapsis and initiate vertical descent. Arrest of vertical free-fall velocity would be accomplished near the planet surface followed by the terminal landing phase. Table A5-1 presents typical maneuver requirements for this landing technique, For reference, the case of no initial lowering of periapsis is included.

As shown by the table, total maneuver requirements are significantly improved by the use of an intermediate orbit for initial lander descent. However, the sensitivity to execution of the apoapsis maneuver is extreme. For example, targeting to 50 km periapsis altitude involves a sensitivity of about $\pm$ 14 km per mps. The associated uncertainty in descent arrest requirement is non-linear and varies from 70 to 170 mps/mps.

The foregoing sensitivities would impose severe penalties on lander propulsion system sizing and terminal descent sensors. Accordingly, it is judged that the 3-impulse landing technique is impractical unless periapsis lowering is accomplished gradually by the orbiter spacecraft.

A 2-impulse landing technique with basically different sensitivities is

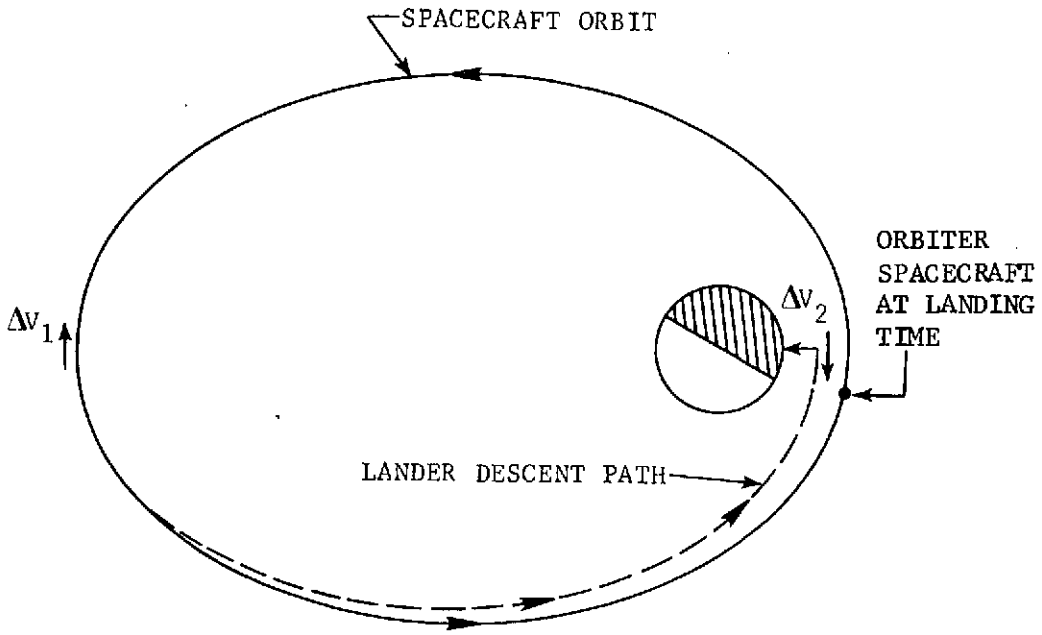

3 IMPULSE LANDING TECHNIQUE

BOTH TECHNIQUES: FINAL RETRO NEAR SURFACE TO ARREST VERTICAL FREE FALL VELOCITY

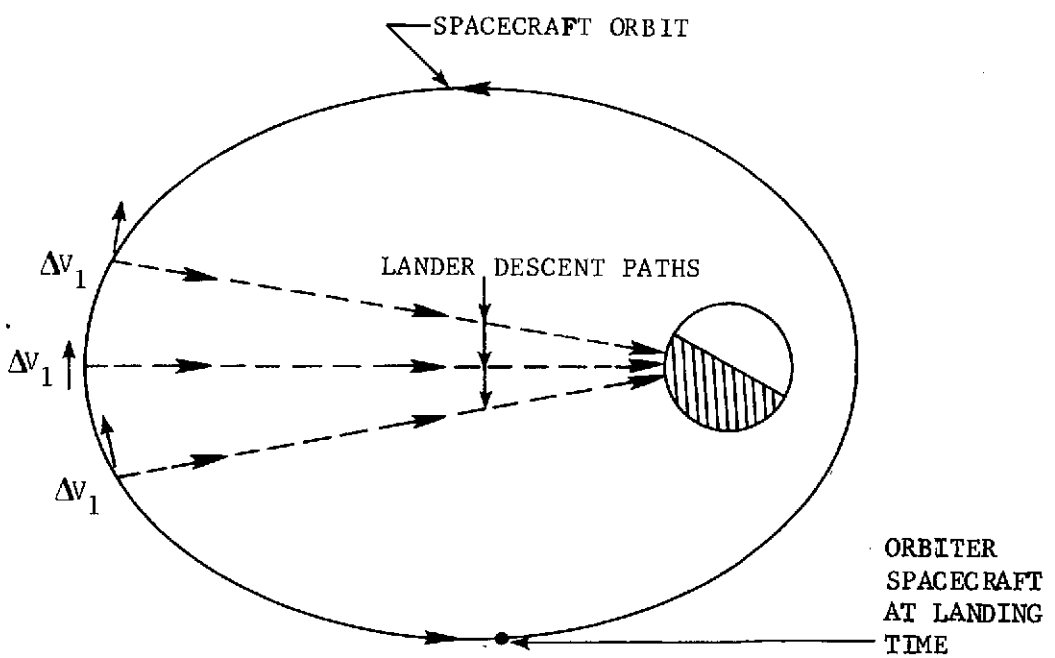

2 IMPULSE LANDING TECHNIQUE

FIGURE A5-1 LANDING TECHNIQUE OPTIONS

TABLE A5-1 VELOCITY MANEUVERS FOR 3-IMPULSE LANDING TECHNIQUE

INITIAL ORBIT: PERIAPSIS ALTITUDE = 500 km
ECCENTRICITY = .8

PERIAPSIS OF LANDER DESCENT ORBIT (km)	500	100	50	0
APOAPSIS MANEUVER TO LOWER PERIAPSIS (ΔV_1, MPS)	0	26.33	29.80	33.32
PERIAPSIS MANEUVER TO INITIATE VERTICAL FREE-FALL (ΔV_2, km/sec)	3.688	3.996	4.039	4.084
SURFACE CONTACT VELOCITY FOR FREE-FALL FROM LANDER DESCENT ORBIT PERIAPSIS (km/sec)	1.762	.848	.605	0
TOTAL VELOCITY MANEUVERS (km/sec)	5.450	4.870	4.674	4.117

also depicted on Figure A5-1. For this case, the apoapsis maneuver is sized to initiate near-vertical free-fall immediately. Magnitude errors in execution of this maneuver produce a residual component of horizontal velocity which will multiply by a factor of about 11 by the time of surface approach. However, the vertical component of surface (or near surface) velocity is insensitive to both magnitude and direction errors. Table A5-2 summarizes maneuver requirements for the 2-impulse landing technique.

TABLE A5-2 VELOCITY MANEUVERS FOR 2-IMPULSE LANDING TECHNIQUE

Initial Orbit: Periapsis Altitude = 500 km, Eccentricity = .8

True anomaly at lander descent initiation (deg)	180 (apoapsis)	170 & 190 (apoapsis $\pm$ 10)
Maneuver Required to Stop Horizontal Velocity (ΔV_1, mps)	409.8	434.7
Surface Contact Velocity for Free-Fall from Maneuver Altitude (km/sec)	4.067	4.067
Total Velocity Maneuvers (km/sec)	4.477	4.487

As shown by the table, the horizontal component of velocity varies only about 25 mps for orbit true anomaly $\pm$ 10 deg from apoapsis. Accordingly, propulsion system sizing could easily accommodate landing site selection over a 20 deg surface range and maintain vertical lander descent. For the technique of stopping the horizontal velocity component only, the remaining vertical component of velocity produces about the same surface contact velocity and landing time for all lander descent paths.

While this study did not intend to recommend a landing method, the 2-impulse technique appears to exhibit some advantages and has been selected for representative calculations of lander sizing.

Table A5-3 presents a typical lander weight history predicated on a final landed weight of 50 kg. This value has not been confirmed by detailed design, but represents a preliminary estimate for a vehicle with the following design characteristics.

1) 5 kg of science instrumentation
2) Planet night-side operation
3) 5-watt SNAP power supply
4) Shock absorbing pads to accommodate vertical contact velocities to about 25 mps
5) Self-righting roll cage to accommodate horizontal contact velocities to about 50 mps.
6) Hydrazine monopropellant propulsion for de-orbit and terminal descent; solid rocket motor for main retro propulsion.
7) Terminal descent velocity budget of 100 mps.

For the example shown, about 400 kg of orbited weight must be allocated to lander systems. An additional 25 kg or so would be required for lander support systems such as a spin table, thermal protection in orbit, etc. Relating these values to the performance capabilities presented on Figure III-4 for the high performance 1988 mission opportunity indicates a requirement for the Shuttle/Centaur class launch vehicle. An alternative which could possibly support a Titan IIIE/Centaur class orbiter/lander mission would be the multiple Venus swingby mission opportunities displayed on Figure I-3.

TABLE A5-3

WEIGHT HISTORY FOR A SMALL MERCURY LANDER

INITIAL WEIGHT SEPARATED FROM ORBITER	403.1 kg
APOAPSIS MANEUVER PROPELLANT (ΔV=410 mps, Specific Impulse = 235 sec)	65.7
PRIMARY RETRO PROPELLANT (ΔV=4.067 km/sec, Specific Impulse = 290 sec)	256.7
RETRO MOTOR WEIGHT JETTISONED (Propellant Fraction = 0.9)	28.5
FINAL DESCENT INITIAL WEIGHT	52.2
TERMINAL DESCENT PROPELLANT (ΔV = 100 mps, Specific Impulse = 235 sec)	2.2
TOTAL LANDED WEIGHT	50.0